Fall 12-7-2021

WINDBLOWN TRANSPORT OF TOXIC METALS IN AIRBORNE PARTICULATE MATTER NEAR THE JACKPILE-PAGUATE URANIUM MINE ON LAGUNA PUEBLO, NEW MEXICO

Savannah S. LaRosa-LoPresti

Savannah LaRosa-LoPresti
Candidate

Earth & Planetary Sciences
Department

This thesis is approved, and it is acceptable in quality and form for publication:

Approved by the Thesis Committee:

, Dr. Joseph Galewsky

, Dr. Adrian Brearley

, Dr. Louis Scuderi

WINDBLOWN TRANSPORT OF TOXIC METALS IN AIRBORNE PARTICULATE MATTER NEAR THE JACKPILE-PAGUATE URANIUM MINE ON LAGUNA PUEBLO, NEW MEXICO

BY

SAVANNAH LAROSA-LOPRESTI

B.S., ENVIRONMENTAL SCIENCE, UNIVERSITY OF NEW MEXICO, 2019
B.A., WOMEN STUDIES, UNIVERSITY OF NEW MEXICO, 2019

THESIS

Submitted in Partial Fulfillment of the
Requirements for the Degree of

Master of Science

Earth and Planetary Sciences

The University of New Mexico
Albuquerque, New Mexico

May, 2022

ACKNOWLEDGMENTS

I am immensely grateful to the Pueblo of Laguna for partnering with the UNM METALS Superfund Research Program and allowing us to access their sites, to perform and translate research for their knowledge and records, and to assist us in furthering scientific understanding of windblown transport of respirable toxic metal mixtures.

I am very thankful to my advisors, Joe Galewsky and Adrian Brearley, and to all of my committee members for guiding and supporting me throughout this program and the research we've completed, and for sticking with me through my personal health struggles. I would also like to thank Dr. Abdulmehdi Ali for his guidance and supervision in the analytical chemistry lab. A big thank you to the UNM METALS Superfund Research Center and all associated staff members for their dedicated work to tribal communities and for supporting me in being a part of this research.

I appreciate the support and care of my friends and family. To my best friend, Rachel, thank you for always being a listening ear when I have a lot to say and just need to be heard. Thank you to my amazing partner, Rene. You are a light in my life; I am blessed to shine together with you and to be illuminated by your kind soul in my darkest times. Your love and support throughout the duration of this work has been healing, motivating, and inspiring.

WINDBLOWN TRANSPORT OF TOXIC METALS IN AIRBORNE PARTICULATE MATTER NEAR THE JACKPILE-PAGUATE URANIUM MINE ON LAGUNA PUEBLO, NEW MEXICO

by

Savannah LaRosa-LoPresti

B.S., Environmental Science, University of New Mexico, 2019
B.A., Women Studies, University of New Mexico, 2019
M.S., Earth and Planetary Sciences, University of New Mexico, 2022

ABSTRACT

Abandoned uranium mines across the U.S. disproportionately affect indigenous communities who suffer numerous intergenerational health consequences from chronic exposure to toxic metal mixtures. The Jackpile-Paguate Uranium Mine on Laguna Pueblo in west-central New Mexico was designated a Superfund Site in 2013 and exposure risks from inhalation of toxic metals in airborne particulate matter are of concern for the local tribal communities. This research aims to examine atmospheric parameters driving windblown transport of respirable particulate matter in the region, to determine concentrations of heavy metals including U, V, Pb, and As due to the link with potential health risks, and to analyze the mineralogic characteristics of metal-bearing particulate matter in the inhalable size fraction. The results indicate the dominant atmospheric parameter controlling dust transport in a semiarid region with variable topography is low relative humidity ≤35% due to the effect on

soil moisture and the subsequent prevention of the formation of aggregate particles that are more difficult to entrain by wind. Local meteorological stations are compared to regional climate models and prove to be significantly more accurate for wind data, highlighting the importance of maintaining the local stations for future analyses. Concentrations of toxic metals U, Pb, As, Cu, Zn, Cd, Mo, and Co are enriched in particulate matter samples relative to crustal average values. Standards associated with inhalation of toxic metals in airborne particulate matter do not currently exist; an indirect comparison to OSHA worker standards is observed in this research but does not provide information for potential health risks. Microscopy analyses revealed the presence of uranyl vanadate and uranyl arsenate minerals in the inhalable size fraction as well as coarser size fractions, many of which appear to be susceptible to erosion and fragmentation during windblown transport. Based on this information, inhalation of airborne particulate matter has been found to be a potential exposure pathway for the local tribal communities at Laguna Pueblo.

Keywords: Jackpile-Paguate Uranium Mine, Laguna Pueblo, toxic metal mixtures, respirable particulate matter, inhalable size fraction, inhalation exposure risk

TABLE OF CONTENTS

LIST OF FIGURES

LIST OF TABLES

CHAPTER 1- INTRODUCTION

Significance of the Study

Indigenous communities in the United States are disproportionally affected by abandoned uranium mines (AUMs) and suffer numerous intergenerational health consequences from chronic exposure to toxic metal mixtures. There are more than 4,000 AUMs across the Western United States and over 600,000 indigenous people live within 10 km of these numerous sites (Lewis et al., 2017). While uranium is a naturally occurring element and makes up about 0.0003% of the Earth's crust, anthropogenic activities such as mining, transporting, and processing ore release additional toxic metal mixtures into the environment that threaten human health (CCME, 2007; Martin et al., 2016). The USEPA does not currently have national standards for heavy metals in airborne particulate matter and most AUM exposure research has focused on hydrologic studies due to concerns for ingestion by local communities. Inhalation of airborne particulate matter may be a significant exposure pathway near AUMs, if it contains harmful concentrations of heavy metals. Serious health risks including various cancers and respiratory diseases are now associated with inhalation exposure to heavy metals such as uranium (U), vanadium (V), copper (Cu), and arsenic (As); therefore, minimization of health risks for current and future generations depends on the expansion of scientific understanding of airborne transport and mineralogic characteristics of toxic metal mixtures in airborne particulate matter near AUMs (Committee on Uranium Mining in Virginia, 2011; Riley, 2019).

The Jackpile-Paguate Uranium Mine (Jackpile or Jackpile Mine) located in west-central New Mexico at Laguna Pueblo (Laguna or the Pueblo of Laguna) was designated a Superfund Site by the USEPA in 2013 after elevated levels of toxic metals were detected in the

local rivers. During its operation from 1952 to 1982, the Jackpile Mine produced 25 million tons of uranium ore that was transported 40 miles west on the Santa Fe Railroad to Anaconda's Bluewater Mill (U.S. Environmental Protection Agency, 2017). The Jackpile Mine (Fig. 1) disturbed approximately 400 million tons of rock, consisting of 9 underground mines and 3 open pits, as well as several waste dumps, protore stockpiles, and topsoil stockpiles (U.S. Bureau of Land Management et al., 1986). Reclamation work was completed by Laguna Construction Company from 1989 to 1995; however, this left the mine untouched for roughly 7 years prior to the start of reclamation, allowing toxic metal mixtures to be exposed to erosion and atmospheric distribution throughout the region during that time (Dixon, 2015; U.S. Bureau of Land Management et al., 1986).

The UNM Metal Exposure and Toxicity Assessment on Tribal Lands in the Southwest (UNM METALS) Superfund Research Center has several site-specific projects funded by the National Institute of Environmental Health Sciences (NIEHS), one of which is to estimate inhalation exposure risks for local tribal communities at Laguna Pueblo. With permission from the Pueblo of Laguna and their Environmental and Natural Resources Department (ENRD), UNM METALS researchers from the Department of Earth and Planetary Sciences and the College of Pharmacy are assessing toxic metal transport in airborne dust. Particulate matter (PM) with an aerodynamic diameter of $PM_{2.5}$ and smaller can penetrate the lungs and enter the bloodstream, while $PM_{2.5} – PM_{10}$ can cause lung inflammation but is considered less of a hazard to human health (Martin et al., 2016; Xing et al., 2016). Estimation of inhalation exposure risks for the local tribal communities is dependent on the inhalable size fraction of

airborne dust PM_{10} and smaller with an emphasis on $PM_{2.5}$ and PM_1 due to increased health risks.

A regulatory framework from the U.S. Atomic Energy Commission for the mining and milling of uranium did not exist during the operation of the Jackpile Mine, leading to a legacy of environmental contamination and severe health issues (Lewis et al., 2017; Riley, 2019). Concerns from the community at Laguna Pueblo remain today as they continue to experience numerous intergenerational health consequences, including various types of cancers, kidney disease, hypertension, breathing problems and respiratory diseases (Riley, 2019). Occupational exposures likely contributed to local health issues, as most of the population of Laguna Pueblo was employed at Jackpile during its operation, but no comprehensive health studies have been conducted near the site. A case study, "Uranium and the Navajo Nation" highlights the disproportionate impacts of uranium mining on Native communities, stating Native miners had higher rates of nonmalignant respiratory diseases and death due to lung cancer compared to non-Hispanic white miners (Lewis et al., 2017). In all populations, exposure to toxic metal mixtures have been found to increase kidney and cardiovascular diseases, neurocognitive disorders, and various cancers (Lewis et al., 2017; Liu & Lewis, 2014; Niu et al., 2013); therefore, the occupational workers at Laguna and their families were likely impacted by increased exposure during the 30-year mining process.

Many of the Jackpile Mine workers from Laguna Pueblo are alive today and have spoken directly with UNM METALS researchers in 2019, recalling that they were not required to wear protective gear while mining, such as face masks and gloves, nor were they warned about the potential hazards of uranium, other heavy metals, or radiation. Workers also claim

that they were not informed of the potential health risks associated with transporting toxic metals home to their families in the form of dust on their clothes. At the peak of its operation, Jackpile was mined 24 hours a day, 7 days a week and explosive blasts used for ore extraction could be felt in Paguate Village 2-3 times a day (Sittnick, 1998). Several Laguna community members told UNM METALS researchers that they remember the resulting dust clouds blowing into the village multiple times a day and recall that the foundations of their houses occasionally cracked. While it is not possible to estimate past inhalation exposure risks, focusing on modern dust transport mechanisms and mineralogic characteristics of toxic metal mixtures in airborne particulate matter will address concerns for ongoing inhalation risks to current and future generations at Laguna Pueblo. Data collected for this research provides the Pueblo of Laguna with current atmospheric and mineralogic data directly from their land for their sovereign decision-making.

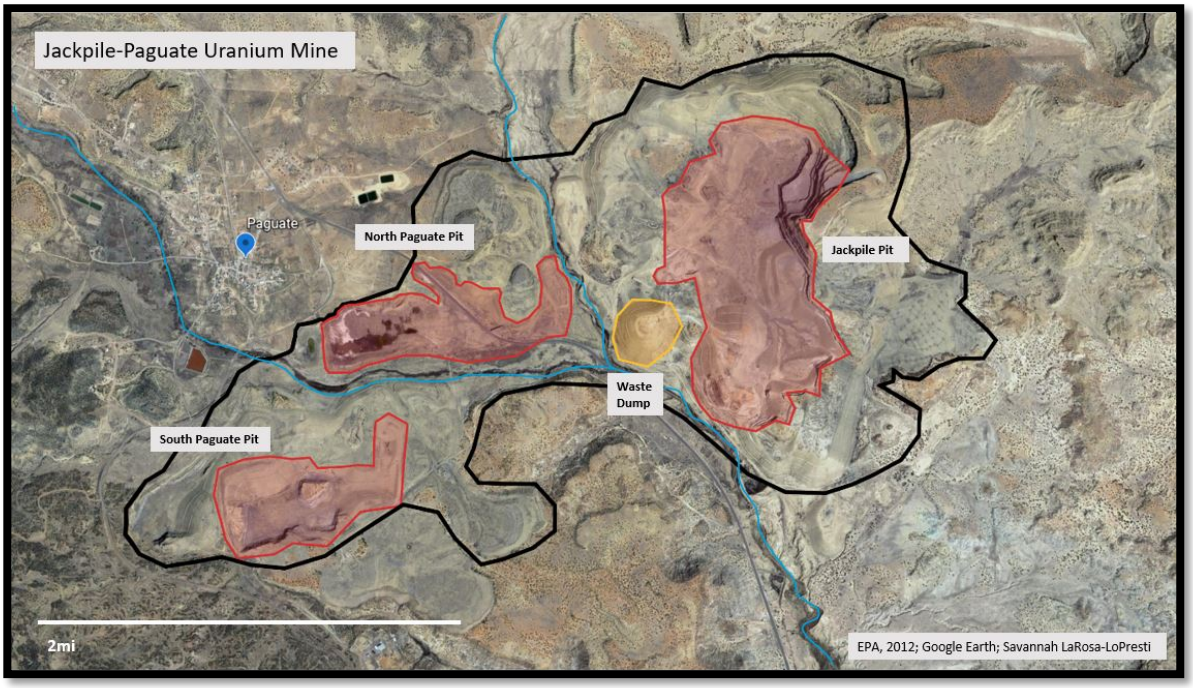

Figure 1: Map of Jackpile-Paguate Uranium Mine on Laguna Pueblo. Includes an outline of the Jackpile Mine area, 1 major waste dump and the 3 open pit mines: Jackpile Pit, North Paguate Pit and South Paguate Pit.

Research Questions

This research aims to characterize the meteorological parameters controlling transport of airborne particulate matter in the inhalable size fraction in a semiarid region with highly variable topography. A possible threshold for relative humidity as a parameter determining respirable particulate matter transport throughout the region is analyzed. Such a threshold may provide a constraint to begin developing a warning system for local tribal communities during high particulate matter conditions influenced by local meteorological conditions. This study also aims to evaluate the presence of a relationship between wind speed and respirable particulate matter concentrations. Preliminary analyses suggested a negative relationship between wind speed and concentration, where slow wind speeds were associated with higher particulate matter concentrations.

To estimate inhalation exposure risk to the local tribal communities at Laguna Pueblo, the concentrations and characteristics of toxic metal mixtures must be evaluated and quantified. This study aims to address which toxic metals are present and in what concentrations, as well as the mineralogic characteristics of respirable U-bearing particles from local samples. There is an emphasis on particulate matter containing toxic metal mixtures in the inhalable size fraction due to increased health risks associated with inhalation of such particles. Particle susceptibility to erosion during transport is also considered as a mineralogic characteristic of observed U-bearing particles. Evaluation of inhalation exposure risks to local tribal communities at Laguna Pueblo can be assessed using atmospheric, mineralogic, and geochemical analyses with comparisons to crustal average concentrations of toxic metals.

CHAPTER 2 – BACKGROUND

Climate

The Jackpile Mine on Laguna Pueblo is located in a semiarid region characterized by minimal precipitation, copious amounts of sunshine, and low relative humidity (NOAA, 2000). The region also experiences large diurnal and annual temperature ranges in response to these parameters. Precipitation ranges from less than 10 inches to more than 20 inches in areas of higher elevation (DuBois, 2020). Precipitation is highest in the summer months during the local monsoon season and characterized by brief and intense thunderstorms that are brought up from the Gulf of Mexico with southeasterly circulations. Precipitation in the winter months occurs mainly as snow in mountain areas and occasionally in valley areas; winter storms are typically brought in from the Pacific Ocean with a westerly circulation (NOAA, 2000). The elevation of Laguna Pueblo varies widely from 5,100 ft – 10,000 ft above sea level (Pueblo of Laguna, n.d.). Highly variable topography, from Mount Taylor west of the Pueblo to large, scattered mesas throughout the region creates local atmospheric conditions which can differ widely from neighboring areas. This can make forecasting local conditions difficult with few local weather stations and with grid-based regional or global models that often cannot resolve small scale processes like those occurring at Laguna. The closest weather station to Laguna is about 35 miles away at the Grants Municipal Airport, which also has limited accuracy at such a distance.

Precipitation is a natural process that reduces airborne particulate matter concentrations; however, a semiarid region like that of Laguna Pueblo may have increased atmospheric dust concentrations due to relatively low annual precipitation and low soil moisture (Zhang et al., 2017). Transport of airborne particulate matter in semiarid regions has been found to be

dependent on relative humidity, where dry conditions reduce the likelihood for water films to develop on particles and prevent the establishment of interparticle cohesion that could reduce suspension by wind (Csavina, 2014). Changes in soil moisture in semiarid regions as a response to changes in atmospheric humidity can be assessed with an estimation of soil matric potential (Neuman & Sanderson, 2008; Ravi et al., 2004; Ravi et al., 2006). The soil matric potential describes the molecular water film that is established when water adheres to many small soil particles through hydrogen bonding and creates aggregates that are more difficult to erode and entrain than individual particles. Neuman and Sanderson (2008) found that the effect of relative humidity conditions between 35% – 45% on completely dry soil is the establishment of a single water layer adsorbed to the surface of the grains; as the relative humidity reaches ~60%, a second water layer forms and increases the soil matric potential. This study was based on smooth quartz plates and other results will vary based on surface roughness but can be applied in terms of the effect of increasing relative humidity on cohesion of particles through water films and the establishment of soil aggregates. Relative humidity <35% does not cause the presence of a complete water layer and leaves soil more susceptible to wind erosion and transport. Temperature has not been found to have a significant influence on soil moisture; however, threshold friction velocity is dependent on soil moisture and influences wind erosion of soils (Ravi et al., 2004). When soil matric potential and therefore soil moisture is higher, the threshold friction velocity increases and can prevent wind erosion and transport (Neuman & Sanderson, 2008). Different soil types have differing soil matric potentials because fine-grained soils provide more surfaces for adhesion; therefore, clayey soils have a higher soil matric potential (less negative) than sandy soils due to their increased ability to maintain water within

aggregates (Neuman & Sanderson, 2008; Ravi et al., 2006). Common soil types were determined from several locations on Laguna Pueblo below the Jackpile Mine where contamination is considered most severe; they vary widely and include sand, loamy sand, sandy loam, silty clay, clay loam, silty clay loam and clay (Gorospe, 2013). The top layer of soils is the region that is used to aid in the assessment of windblown respirable particulate matter and often contains a thin layer of deposited sand.

Wind speed is another known atmospheric parameter that influences dust transport. While high wind speeds are known to produce dust storms in arid and semiarid regions, fine particulate matter of the inhalable size fraction may behave differently in response to wind speed when compared to coarser size fractions. Specifically, PM ≤10 μm can decrease in concentration with increasing wind speeds, with the opposite effect on larger particles due to dust resuspension under high wind conditions (Zhang et al., 2017). The average wind speed observed from locally collected data at Laguna Pueblo is 2.13 m/s; combining this data with previous research, low wind speeds are defined from 0 m/s up to 2.2 m/s, while high wind speeds are defined from 2.4 m/s to ≥4.4 m/s (Zhang et al., 2017). The effect of wind speed on $PM_{2.5}$ may have a stronger negative impact than on PM_{10}, indicating that finer particulate matter is less susceptible to transport at high wind speeds but more susceptible to transport under conditions with slow wind speeds. Additionally, particles with a diameter ≤20 μm can have a lifetime of up to 1-2 weeks in the atmosphere after initial suspension (Kok et al., 2012).

Atmospheric dispersion of heavy metal-bearing particulates is assumed to have occurred for the duration of the roughly 30-year mining process at Jackpile; however, windblown particulate matter likely represents a combination of contaminated particulates from

the mining processes as well as windblown dust from distant sources, which dilutes the local soil and likely adds a new carbonate component from older eroded soil carbonate (Naiman et al., 2000). The topsoil at Laguna is the main source of airborne particulate matter and consists of a mixture of local and distant materials that are subject to daily resuspension in response to local meteorological parameters. It is unknown if the reclamation efforts were sufficient to prevent ongoing erosion of the mine site from local wind and precipitation events over the last 26 years; however, researchers have identified uraniferous sandstone outcrops and U-bearing strata exposed within the mine area that are likely subject to climate induced erosional processes and subsequent particulate transport by wind. The National Priority Listing (NPL) for the site concluded that the reclamation was "incomplete" and primary contaminants include uranium (U), arsenic (As), barium (Ba), cobalt (Co), copper (Cu), lead (Pb), manganese (Mn), vanadium (V), selenium (Se) and zinc (Zn) (U.S. Environmental Protection Agency, 2015).

Impacts of Local Geomorphology

Climate is the determining factor for chemical, mechanical, and biological weathering and active erosional processes from intense wind and precipitation events are a significant driver of geomorphic processes in the region, contributing to increased airborne particulate matter concentrations (Brown, 2017; Huggett, 2017). The three most common erosional events that occur in semiarid climates are mass movements, fluvial processes, and aeolian processes. Sparse vegetation and loose gravel material are also characteristic of the region and contribute to erosional processes that have shaped the landscape over time (NPS, 2019). Dominant land features in the region are valleys that have deepened and widened over time, scattered bedrock

mesas capped with Dakota sandstone and erosional pediment surfaces between mesa tops and valley floors that are mostly comprised of gravelly alluvium (Wells, 1989). Most overlying shales and mudstones on mesas have been eroded; the Jackpile deposit was also eroded to some extent before the Dakota sandstone was deposited on top, exposing the strata at the surface. Surficial deposits have become part of the local geology and include gravels over pediment remains, colluvial deposits next to mesas and mixed aeolian and fluvial deposits on mesa tops and valley floors (Moench & Schlee, 1967).

The local geomorphology was significantly modified by the mining and reclamation processes, which severely altered the landscape. Of the 7,868 acres leased by Anaconda Mining Company, 2,656 acres were disturbed for mining and then buried during the reclamation process; during this time, roughly 400 million tons of rock were moved within the mine area (U.S. Environmental Protection Agency, 2017). The reclamation consisted of burying the mine in layers of soil and shale, adjusting slope angles, and revegetating to prevent extensive erosion and subsequent release of toxic metal mixtures into the environment (U.S. Bureau of Land Management et al., 1986).

Mineralogy & Geology

The Jackpile Mine is located on the eastern section of the Grants Mineral Belt in the Laguna District on the south margin of the San Juan Basin. The Jackpile uranium deposit is the largest in the district and is composed of several semi-tabular ore layers up to 15 m in total thickness with an average width of 609 m (Moench & Schlee, 1967). The Jackpile Sandstone Member was considered viable for local economic usage due to a high U_3O_8 content, which

averaged 0.23% for the first 3 million tons and 2.2% for the total production up to 1963; it is contained in the uppermost section of the Morrison Formation that was established during the Late Jurassic and lies beneath the Dakota Sandstone (Moench & Schlee, 1967; Wilton, 2017). The Morrison formation is an accumulation of fluvial deposits from a system of braided streams with a northeasterly trend.

Sandstones are common in the area and act as the host material for uranium ore at the Jackpile Mine, with much of the ore content found in carbonaceous matter (Adams et al., 1978; Moench & Schlee, 1967). Sandstone lenses are cemented with calcite, silica, and clays including kaolinite ($Al_2Si_2O_5(OH)_4$); clay content decreases down through the sequence while calcite content increases (Moench & Schlee, 1967; Nash, 1968; Wilton, 2017). Other common minerals in the area are quartz and some feldspars; minor phases include tourmaline, rutile, magnetite, garnet, and sillimanite (Moench & Schlee, 1967). Elements enriched in the ore are vanadium, molybdenum, and selenium (Adams et al., 1978). Uraninite and coffinite are the primary ore minerals found in carbonaceous matter within the sandstone, but in some areas including the South Paguate Pit, oxidized uranium-vanadium minerals tyuyamunite [$Ca(UO_2)_2V_2O_8 \cdot (5\text{-}8)H_2O$] and carnotite [$K_2(UO_2)_2(VO_4)_2 \cdot 3H_2O$] were produced (Moench & Schlee, 1967; Nash, 1968; Wilton, 2017).

Previous analyses of particulate matter from Paguate Church attic containing a legacy of mine dust that has remained untouched since the start of operations at Jackpile was performed by Dr. Adrian Brearley from UNM Department of Earth and Planetary Sciences. His research revealed clusters of nanoparticles consisting of two uranyl vanadate minerals: carnotite and tyuyamunite, which is consistent with local geology. However, the dominant ore

minerals coffinite and uraninite were not found, suggesting only the oxidized minerals are present in the respirable dust fraction and not the reduced minerals. Additionally, U-rich minerals were found only in the smallest size fractions (< $PM_{2.5}$), which is consistent with previous research that has determined that there are enrichments in U and other trace metals in the inhalable size fraction (Brown, 2017; Martin et al., 2016). However, these previous studies did not provide any mineralogical data on the characteristics of the trace metals.

CHAPTER 3 - METHODS

Regional & Local Climate Analyses

Local meteorological stations were deployed at several locations at Laguna Pueblo in April of 2019: Paguate Village, the Mine Yard, Mesita Village, and Old Laguna Village (Fig. 2). The equipment utilized for climate analyses includes 4 Kestrel 5500 Weather Meters, one at each site, and one DustTrak DRX Aerosol Monitor 8535 located at the Paguate Village site. The Kestrel Meters collect local meteorological data at 10-minute intervals; the DustTrak Monitor measures dust mass and size fraction, specifically PM_1, $PM_{2.5}$, PM_4 and PM_{10}, at 10-minute intervals. Models for regional climate utilized in this work are based on North American Regional Reanalysis (NARR) data obtained from the National Oceanic and Atmospheric Administration (NOAA). This NARR model is produced by the National Centers for Environmental Prediction (NCEP) and is derived from several observational datasets across the region that are assimilated to produce the reanalysis model; datasets include radiosondes, surface observations, pilot balloon observations, aircraft temperatures and winds, and satellite data from polar and geostationary satellites. These data provide a long-term picture of weather

over North America from 1979 to present; the daily surface level model uses 3-hour collection intervals. The wind direction and wind speed data from the model represent conditions 10m above the surface; relative humidity data represents 2m above the surface. This model is used for comparison to local meteorological data at Laguna Pueblo to determine accuracy and importance of the local stations. (NCEP Reanalysis data provided by the NOAA/OAR/ESRL PSL, Boulder, Colorado, USA: https://psl.noaa.gov/data/gridded/data.narr.monolevel.html).

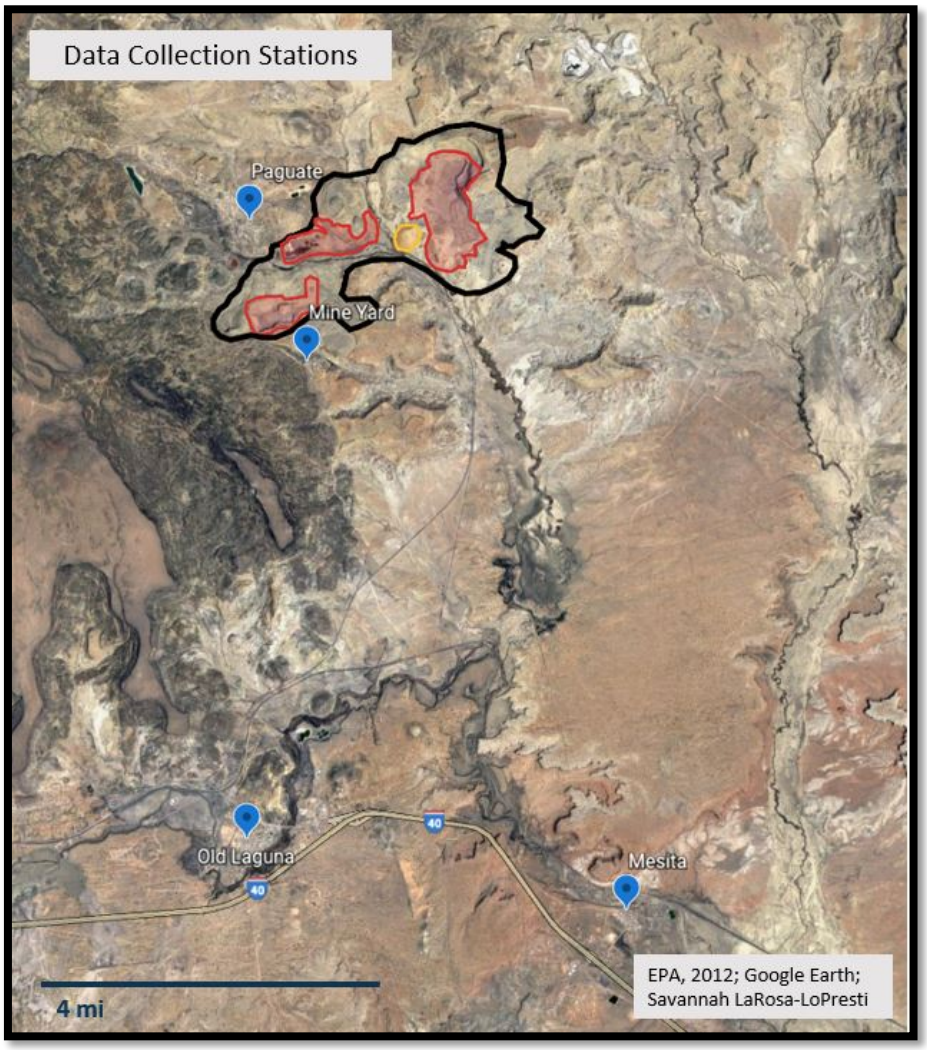

Figure 2: Map of data collection stations at Laguna Pueblo. Image includes the outline of the Jackpile-Paguate Uranium Mine and the 4 blue icons identify the locations of the 4 data collection stations.

Soil Matric Potential

Soil moisture is an important variable controlling soil susceptibility to dust transport. Without direct measurements for soil moisture in this study, it has been estimated using soil matric potential values based on average relative humidity and temperature data from the local meteorological stations. A combination of the Boyle-Charles law (perfect gas law) and the first law of thermodynamics yields the equation for soil matric potential in units of energy per unit mass of water in the soil. It uses directly measured relative humidity and temperature values and is effective when direct measurements of soil moisture cannot be made (Campbell, 2016; Neuman & Sanderson, 2008).

Soil matric potential equation derivation (Campbell, 2016):

The first law of thermodynamics, where dE is energy required to create an infinitesmal volume of water vapor in an adiabatic system, p is pressure, and dV is volume change.

$$dE = -pdV$$

The Boyle-Charles law (perfect gas law), where n is the number of moles, R is the universal gas constant, 8.314 J/mol*K and T is temperature in Kelvin.

$$pV = nRT$$

After rearranging terms and taking the derivative of both sides.

$$dV = -\frac{nRT}{p^2}dp$$

Now this equation is substituted for dV in the first equation.

$$dE = \frac{nRT}{p} dp$$

The equation then becomes the total energy required to go from the vapor pressure of pure water (p_o) to the vapor pressure of water in the soil (p).

$$E = nRT \int_{p_o}^{p} \frac{dp}{p} = nRT \ln\left(\frac{p}{p_o}\right)$$

After dividing both sides by the molar mass of water and reducing terms, the final equation represents the soil matric potential expressed as the energy per unit mass of water in the soil.

$$\boxed{\psi = \frac{RT}{M_w} \ln(h_r)}$$

The ratio of vapor pressure to the saturation vapor pressure is relative humidity, h_r and M_w is the molar mass of water, 18.02 g/mol.

The soil matric potential value is always negative relative to the atmospheric potential in arid conditions where there is an absence of bulk pore water; therefore, the more negative a value is, the lower the pressure potential, indicating less particle cohesion. These conditions favor unsaturated soils in response to local relative humidity (Neuman & Sanders, 2008). Soil matric potential values equal to or close to 0 indicate completely saturated soil. The time period utilized for soil moisture estimations is the meteorological summer (June 1st – August 31st, 2019). This period was selected for this study because there are not currently enough data to

fully analyze other seasons of the year; however, a seasonal approach to estimating soil moisture may be necessary due to the associated changes in temperature and relative humidity. Conditions of highest and lowest relative humidity, as well as the seasonal average relative humidity are used for soil matric potential estimation values. Only the seasonal average temperature value was utilized for these calculations due to the lack of significant dependence of temperature variations on soil moisture (Ravi et al., 2004).

Sample Collection

Particulate matter samples were collected using 2 Tisch High Volume Air Samplers exposed biweekly for 24-hour periods at Old Laguna Village and Mesita Village during 2019 (Fig. 2); however, samples 1013 and 1014 were exposed for 96-hours each. The 8" x 11" polytetrafluoroethylene (PTFE) filters were weighed before and after sample collection (Table 1). Filter numbers 1003 – 1008 were analyzed using microscopy, while samples 1001 – 1015 were analyzed using ICP-MS, excluding sample 1002 which was used as a calibration filter. The air samplers collect particulate matter of all sizes and do not filter for particulates of the inhalable size fraction.

Table 1: Particulate matter samples collected using Tisch High Volume Air Samplers

Filter Number	Pre-Sample Weight (g)	Post-Sample Weight (g)	Total Mass (µg)	Sample Location	Start Date	End Date	Total Time (hrs)	Flow Rate (m^3/min)	Total Volume (m^3)	Concentration (µg/m^3)
1001	2.71575	2.89966	183910	Laguna	5/31/19	6/1/19	23:52	1.139	1631.51	112.723
1002	2.73689	2.83632	99430	Calibration	N/A	N/A	0:00	N/A	N/A	N/A
1003	2.71809	2.92724	209150	Mesita	5/22/19	5/23/19	25:39	1.133	1744.19	119.912
1004	2.63454	2.78277	148230	Mesita	5/31/19	6/1/19	24:00	1.157	1666.4	88.9522
1005	2.7299	2.7703	40400	Laguna	7/25/19	7/26/19	23:36	1.148	1625.1	24.86000
1006	2.79275	2.8396	46850	Mesita	7/25/19	7/26/19	24:35	1.149	1695.93	27.6249
1007	2.69804	2.75595	57910	Laguna	8/28/19	8/29/19	23:35	1.153	1631.05	35.5047
1008	2.69941	2.7635	64090	Mesita	8/28/19	8/29/19	24:15	1.155	1680.77	38.1313
1009	2.72579	2.78362	57830	Mesita	7/10/19	7/11/19	24:44	1.151	1708.52	33.8480
1010	2.67731	2.74825	70940	Laguna	7/10/19	7/11/19	24:39	1.154	1707.39	41.5487
1011	2.672	2.69615	24150	Laguna	11/8/19	11/9/19	24:30	1.117	1642.55	14.7027
1012	2.68325	2.72829	45040	Mesita	11/8/19	11/9/19	24:30	1.126	1655.78	27.2016
1013	2.7154	2.77835	62950	Laguna	11/26/19	11/30/19	96:00	1.103	6350.97	9.91187
1014	2.7693	2.8226	53300	Mesita	11/26/19	11/30/19	96:00	1.108	6379.72	8.35459
1015	2.7168	2.77875	61950	Laguna	12/11/19	12/12/19	24:15	1.111	1616.96	38.3126

Mineralogical Analyses

The particulate matter was imaged with second and backscattered electron imaging using a FEI Quanta 3D Field Emission Gun (FEG) Scanning Electron Microscope (SEM) in the Department of Earth and Planetary Sciences at the University of New Mexico. This instrument is equipped with an EDAX GENESIS EDS system fitted with an Apollo 40 mm2 SDD EDS detector. Secondary electron imaging provides information about the surface characteristics of the sample, while backscattered electron imaging provides qualitative information on the chemistry of the materials that are being imaged. Energy Dispersive X-ray Spectrometry (EDS) was used to perform X-ray microanalysis on sample particulate matter to determine mineralogic composition. Sample preparation for SEM analyses involved a filter agitation process by which particulate matter in the smaller size fraction were selected for; the overall abundance of metal-bearing particulates was not determined from this. A detailed procedure for sample preparation of the filters for microscopy can be found in APPENDIX I. Once prepared,

samples were analyzed under the microscope using the backscattered electron detector (BSED) to identify mineral particulates with high atomic numbers, specifically uranium. The SEM was operated at an accelerating voltage of 30 kV in analytical mode, using a beam current of 8-16 nA, providing high X-ray count rates for EDS analysis; conditions were adjusted during image production to lower beam currents and accelerating voltages to produce higher quality images and to better assess particulate morphology. A random observation method was used to identify particles on the filter pieces, where 10-15 areas selected at random were observed on each filter piece before moving on to the next filter. The samples analyzed using SEM are from filters 1003, 1004, 1006, and 1008 (Mesita Village), and 1005 and 1007 (Old Laguna Village).

Analysis of Toxic Metal Concentrations

Concentrations of toxic metals and several other elements were analyzed using Inductively Coupled Plasma Mass Spectrometry (ICP-MS). Sample preparation included acid digestion of samples using HF, HCl and HNO_3. A detailed procedure for sample preparation of filter sections for ICP-MS analyses utilized in this research can be found in APPENDIX II. The samples used for analysis are from filters 1001-1015, excluding 1002 which was a calibration filter and was not used for analyses. Triplicate sample sets were used for analysis with ICP-MS, consisting of 3 sections of the same filter for each sample, i.e., sample B1-1001 is from the same filter as B2-1001 and D1-1001. Bar graphs in this study showing sample sets 1, 2 and 3 refer to samples from filter sections B1, B2 and D1, respectively (APPENDIX II). The elements analyzed were U, V, As, Pb, Co, Cd, Cu, Ti, Cr, Mn, Ni, Mo, Ba, Sr, Sn, Li, La, Ce, and Zn.

The absolute concentration values for each element were unable to be directly determined; therefore, this research utilizes normalized ratio values. Elemental ratios to both titanium (Ti) and chromium (Cr) were calculated. These elements were chosen, because Ti, in particular, is considered to be relatively immobile in rocks and soils that have undergone a variety of geochemical processes. The normalization process involved calculating the ratio of each element over Ti (or Cr) divided by the same ratio based on crustal averages. The normalized ratio for Ti/Cr was also analyzed for accuracy to crustal average values and was relatively consistent, confirming that these are valid ratioing elements for normalization. The Ti/Cr normalized plot allows for an estimation of the absolute concentrations of U, V, As and Pb that were calculated based on the crustal average value for Ti, which is 5560 ppm (Table 7).

Limitations & Assumptions

Due to COVID-19 restrictions and resulting setbacks to data collection and equipment site access, this research resulted in a smaller portion of meteorological data collection than originally proposed. Therefore, the time-period utilized for meteorological data collection is April 2019 to November 2019. Researchers were unable to move equipment between sample stations for data collection from each site, resulting in dust mass and size fraction data from just 1 performance site, rather than the 4 sites originally planned and particulate matter samples from 2 of 4 planned sites. Procedures for sample preparation for ICP-MS analysis of toxic metal concentrations in particulate matter samples collected from Laguna Pueblo are still in the process of being developed for accurate results after repeated, supervised attempts to determine absolute elemental concentrations; as a result, this research utilizes normalized elemental ratio

values for analyses, rather than absolute concentrations. Estimates of absolute concentrations are made based on crustal average values for Ti.

CHAPTER 4- RESULTS

Regional & Local Climate

The meteorological parameter identified as being most important in controlling dust transport of respirable particulate matter is relative humidity, especially as it relates to soil moisture and subsequent susceptibility of respirable particulate matter to windblown transport. Wind speed may also be an important parameter influencing dust transport in the region. Correlation between the 4 local stations was determined for relative humidity ($R^2 = 0.86$), temperature ($R^2 = 0.84$), wind direction ($R^2 = 0.36$), and wind speed ($R^2 = 0.41$) all with statistically significant *p*-values ≤ 0.05 (Fig. 3-6). While relative humidity and temperature values do not vary greatly between the local stations, wind direction and speed both show a weak correlation between the 4 local stations, indicating greater variation in these variables across the landscape. Local meteorological station data from Laguna Pueblo were compared with NARR model data for relative humidity, wind direction and wind speed. The NARR model area used for this study includes 4 grid squares that cover the region of Laguna Pueblo that encompasses the 4 local stations (Fig. 7). All figures derived from this model are selectively confined to the area outlined in red.

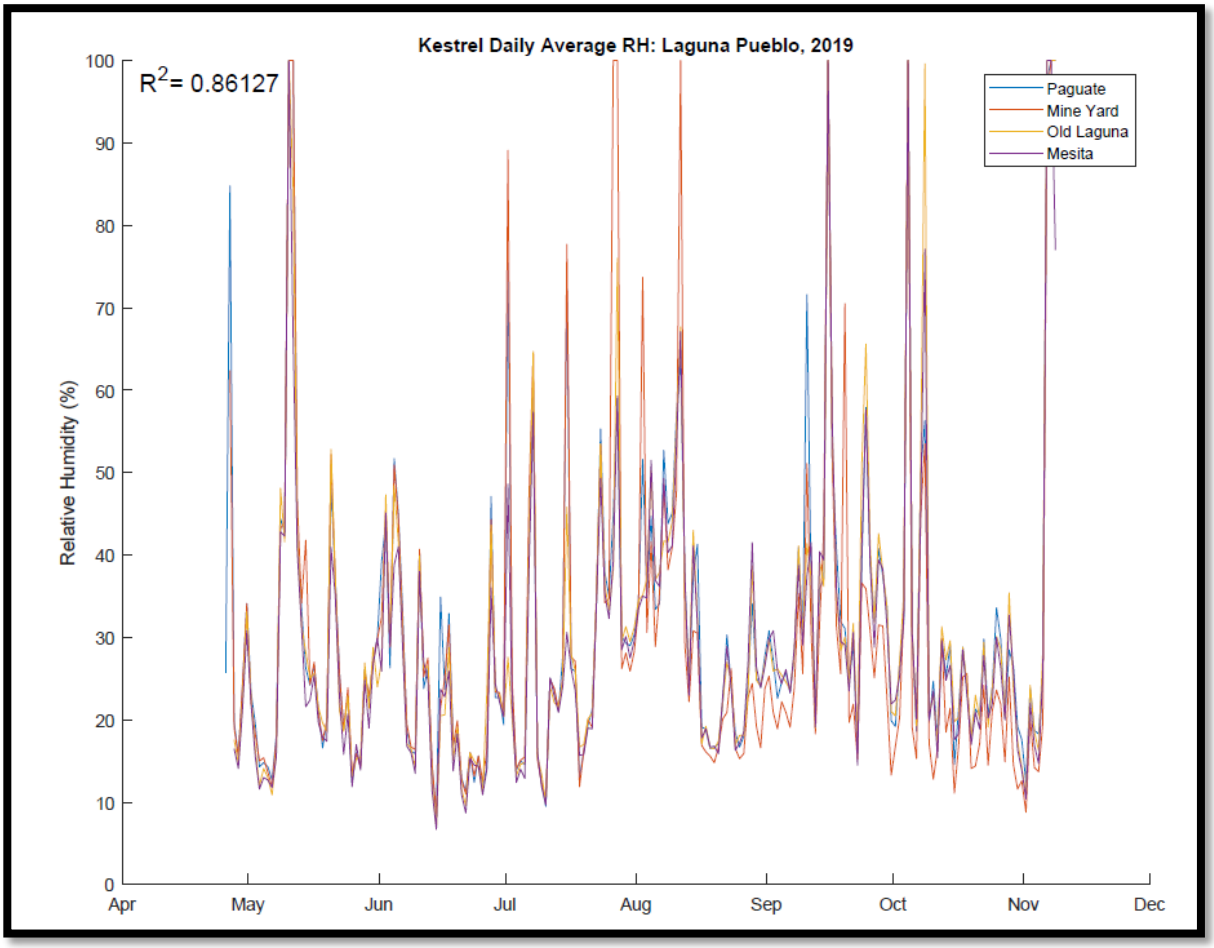

Figure 3: Daily average correlation of relative humidity from all Kestrel meters at Laguna Pueblo. The x-axis shows months of data collection during 2019 and the y-axis is relative humidity in %. Correlation between the 4 sites is statistically significant (p-value ≤ 0.05).

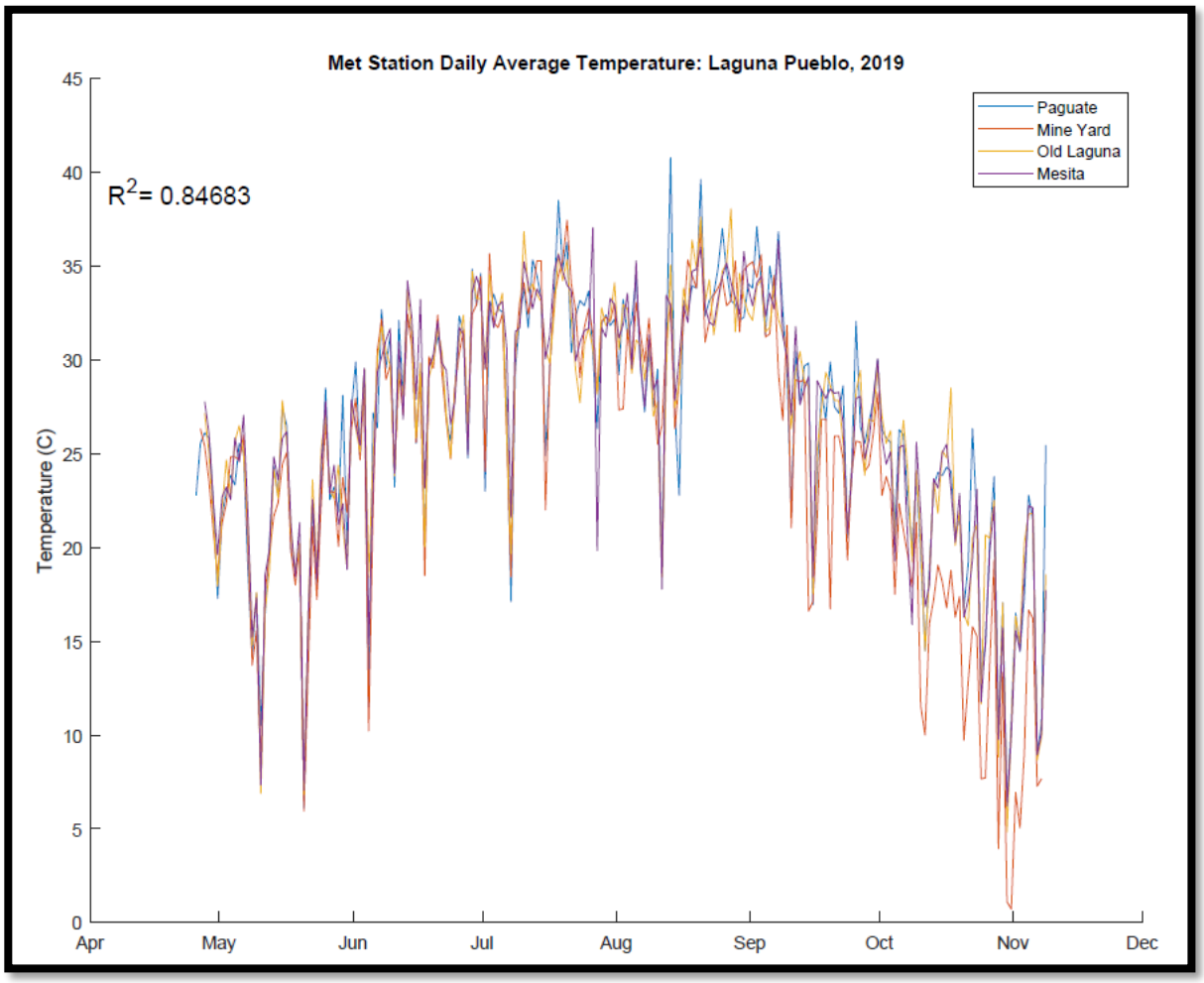

Figure 4: Daily average correlation of temperature from all Kestrel meters at Laguna Pueblo. The x-axis shows months of data collection in 2019 and the y-axis is temperature in °C. Correlation between the 4 sites is statistically significant (p-value ≤0.05).

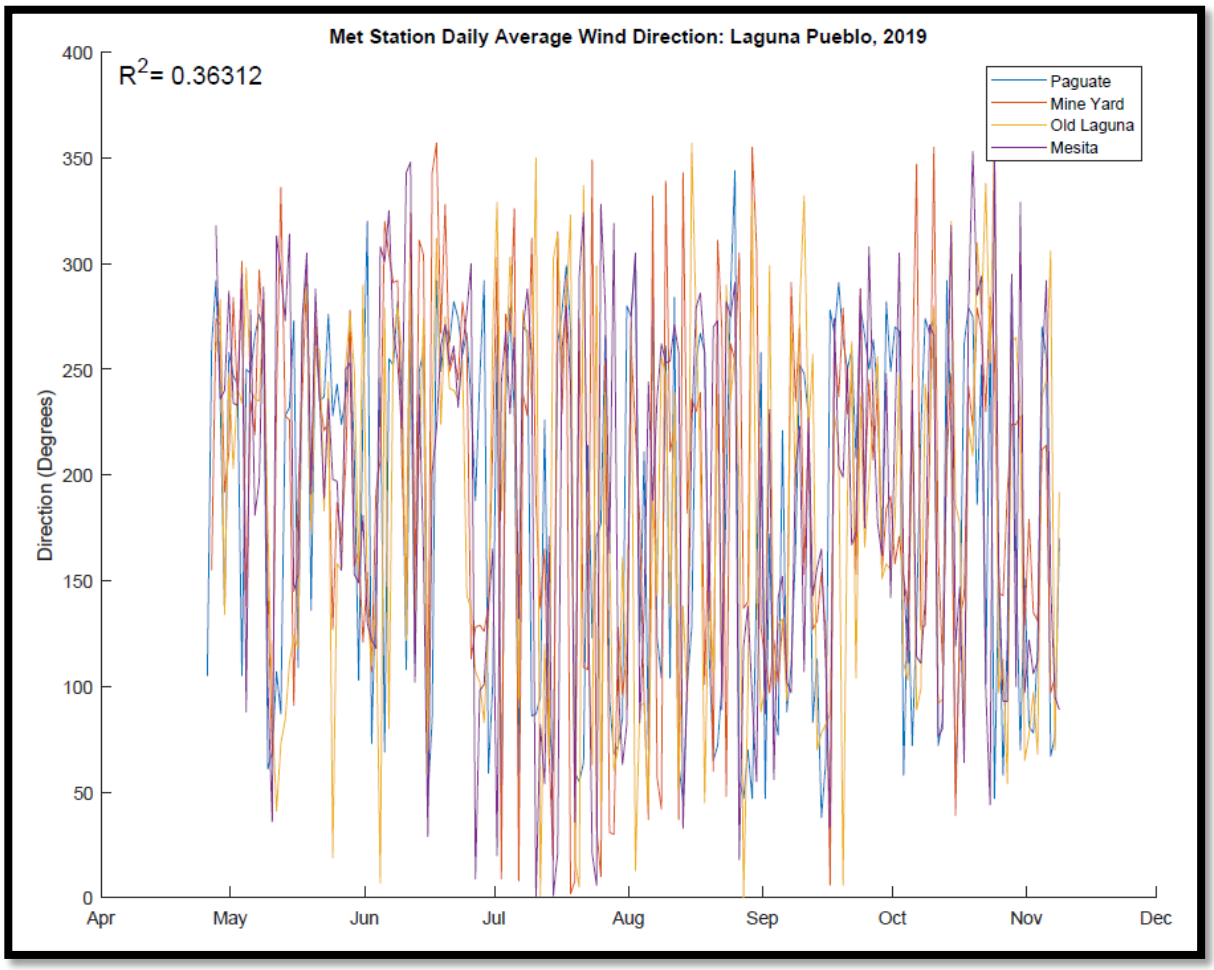

Figure 5: Daily average correlation of wind direction from all Kestrel meters at Laguna Pueblo. The x-axis shows months of data collection in 2019 and the y-axis is wind direction in degrees. Correlation between the 4 sites is statistically significant (p-value ≤ 0.05).

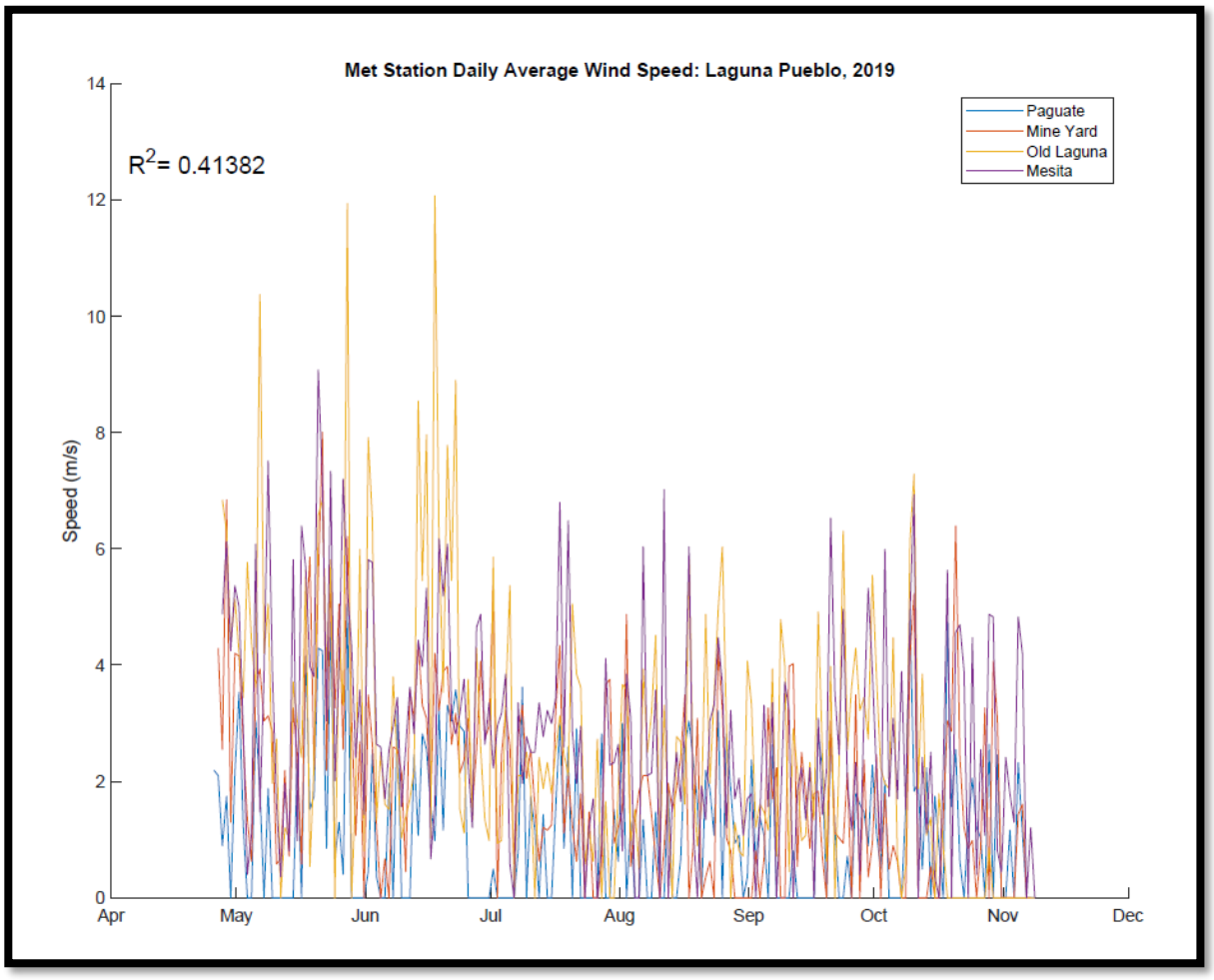

Figure 6: Daily average correlation of wind speed from all Kestrel meters at Laguna Pueblo. The x-axis shows months of data collection in 2019 and the y-axis is wind speed in m/s. Correlation between the 4 sites is statistically significant (p-value ≤ 0.05).

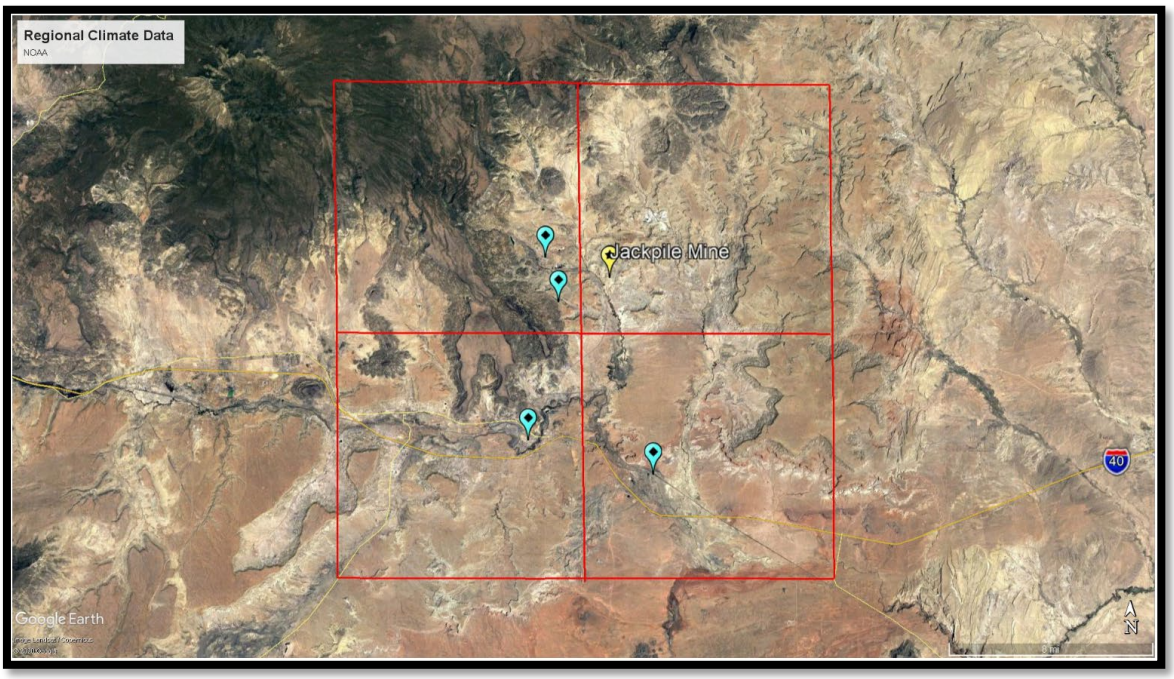

Figure 7: Map of NARR grid area used for analyses outlined in red. The 4 blue icons represent the local meteorological stations, and the yellow icon represents the location of the Jackpile Mine. All NARR model data in the following figures are selectively confined to this area.

Particulate Matter Concentrations

The daily average particulate matter concentration at Paguate village is compared to the annual National Ambient Air Quality Standards (NAAQS) due to the health risks associated with elevated $PM_{2.5}$ despite the presence or absence of toxic metal mixtures. The average annual NAAQS for $PM_{2.5}$ is 15 $\mu g/m^3$ and the average at Paguate Village exceeds this value at 21 $\mu g/m^3$ for a similar period (Fig. 8). The 24-hour NAAQS for $PM_{2.5}$ is 35 $\mu g/m^3$ and there are 6 days at Paguate Village that exceed this value. Due to the lack of data beyond the period from April 2019 to November 2019, seasonal variations and patterns were unable to be addressed. There may be significant changes throughout the year, and the particulate matter concentrations observed from Paguate Village indicate higher concentrations for summer and fall months, and possibly lower concentrations during winter months.

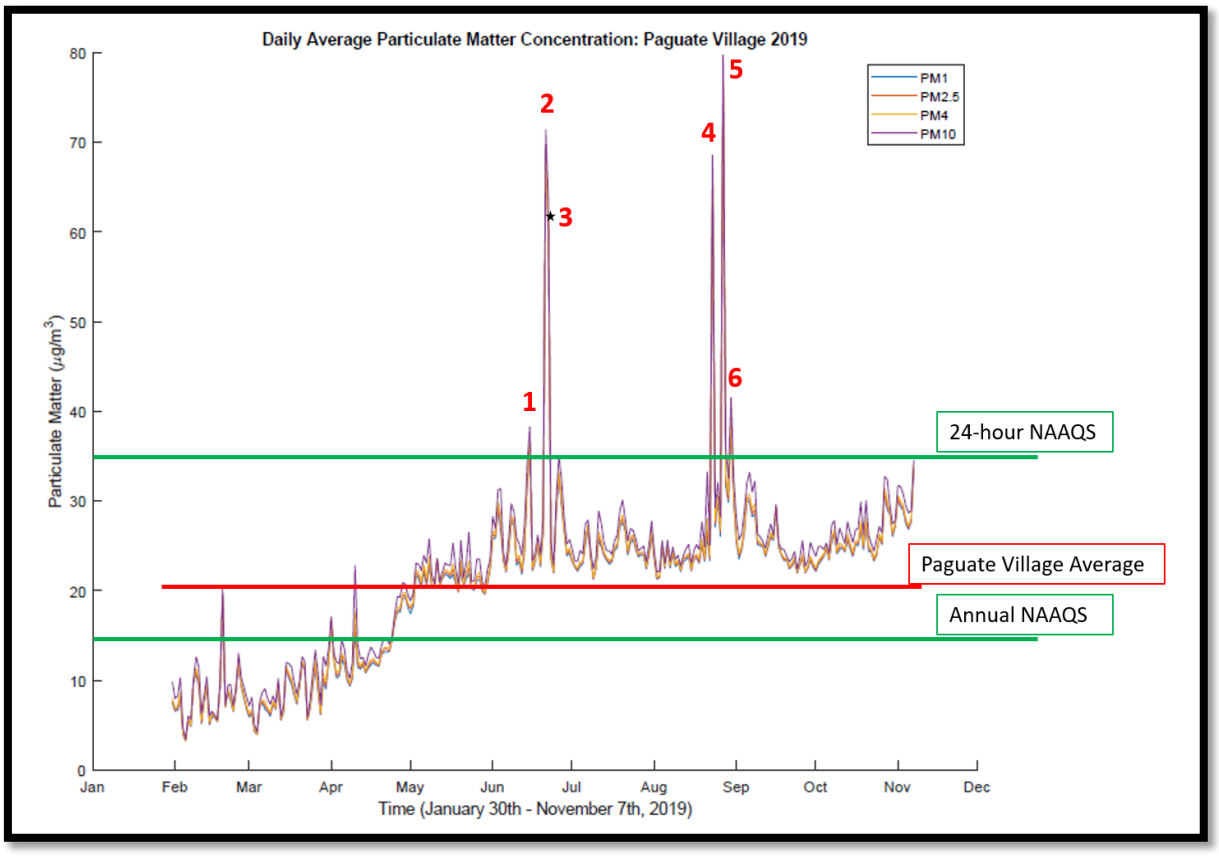

Figure 8: Daily average particulate matter concentrations at Paguate Village. Particulate matter data include sizes PM_1, $PM_{2.5}$, PM_4, and PM_{10}. The 6 days exceeding the NAAQS are numbered. The green lines indicate 24-hour and annual NAAQS; the red line indicates the annual average PM at Paguate Village.

The meteorological conditions for days that exceed the 24-hour NAAQS have been evaluated to determine which parameters are most significant (Table 2). Relative humidity values are consistently at or below 35%, while temperature values are between 30-38 °C. Wind speeds are generally low, not exceeding the overall average of 2.3 m/s, and the wind direction is variable. Time of day may also be a factor influencing particulate matter concentrations. The most frequent time of day associated with higher $PM_{2.5}$ concentrations is from about hour 20 to hour 5; that is, 8pm-5am (Fig. 10).

Table 2: Daily average meteorological conditions for days with high particulate matter concentrations.

High PM Days	1	2	3	4	5	6
$PM_{2.5}$ Concentration	36 µg/m^3	69 µg/m^3	60 µg/m^3	66 µg/m^3	77 µg/m^3	39 µg/m^3
Relative Humidity	8%	14%	12%	35%	20%	27%
Temperature	31°C	31°C	30°C	32°C	38°C	34°C
Wind Speed	2.3 m/s	1 m/s	1.5 m/s	3.3 m/s	0.2 m/s	0.2 m/s
Wind Direction	W	W	W	NE	SW	SE

Relative Humidity & Soil Moisture

When compared with $PM_{2.5}$ concentrations, daily averages exceeding the 24-hour NAAQS are consistently ≤35% relative humidity (Fig. 9-11). The daily average relative humidity averaged from all 4 stations at Laguna Pueblo for the duration of data collection is 31%, with a maximum value of 100% and a minimum value of 8%. Soil matric potential values were calculated using maximum, average, and minimum relative humidity values calculated from the local meteorological station at Paguate Village (Table 3), resulting in 3 values for matric potential at Laguna. The maximum value is 0 J/g, consistent with what is expected to be a precipitation event resulting in saturated soil at 100% atmospheric humidity. The average value is then -144.9 J/g and the minimum value is -371 J/g, indicating unsaturated soils in both cases with low matric potential and dry soils during periods of low relative humidity ≤31% based on the data used to make these calculations. Average low relative humidity ≤35% at Laguna is consistent with soil matric potential studies that have determined the development of a water layer between particles is prevented without higher atmospheric humidity, leaving soil more susceptible to windblown transport. The findings of this study support this information, in

which low relative humidity is consistent with higher particulate matter concentrations of the inhalable size fraction, likely due to the atmospheric conditions preventing the formation of aggregate particles. A threshold may exist for relative humidity ≤35% as it relates to dust transport of respirable particulate matter; however, this is based on the limited dataset provided in this research. Relative humidity conditions above this threshold allow for stronger interparticle cohesion and the development of aggregates that are more difficult to entrain by wind. Particle size, shape, and density should also be considered as factors that influence entrainment by wind; dust particles tend to have larger interparticle cohesive forces than larger particles, making them less likely to be directly lifted by wind (Kok et al., 2012).

Table 3: Soil matric potential estimation values. A temperature average of 297K was used for each.

	Relative Humidity	**Soil Matric Potential**
Maximum	100%	0 J/g
Average	35%	-144.9 J/g
Minimum	6.7%	-371 J/g

Climatic comparisons between the NARR model and local meteorological data were made to determine the importance of maintaining local data collection sites at Laguna Pueblo. The local data have more instances of extreme values for relative humidity compared to the NARR model (Fig. 12) but are generally consistent otherwise with a strong positive correlation (p-value <0.05). The average relative humidity for 2019 from the NARR model is 38% with a low of 12% and a high of 90%. The model for monthly average and long-term monthly average

relative humidity both indicate decreasing values from January to June, then increasing values through August consistent with local monsoon season, and slight increases into December at a slower rate (Fig. 13-14). The local stations provide valuable meteorological data that is not captured by the regional climate model; they are a useful tool in the eventual development of a local warning system for high particulate matter conditions in the inhalable size fraction.

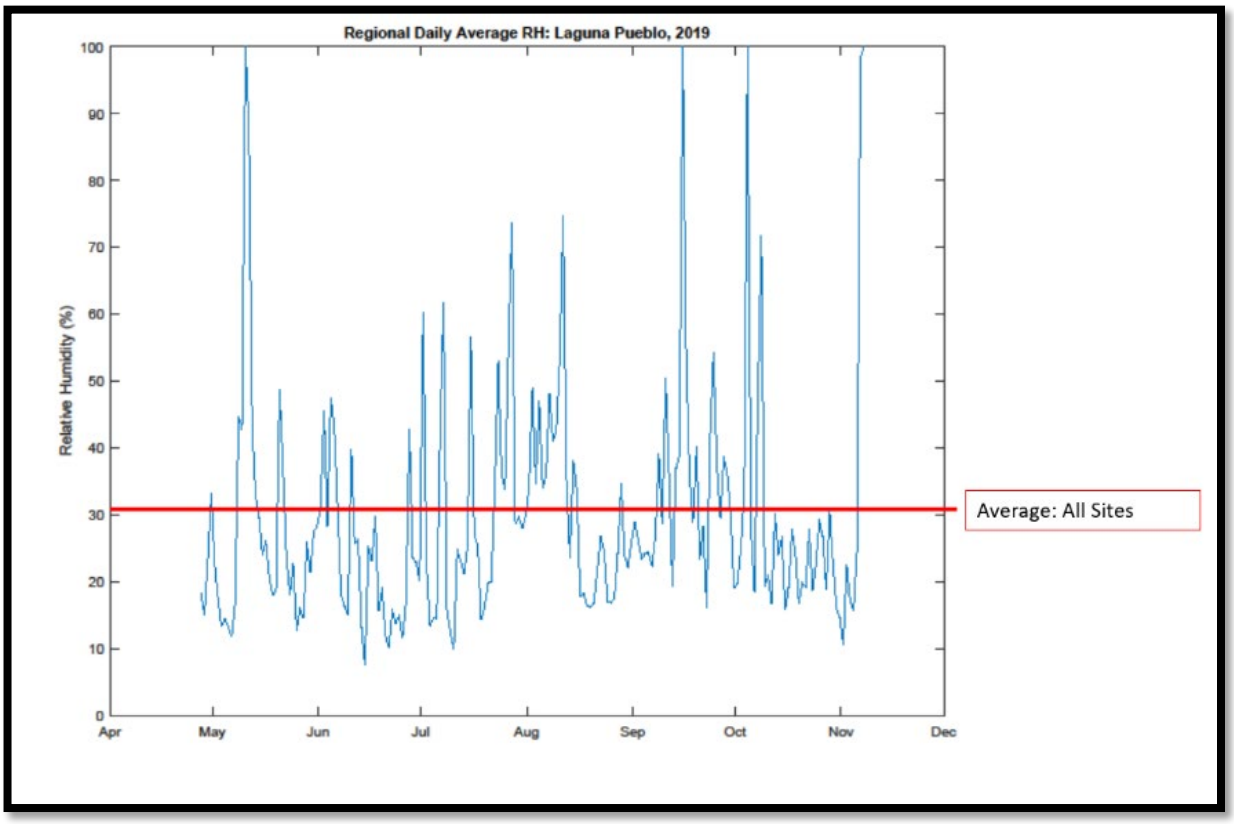

Figure 9: Daily average relative humidity at Laguna Pueblo based on 10-minute data collection intervals averaged from all 4 Kestrel meters. The red line indicates the total average of the dataset; the average daily relative humidity at Laguna Pueblo is 31% for this period.

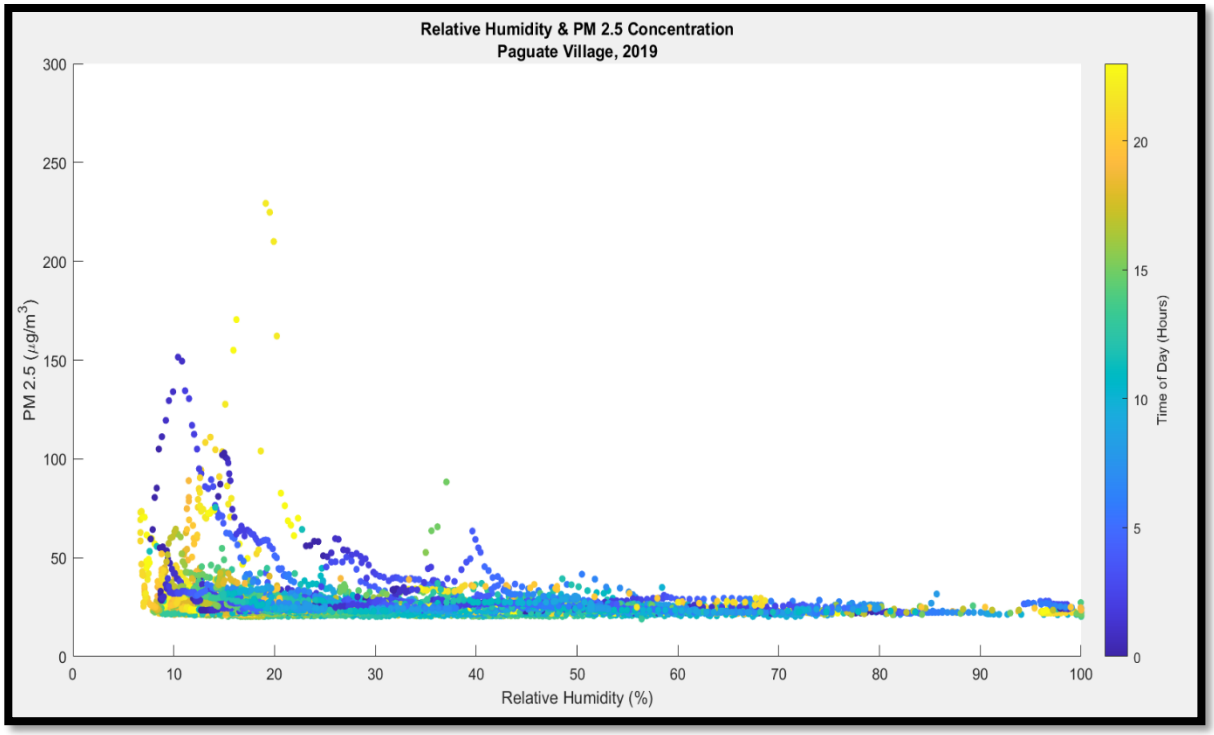

Figure 10: Raw data for $PM_{2.5}$ concentrations and relative humidity at Paguate Village collected at 10-minute intervals from April – November of 2019. The color bar indicates the time of day in hours. The most frequent time of day associated with higher PM concentrations is from about hour 20 (bright yellow) to hour 5 (dark blue); that is, 8pm-5am.

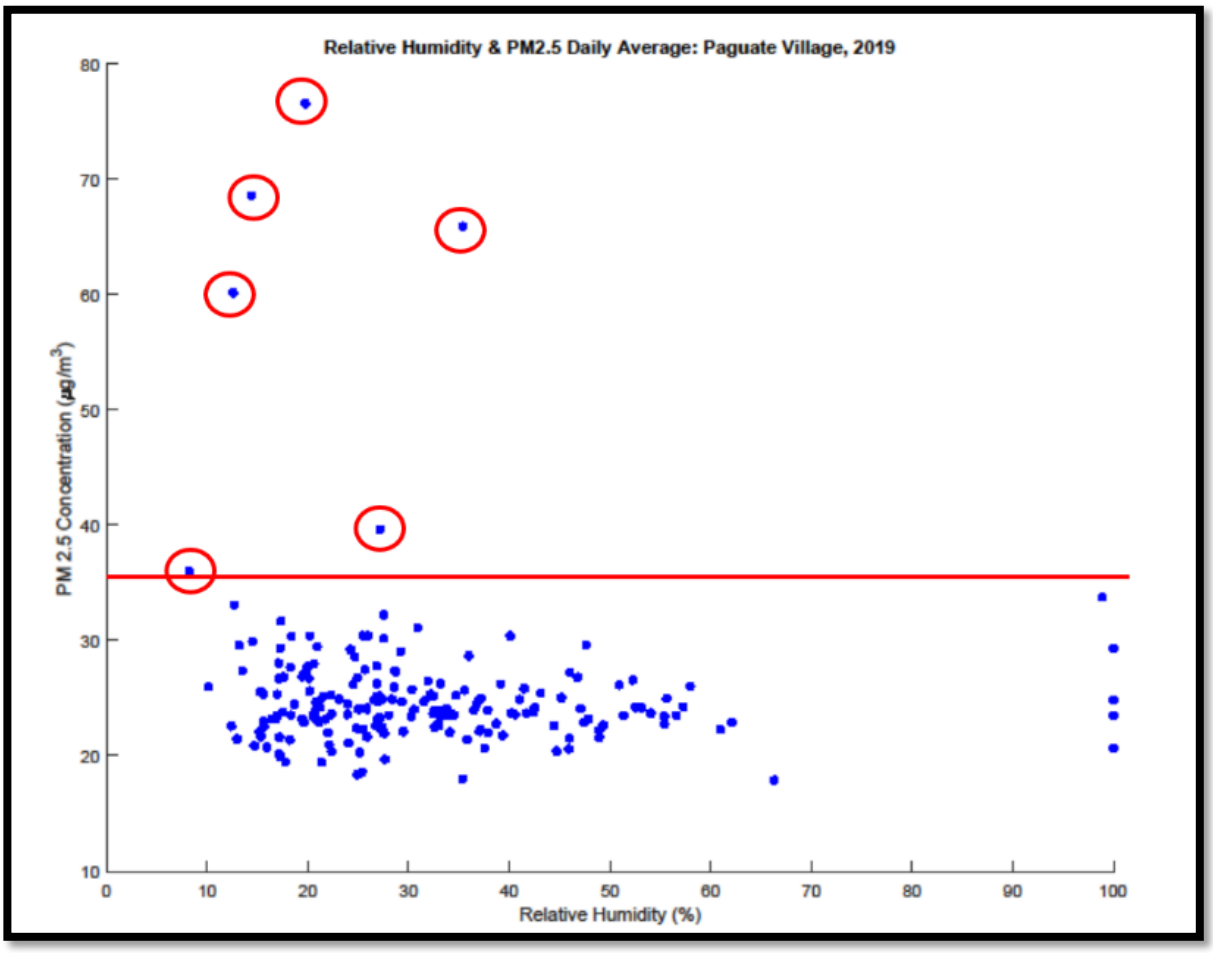

Figure 11: Daily average relative humidity and $PM_{2.5}$ concentrations at Laguna Pueblo. The red line indicates the 24-hour NAAQS; the datapoints circled in red indicate the 6 days with higher $PM_{2.5}$ concentrations exceeding this value. Each of the concentrations exceeding the NAAQS is associated with ≤35% relative humidity.

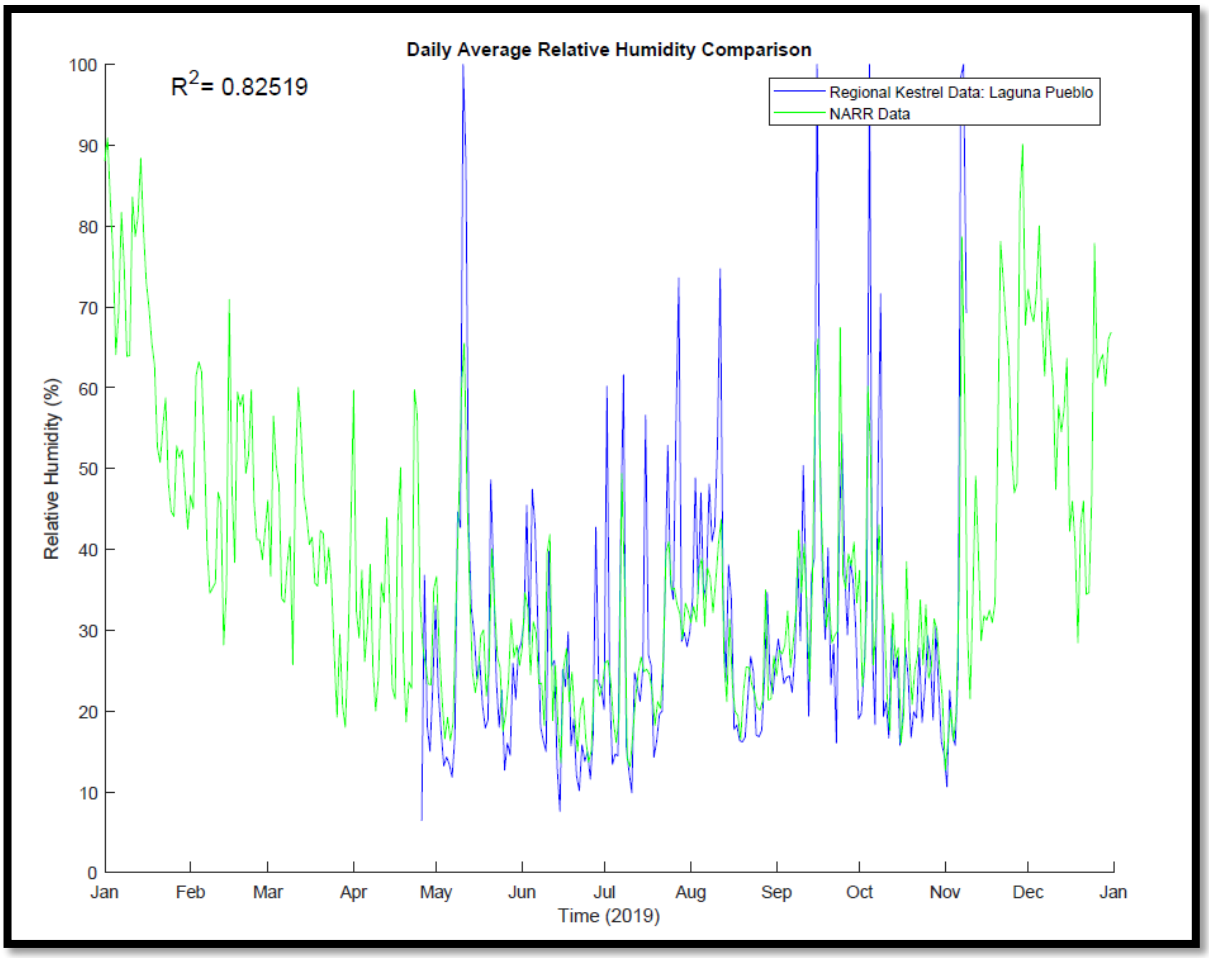

Figure 12: Relative humidity daily average comparison of NARR model (green) and the average of the 4 local meteorological stations (blue). Correlation is statistically significant (p-value ≤ 0.05).

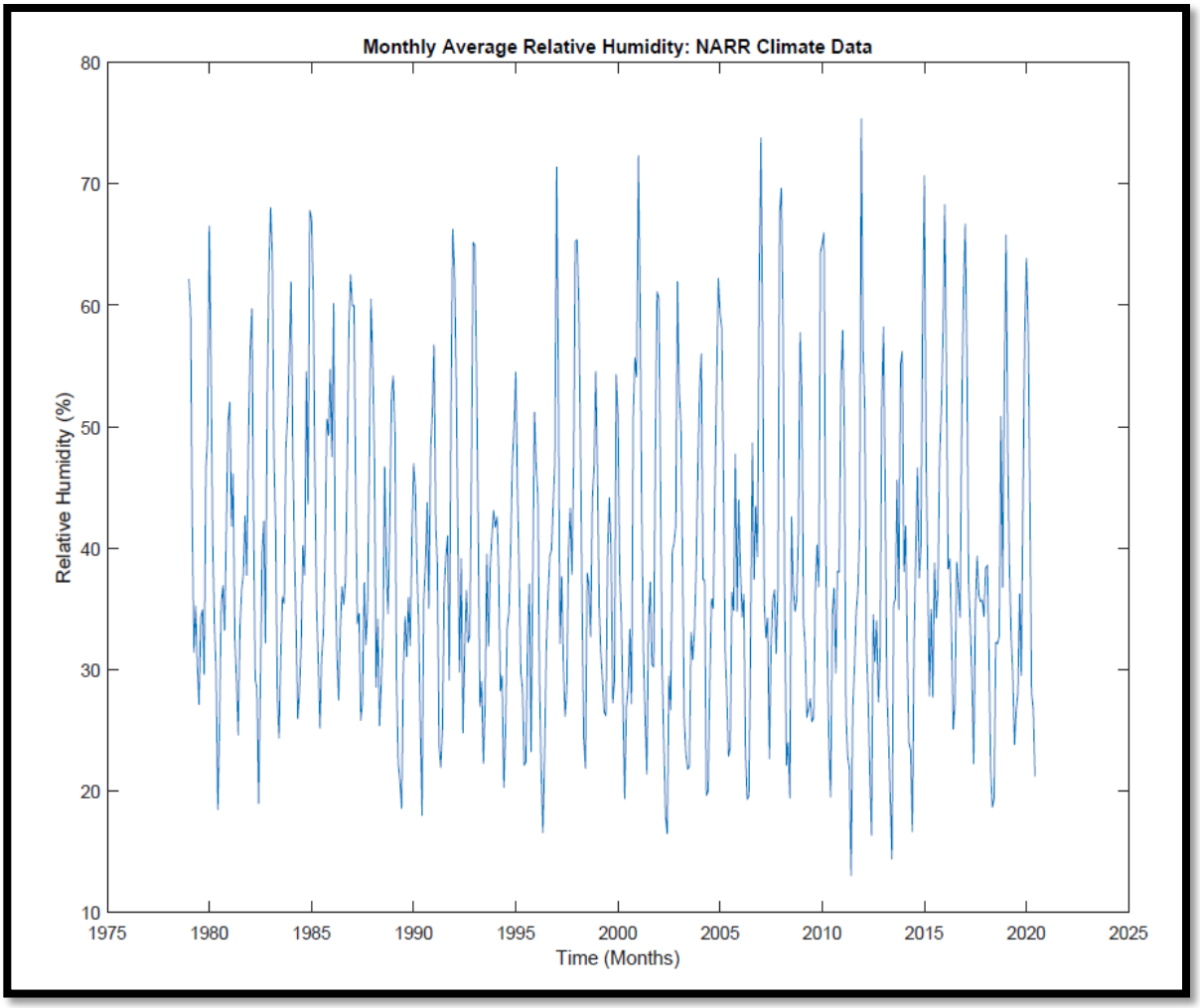

Figure 13: NARR model monthly average relative humidity. Monthly data for the model are from 1979 to 2020 at 2m above the surface.

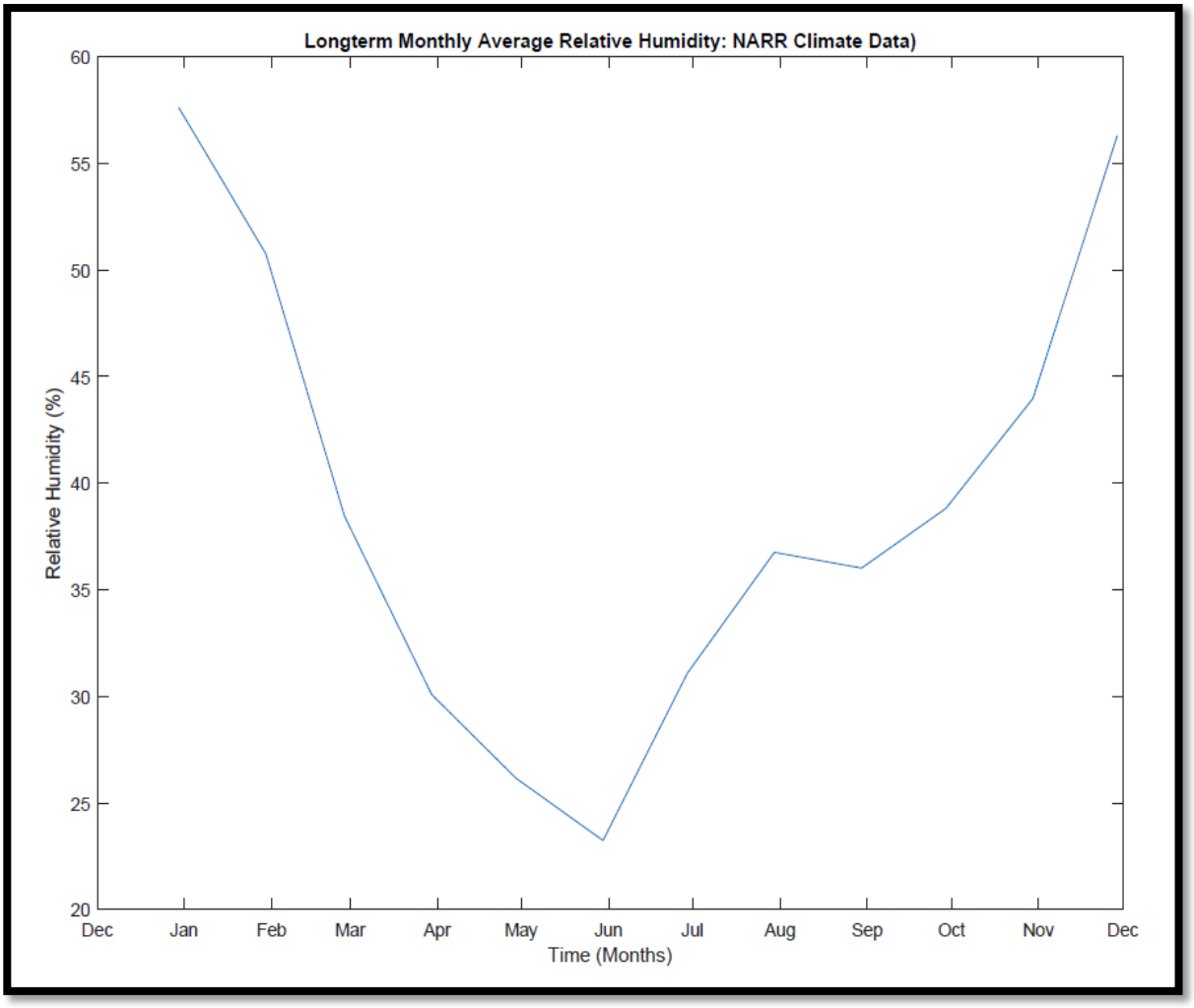

Figure 14: NARR model long-term monthly average relative humidity. Data for the model are from 1979 to 2000 at 2m above the surface. The data show averages for the months over this time period.

Wind Direction & Speed

The wind direction at Laguna Pueblo is dominantly from the west; however, there is some variation between the daily averages from the regional climate model and the local meteorological stations. The NARR model monthly average and long-term monthly average wind rose diagrams have a dominant westerly wind direction with top speeds of 4.5-5 m/s and 2.6-2.8 m/s, respectively (Fig. 15). The monthly average model is a collection of monthly means from 1979 to 2020 at 10m above the surface; the long-term monthly average model is from 1979 to 2000, representing the mean for each month at 10m above the surface. The daily average wind direction and speed are compared between the NARR model and an average of the 4 sites at Laguna Pueblo (Fig. 16). The dominant wind direction from the NARR model is W-NW with top speeds of 8-9 m/s, while the main wind direction from the local stations is W-SW with top speeds of 7-8 m/s. There is a weak correlation for both wind direction and wind speed between the NARR model and the local stations (Fig. 17); wind direction has a weaker correlation than wind speed. Significant differences between these two sources highlight the importance of the local stations as a result of highly variable local topography that characterizes the area. Individual local stations compared to single grid square areas from the NARR model encompassing each station further support these disparities and emphasize the advantage of maintaining local stations for wind direction and wind speed data collection (Fig. 18-20). Additionally, there is significant variation in wind direction and speed between each local station due to the local topography, likely due to the natural geomorphology of the area, as well as the anthropogenic influences on the landscape caused by the mining and reclamation processes. The dominant wind direction at Paguate Village is W; at the Mine Yard the

dominant direction is SW-SE; at Mesita Village the dominant direction is W-NW, with a significant portion of the data showing SW-SE wind as well; at Old Laguna Village the dominant wind direction is SW.

a.

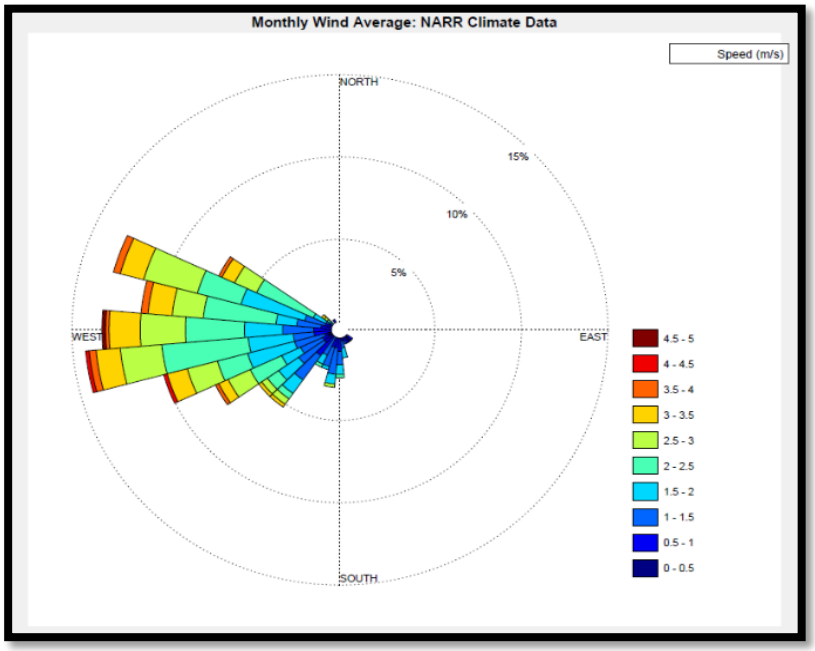

b.

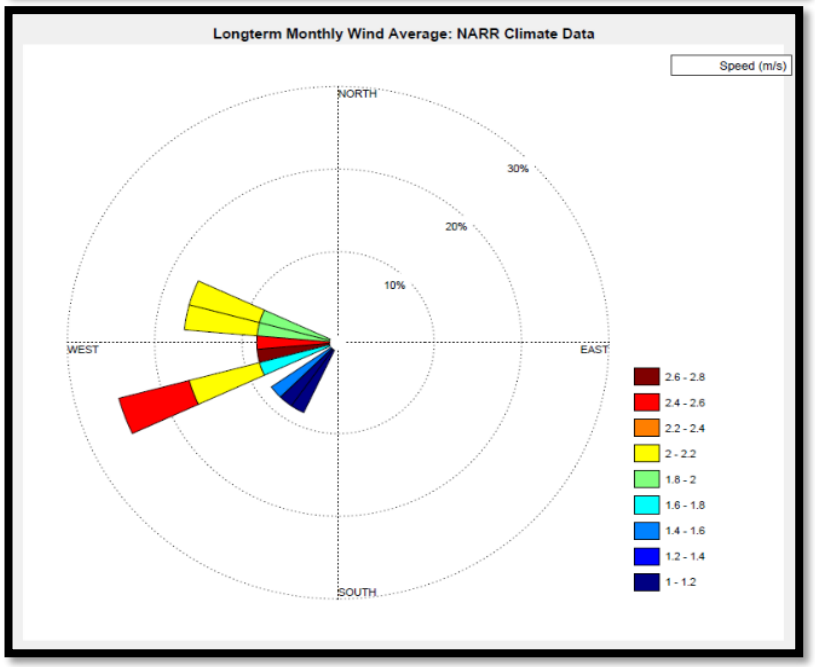

Figure 15: NARR data monthly average (a) and long-term monthly average (b) wind direction and wind speed. Data for the monthly average model are from 1979 to 2020 at 10m above the surface; data for the long-term monthly average are from 1979 to 2000 representing the mean for each month at 10m above the surface.

a.

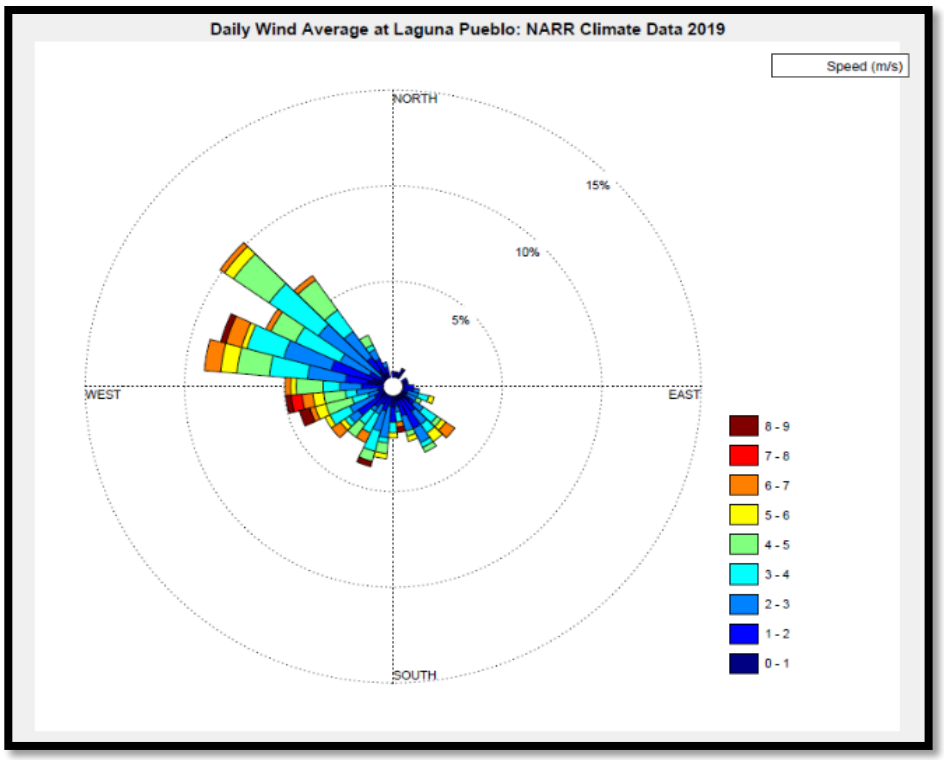

b.

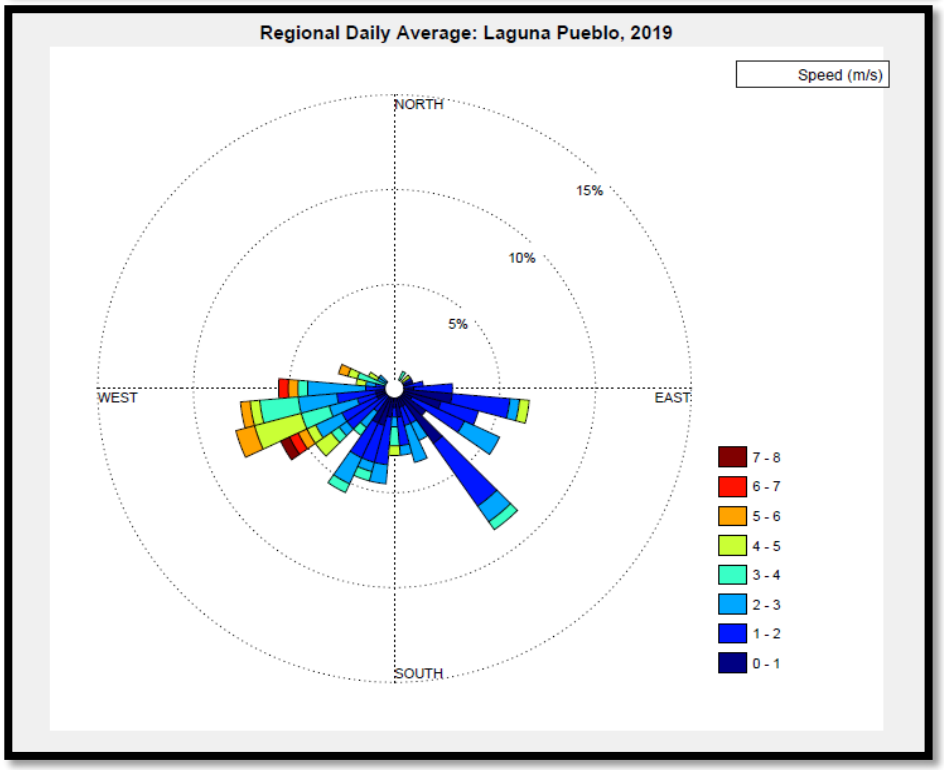

Figure 16: Wind rose diagrams for daily average wind direction and speed from NARR model (a) and the average of the 4 local meteorological stations (b).

a.

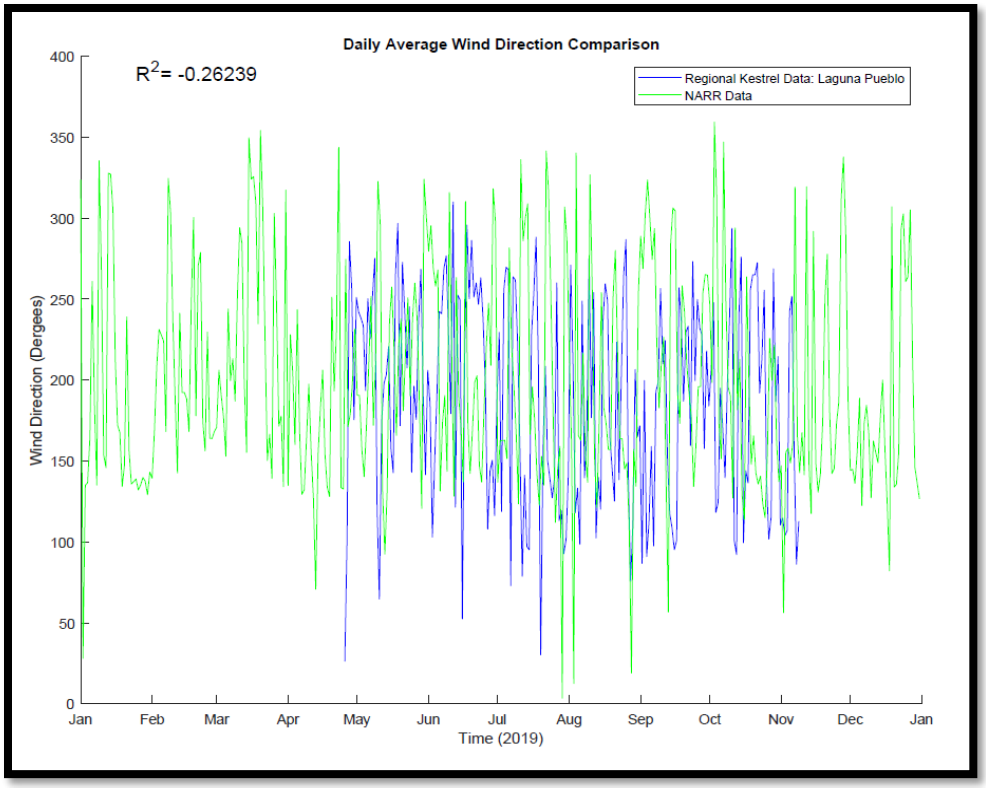

b.

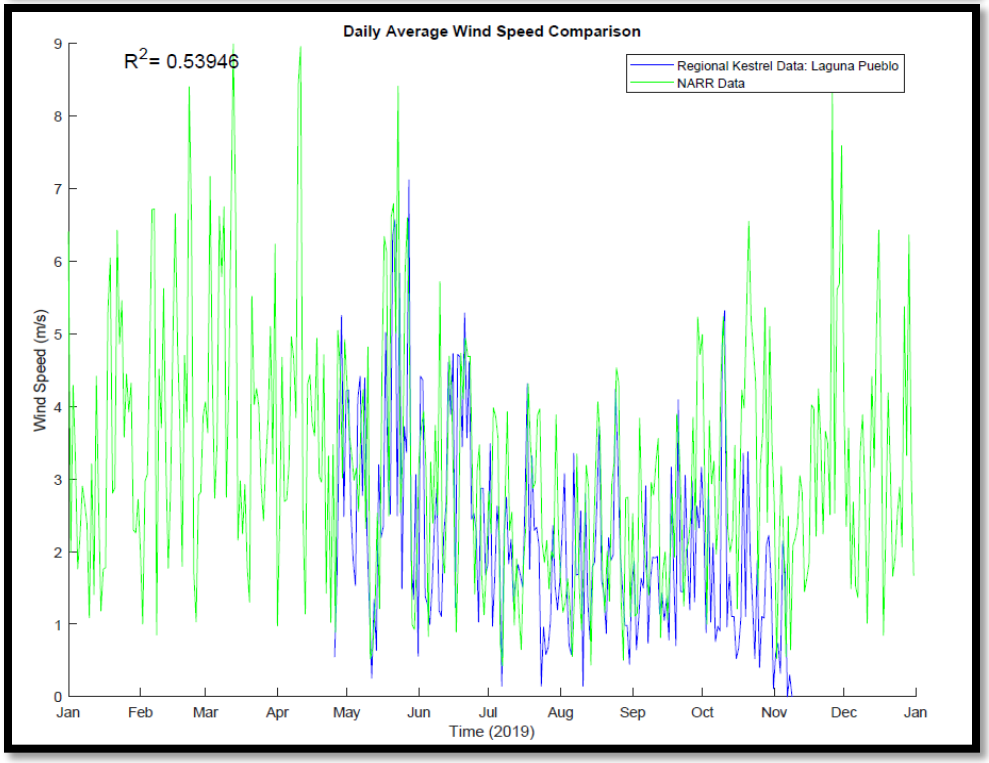

Figure 17: Daily average correlations for wind direction (a) and speed (b) from the NARR model (green) and the average of the 4 local meteorological stations (blue). The model represents data at 10m above the surface; the local data are collected at ~1m above the surface. Correlation for both plots have a statistically significant *p*-value ≤0.05.

a.

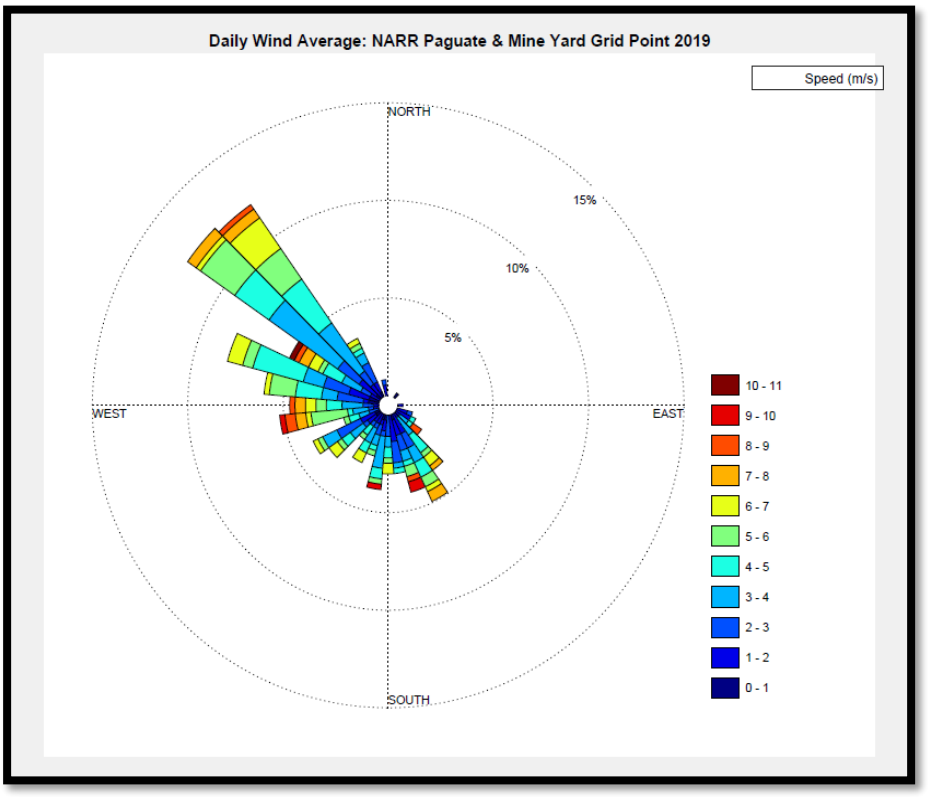
Daily Wind Average: NARR Paguate & Mine Yard Grid Point 2019
Speed (m/s)
NORTH
15%
10%
5%
WEST
EAST
SOUTH
10 - 11
9 - 10
8 - 9
7 - 8
6 - 7
5 - 6
4 - 5
3 - 4
2 - 3
1 - 2
0 - 1

b.

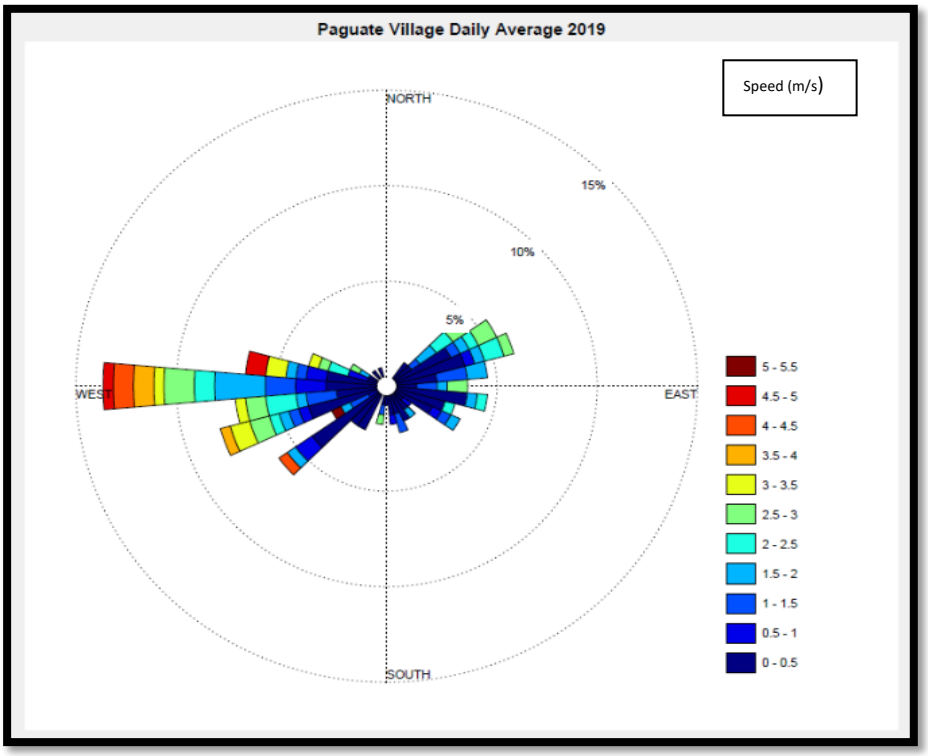
Paguate Village Daily Average 2019
Speed (m/s)
NORTH
15%
10%
5%
WEST
EAST
SOUTH
5 - 5.5
4.5 - 5
4 - 4.5
3.5 - 4
3 - 3.5
2.5 - 3
2 - 2.5
1.5 - 2
1 - 1.5
0.5 - 1
0 - 0.5

c.

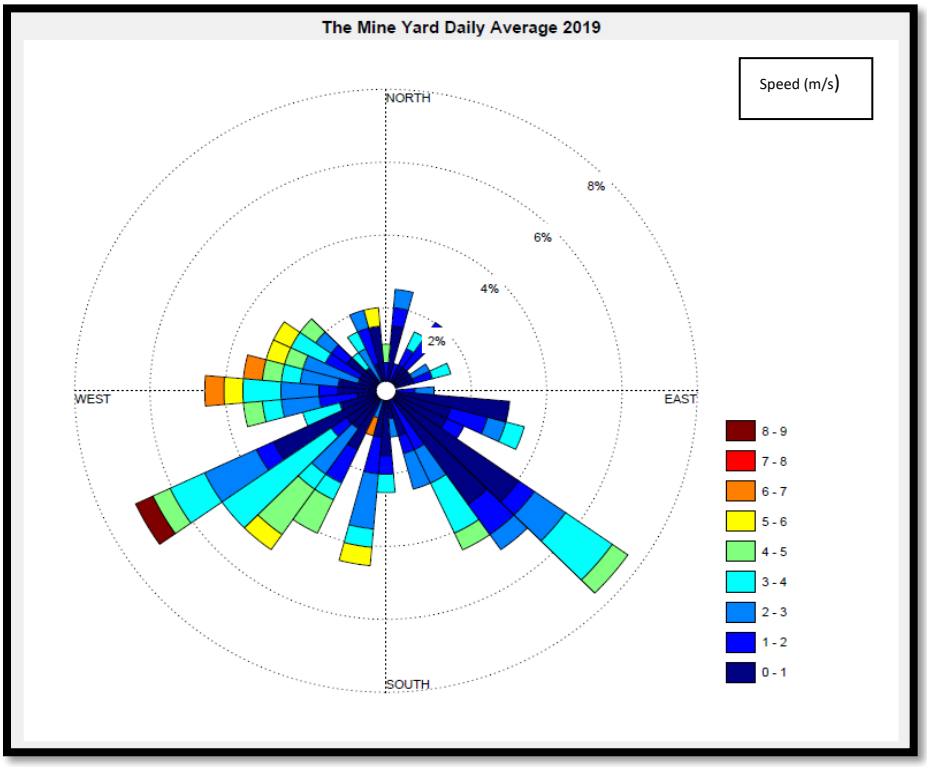

Figure 18: Wind rose diagrams from NARR model (a) and local meteorological stations at Paguate Village (b) and the Mine Yard (c). The NARR model utilizes a single grid square that encompasses both the local Paguate Village station and the Mine Yard station.

a.

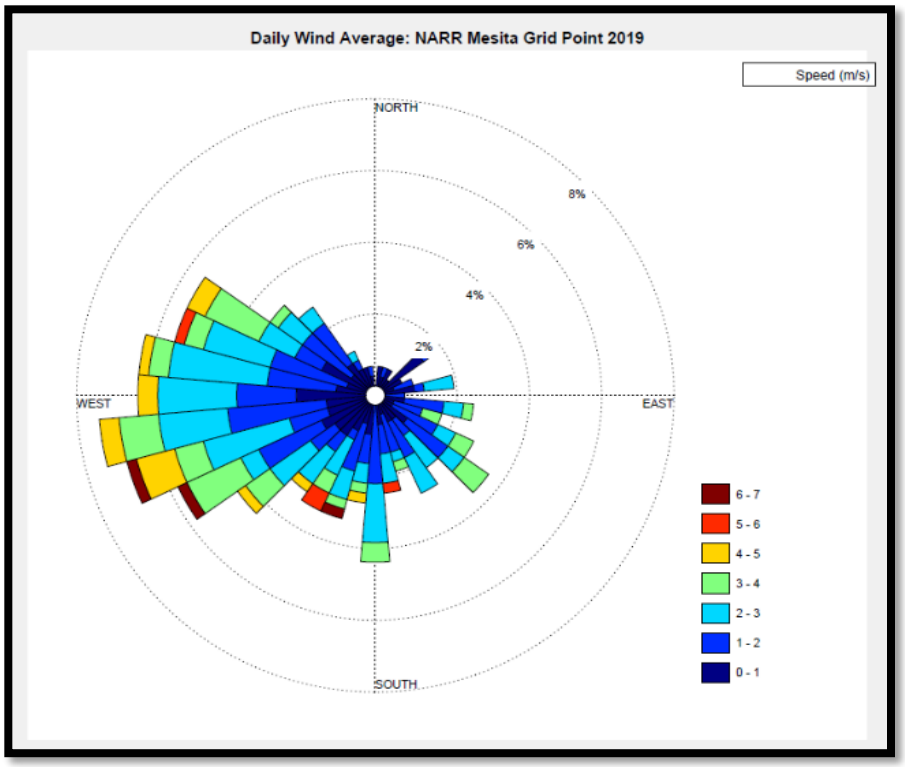

b.

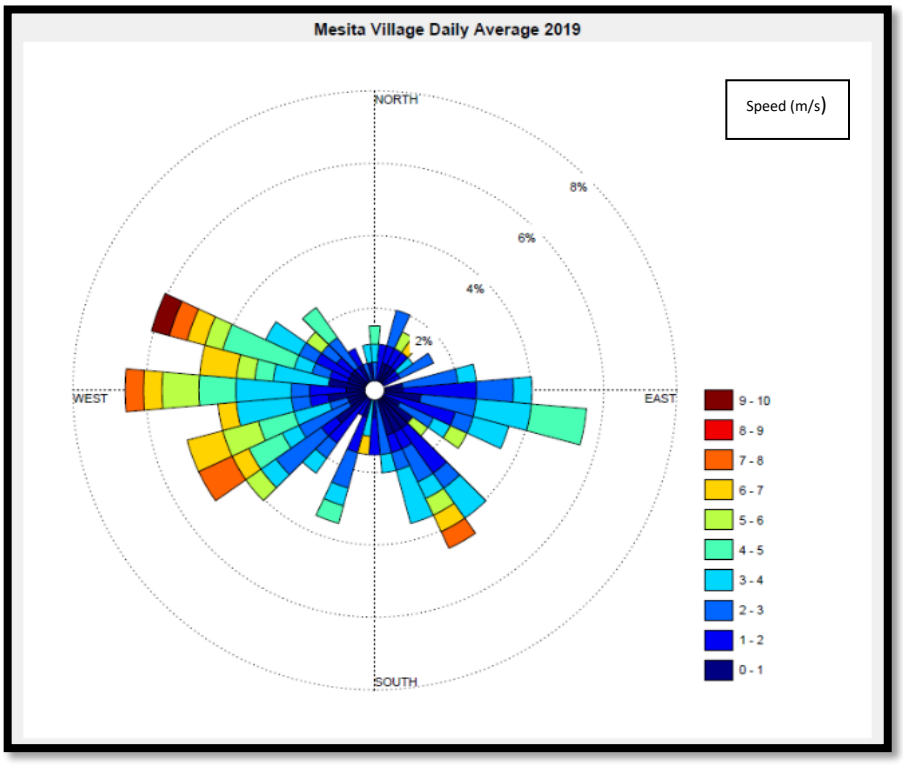

Figure 19: Wind rose diagrams from NARR model (a) and the local meteorological station at Mesita Village (b). The NARR model utilizes a single grid square that encompasses the local station at Mesita Village.

a.

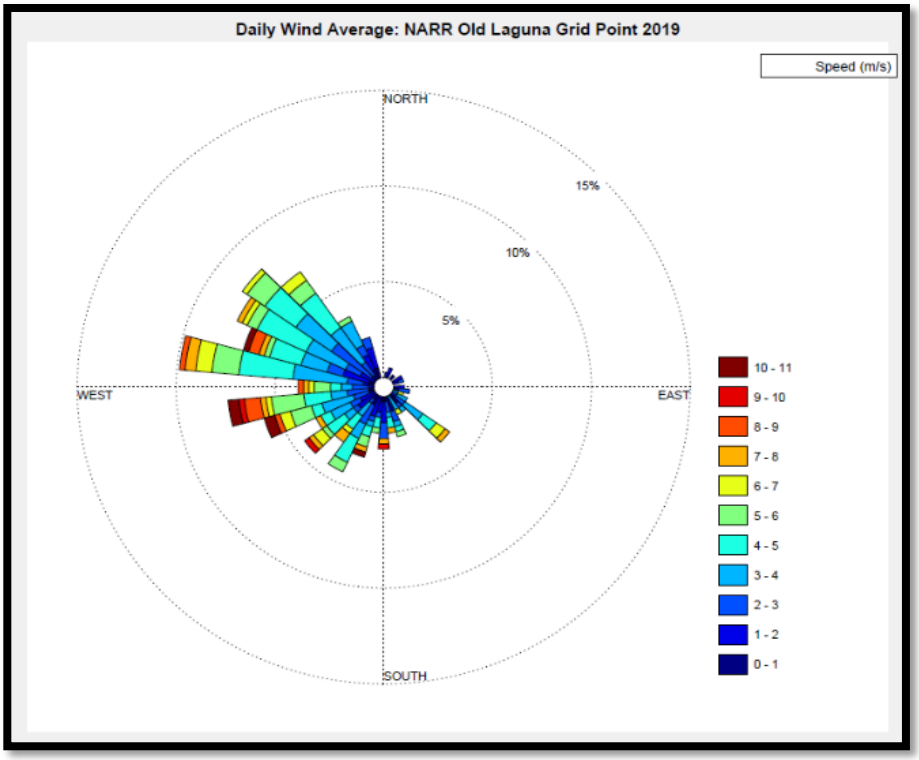

b.

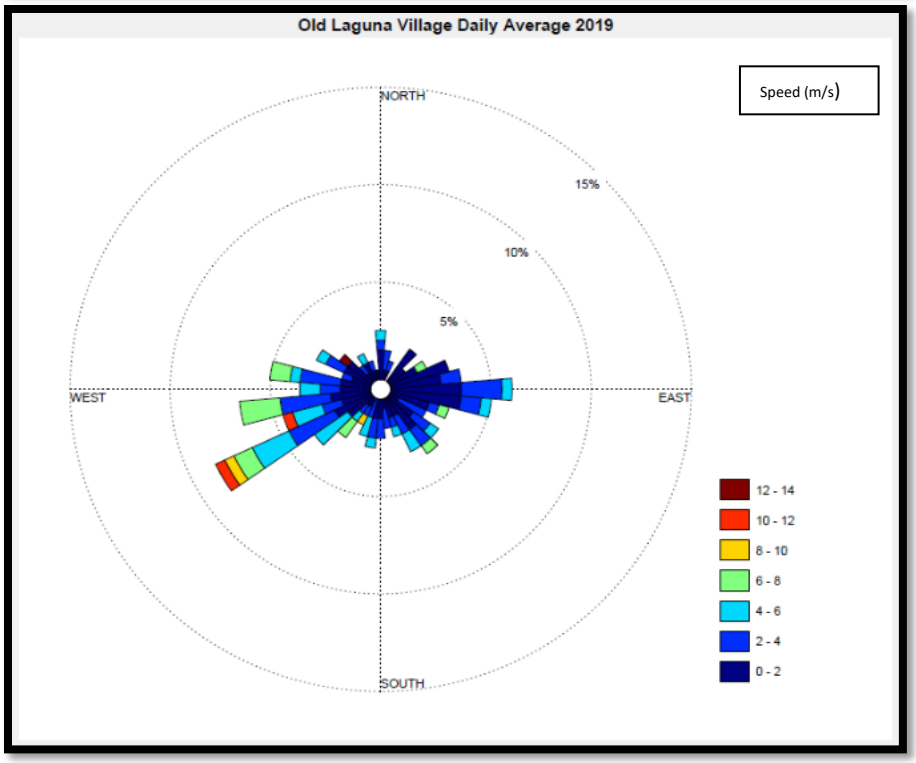

Figure 20: Wind rose diagrams from NARR model (a) and the local meteorological station at Old Laguna Village (b). The NARR model utilizes a single grid square that encompasses the local station at Old Laguna Village.

Wind blowing from the direction of the Jackpile Mine toward Pueblo of Laguna villages was calculated as a percent of the total dataset from both the NARR model and the local meteorological stations (Fig. 21-24). In 2019, the percent of wind moving from the Jackpile Mine toward Paguate Village was 33% based on the NARR model and 49% based on the local station data. The percent of wind moving from the Jackpile to the Mine Yard station was 16% based on the NARR model and 18% based on the local station data. For Mesita Village, the NARR model indicated 6% while the local data indicated 8%. At Old Laguna Village, the NARR model shows 1% of the wind coming from the Jackpile and the local station data shows 8%. Generally, the dominant westerly wind direction is not moving from the mine toward the villages; however, Paguate Village is most exposed to dust transport directly from the mine with about half of the wind moving from the Jackpile. This is also likely due to the proximity of the station, and ultimately Paguate Village, to the mine area. These data provide quantitative information on the potential for transport of airborne particulate matter moving from the Jackpile Mine toward local and populated areas at Laguna Pueblo and suggest which areas may be most exposed to dust transport.

The average wind speed at Laguna Pueblo is 2.13 m/s based on an average of the 4 local meteorological stations. There is very little correlation between wind speeds and respirable particulate matter concentrations; however, slow wind speeds may be more conducive to higher airborne concentrations, but more data collection is necessary to fully evaluate this effect (Fig. 25-26). A relationship between wind speed and relative humidity, as these parameters relate to higher particulate matter concentrations, is also of interest but the data available do not show a significant correlation (Fig. 27). A seasonal effect may also be

present and could be evaluated with a larger dataset. The presence of high $PM_{2.5}$ concentrations during periods of no wind (0 m/s) can likely be attributed to findings from previous studies that suggest the residence time of fine particulate matter ≤20 µm is around 1-2 weeks in the atmosphere after initial suspension. Particulate matter lofted into the atmosphere during climatic events such as local dust storms may potentially linger for an extended period, resulting in the data observed.

a.

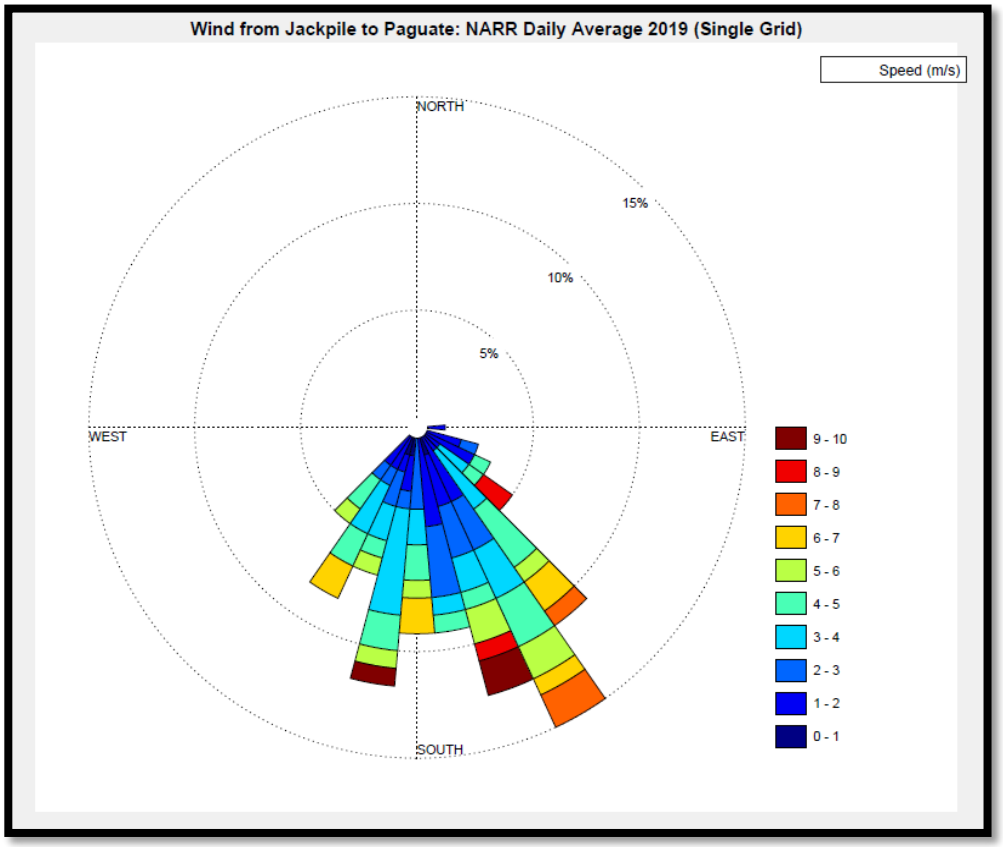

b.

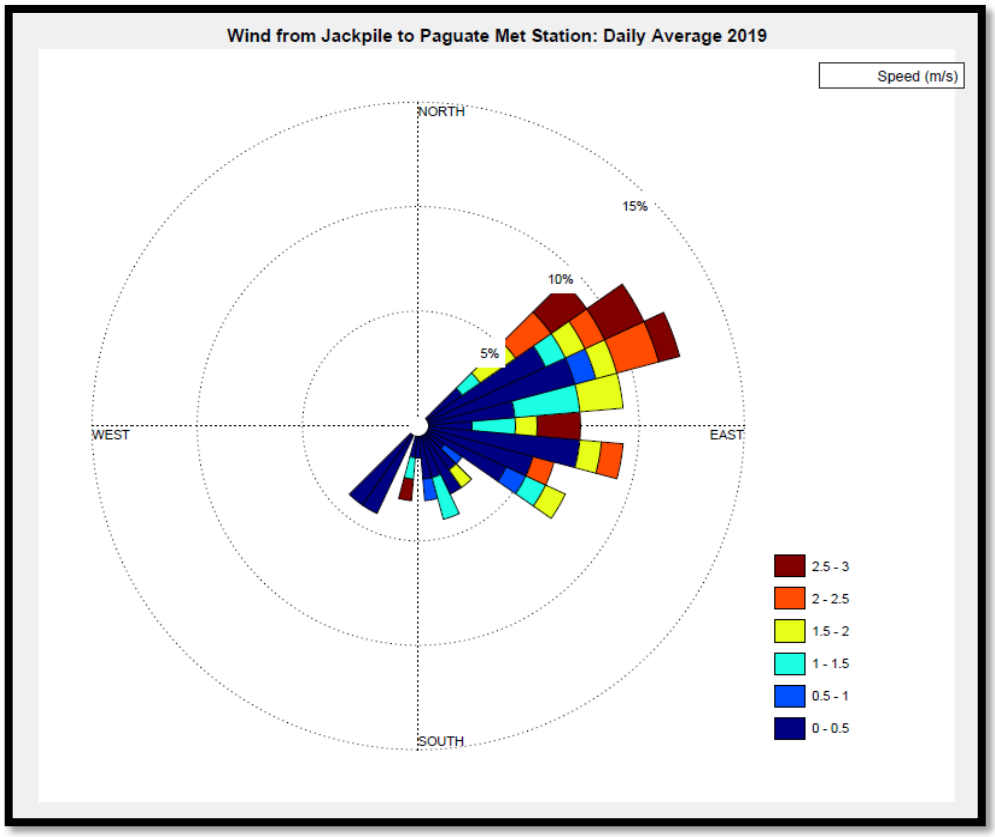

Figure 21: The percent of wind from the Jackpile Mine toward Paguate Village in 2019. The NARR model (a) and the local meteorological station (b) are compared. The NARR model is derived from a single grid square encompassing Paguate Village with 33% of the total wind moving this direction; the local meteorological station shows 49%

a.

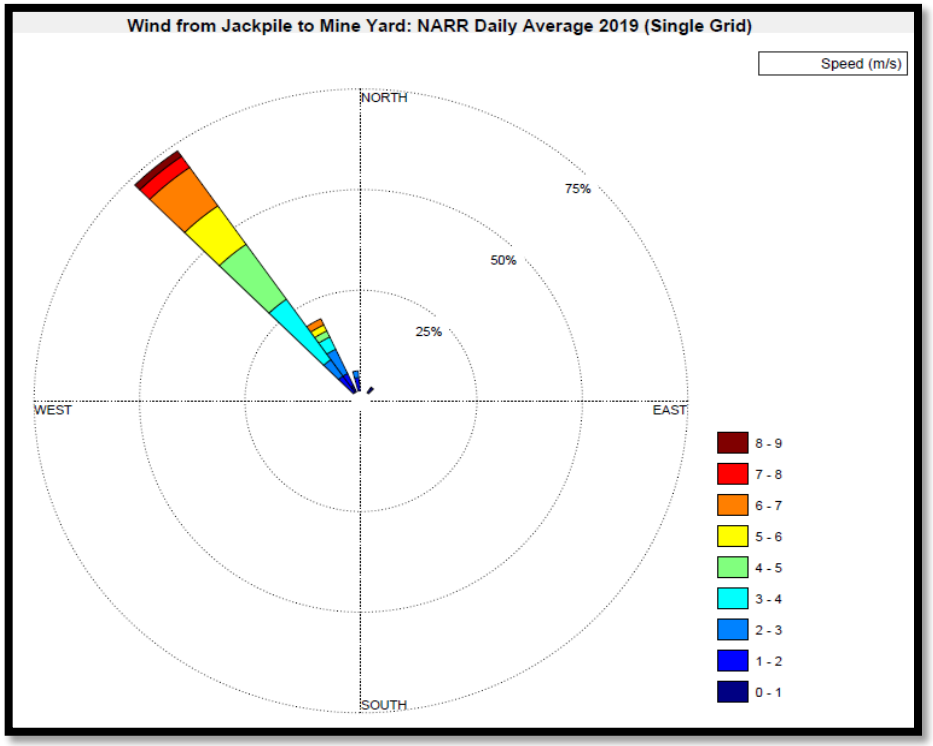

b.

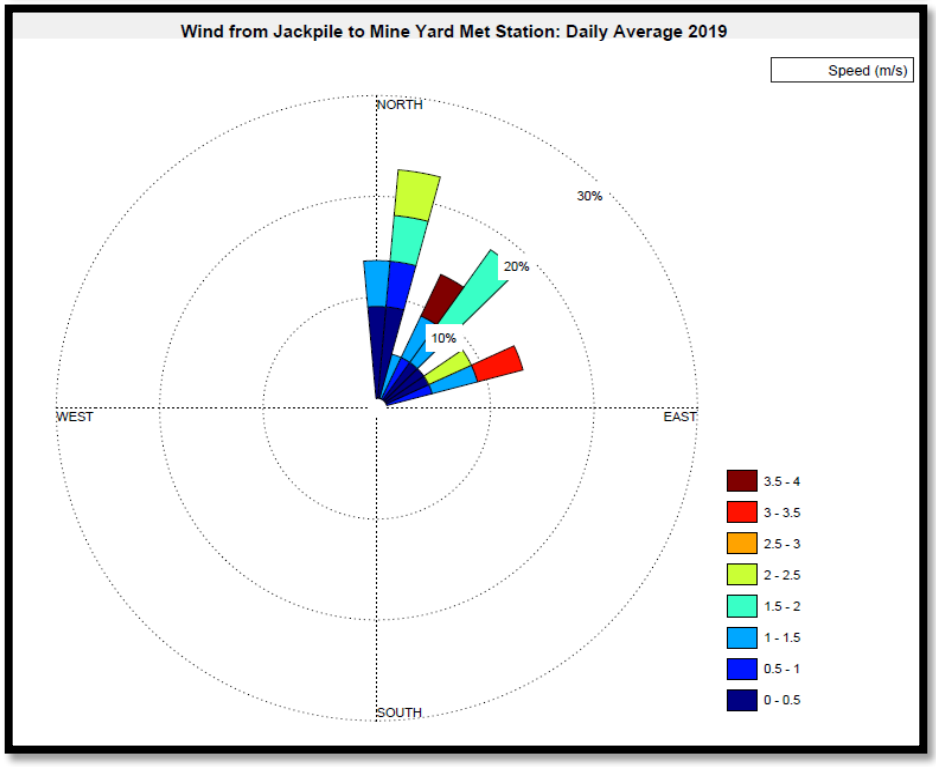

Figure 22: The percent of wind from the Jackpile Mine toward the Mine Yard in 2019. The NARR model (a) and a local meteorological station (b). The NARR model is derived from a single grid square encompassing the Mine Yard with 16% of the total wind moving this direction; the local meteorological station shows 18%.

a.

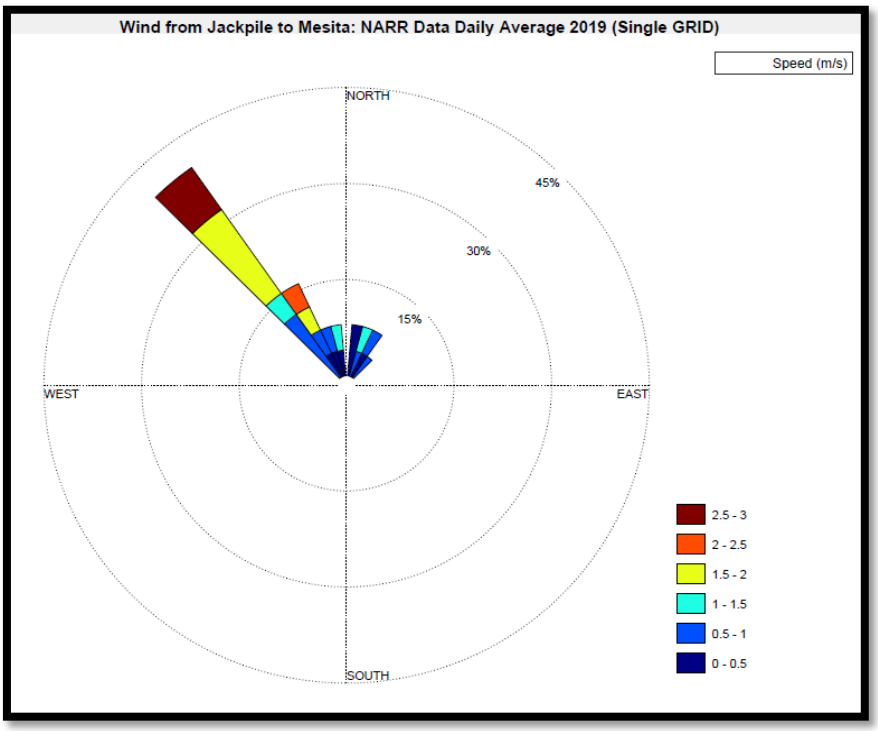

b.

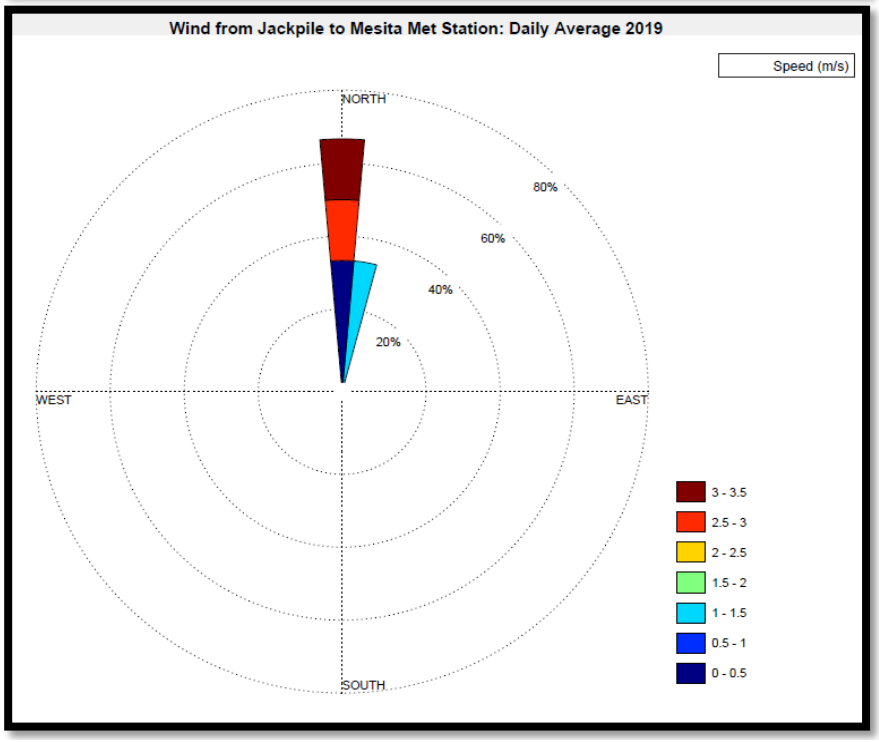

Figure 23: Percent of wind from the Jackpile Mine toward Mesita Village during 2019. The NARR model (a) and the local meteorological station (b) are compared. The NARR model is derived from a single grid square encompassing Mesita Village with 6% of the total wind moving this direction; the local meteorological station shows 8%.

a.

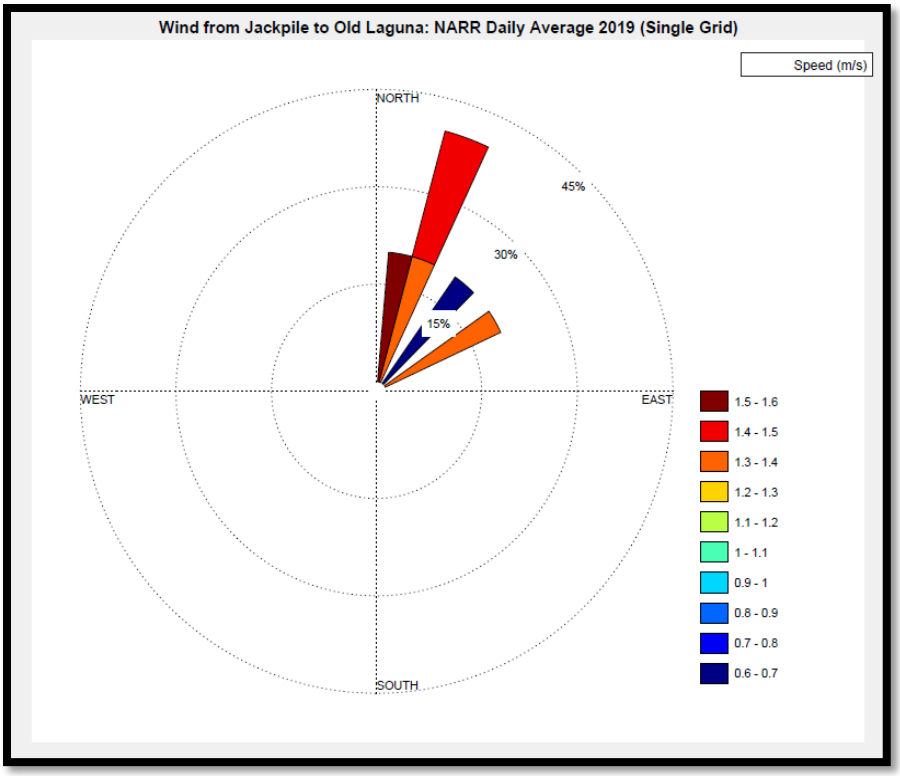

b.

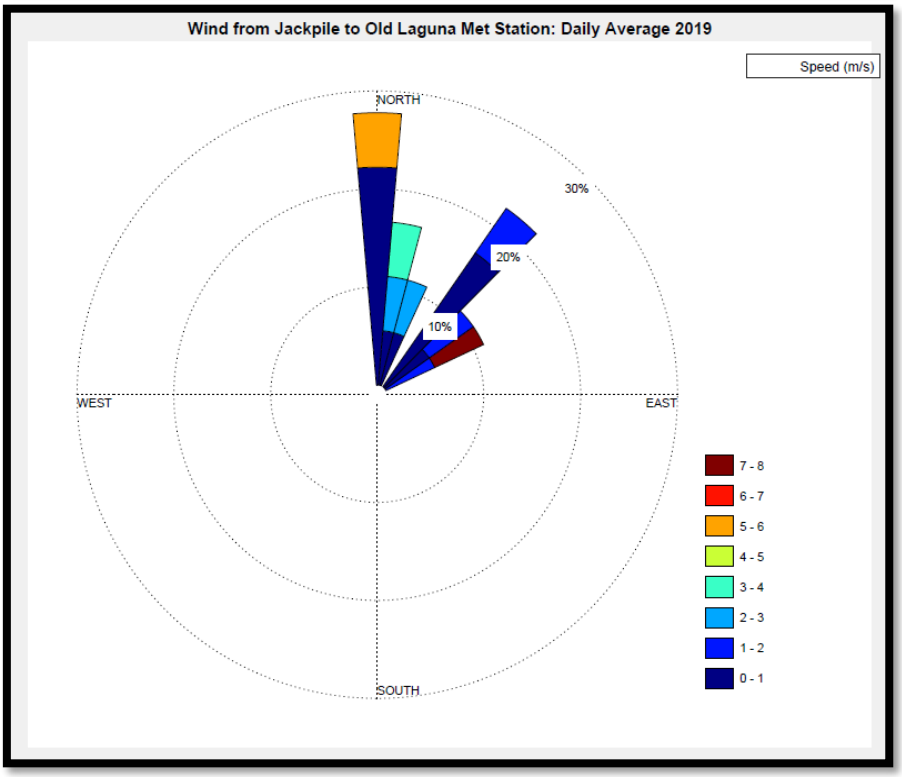

Figure 24: The percent of wind from Jackpile Mine toward Old Laguna Village in 2019. The NARR model (a) and a local meteorological station (b) are compared. The NARR model is derived from a single grid square encompassing the Old Laguna Village with 1% of the total wind moving this direction; the local meteorological station shows 8%.

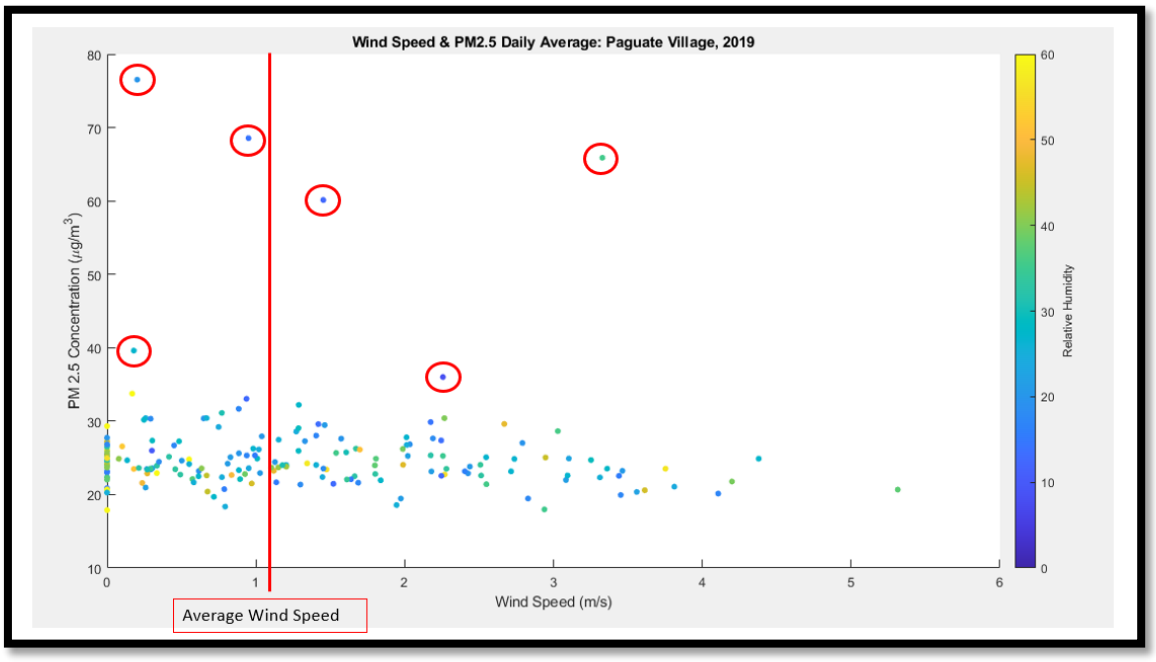

Figure 25: Daily average wind speed and $PM_{2.5}$ concentration at Laguna Pueblo. The circled points indicate the 6 days that exceed the 24-hour NAAQS. The color bar indicates relative humidity in %.

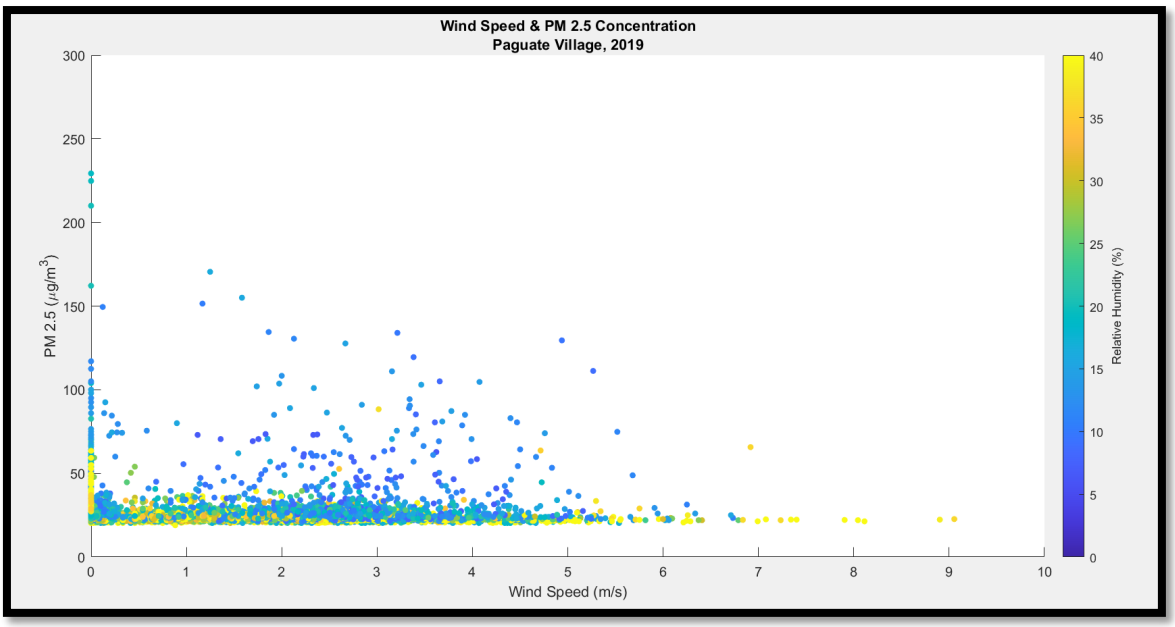

Figure 26: Raw data for $PM_{2.5}$ concentration and wind speed at Paguate Village. The data were collected at 10-minute intervals from April-November of 2019. The color bar indicates relative humidity.

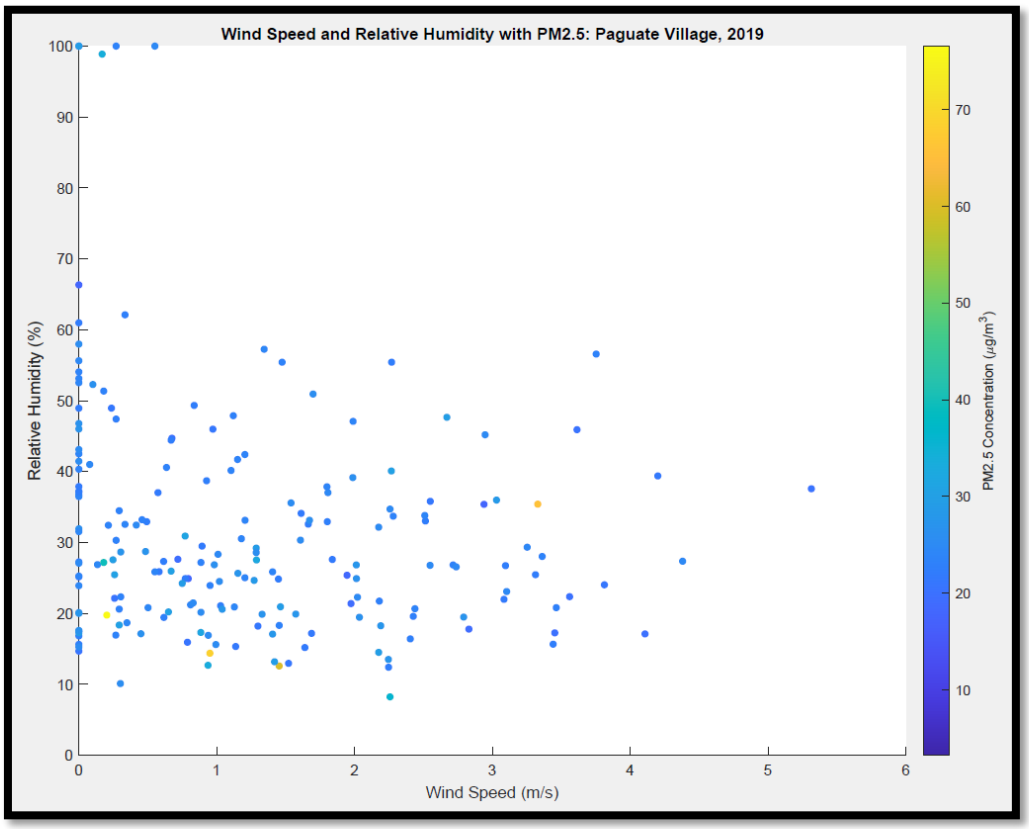

Figure 27: Daily average relative humidity plotted against wind speed at Paguate Village. The color bar indicates $PM_{2.5}$ concentrations.

Mineralogy of Toxic Metals in Particulate Matter Samples

Minerals were identified using EDS and qualitative composite imaging by way of X-ray mapping, including $CaAl_2Si_2O_8$ plagioclase feldspars and $KAlSi_3O_8$ alkali feldspars, as well as several iron oxides, sulfates, and barium sulfates. Sulfur-bearing minerals were identified several times during microscopy analyses. Other minerals identified are rutile, biotite, and calcite. Significant numbers of Cu particles were identified, including submicron particles <600 nm, raising questions for future research pertaining to origin and toxicity. Other metals of concern for potential health risks when present in elevated quantities that were identified in several respirable particles with SEM include Pb, Zn, Cu, Mo, and Co. Quantification of the

abundance of metal-bearing particles was not attempted as part of this research; the focus was identification of the presence of such grains in the samples.

The presence of several U-bearing particles of inhalable sizes were observed in 5 of the 6 samples analyzed; no U-bearing particles were observed on sample 1007 from Old Laguna Village. Uranyl vanadate minerals tyuyamunite and carnotite are present in the inhalable size fraction on several samples. Additionally, a mineral with U and As was observed in 4 instances on 2 samples; this mineral may be the uranyl arsenate mineral abernathyite [$K(UO_2)(AsO_4)\cdot 4H_2O$]. The EDS spectra for one of the uranyl arsenate particles (Fig. 28) displays the presence of both K and Cu, indicating that the mineral in question may be either abernathyite or metazeunerite [$Cu(UO_2)_2(AsO_4)_2\cdot 8H_2O$], but further mineralogical studies are necessary to confirm this identification. The material used to hold the sample is also made of Cu, making it difficult to determine whether this element is part of the chemical composition of the mineral in question. Based on BSE imaging and EDS spectra it is apparent that the larger U-bearing particles that are too large to be inhaled (~20 – 90 μm) are fracturing into smaller particles in the inhalable size range of PM ≤10 μm. In several cases, these particles are <1μm.

Respirable uranyl vanadate and uranyl arsenate particles were observed on samples 1003, 1004, 1005, 1006, and 1008 (Fig. 29-33). Table 4 indicates the total number of U-bearing grains identified on each sample, the sizes measured by diameter, and the minerals identified. Sample 1003 from Mesita Village contains a ~58 μm uranyl arsenate particle that is fragmenting into >20 respirable particles (Fig. 28), the total of which is difficult to accurately determine; therefore, these were not counted individually in the table and were counted as 1 particle. This same method was applied to sample 1008 from Mesita Village and 1005 from

Old Laguna Village, where the largest particle was counted as 1 and the fragmented respirable particles are included in that count.

Table 4: Toxic Metal-Bearing Grains Identified with SEM

Filter Number	Location	Metal-Bearing Minerals Identified	Number of Grains	Grain Sizes (µm)	Wind from Jackpile
1003	Mesita	Uranyl Arsenate; Uranyl Vanadate	7	0.137 – 9.25, 58.6	0.007 %
1004	Mesita	Uranyl Vanadate	6	0.391 – 9.13	0 %
1005	Laguna	Uranyl Vanadate	8	1.04 – 8.07, 19.9, 24.2	11 %
1006	Mesita	Uranyl Vanadate	2	0.391 – 1.13	13 %
1007	Laguna	N/A	0	N/A	43 %
1008	Mesita	Uranyl Arsenate	2	0.274 – 1.43, 14.5, 87.5	9 %

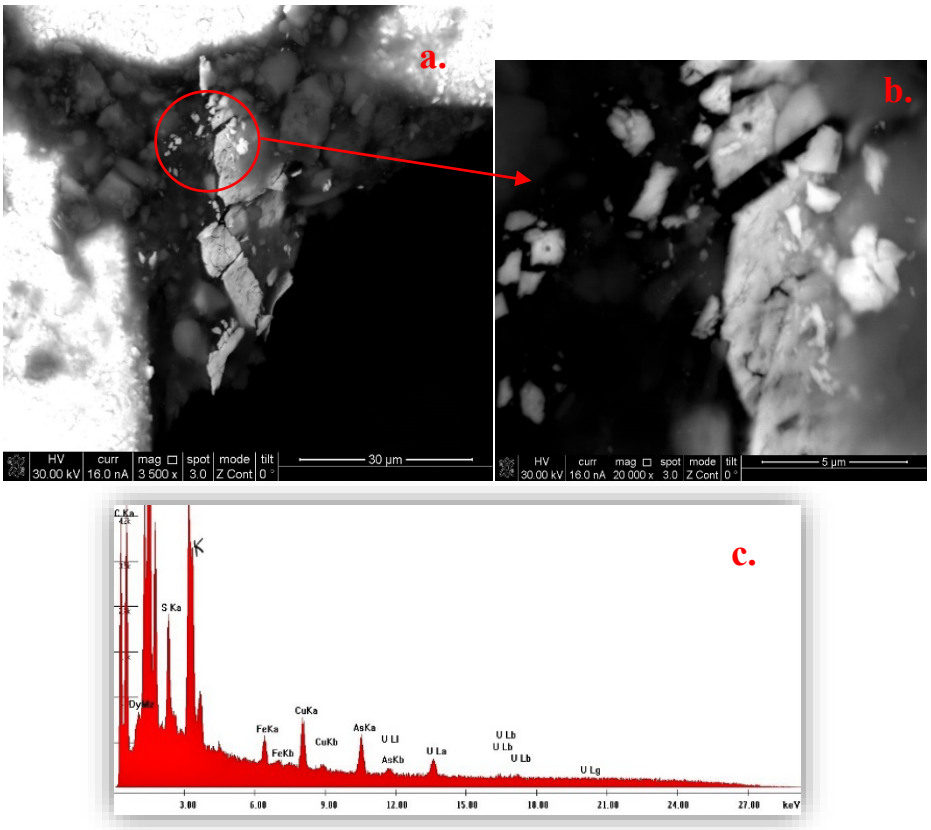

Figure 28: Particulate matter sample 1003 from Mesita Village showing a large 58.6 µm particle fragmenting into several respirable particles ranging from 0.137 – 6.74 µm in diameter.

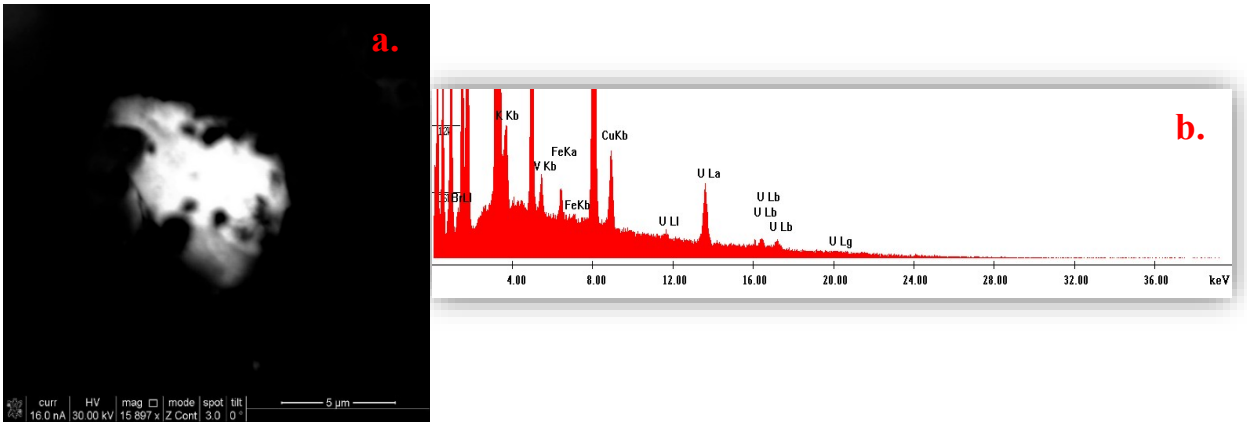

Figure 29: Backscattered electron image and EDS spectrum of particulate matter sample 1003 from Mesita Village containing a 9.25 µm uranyl vanadate particle.

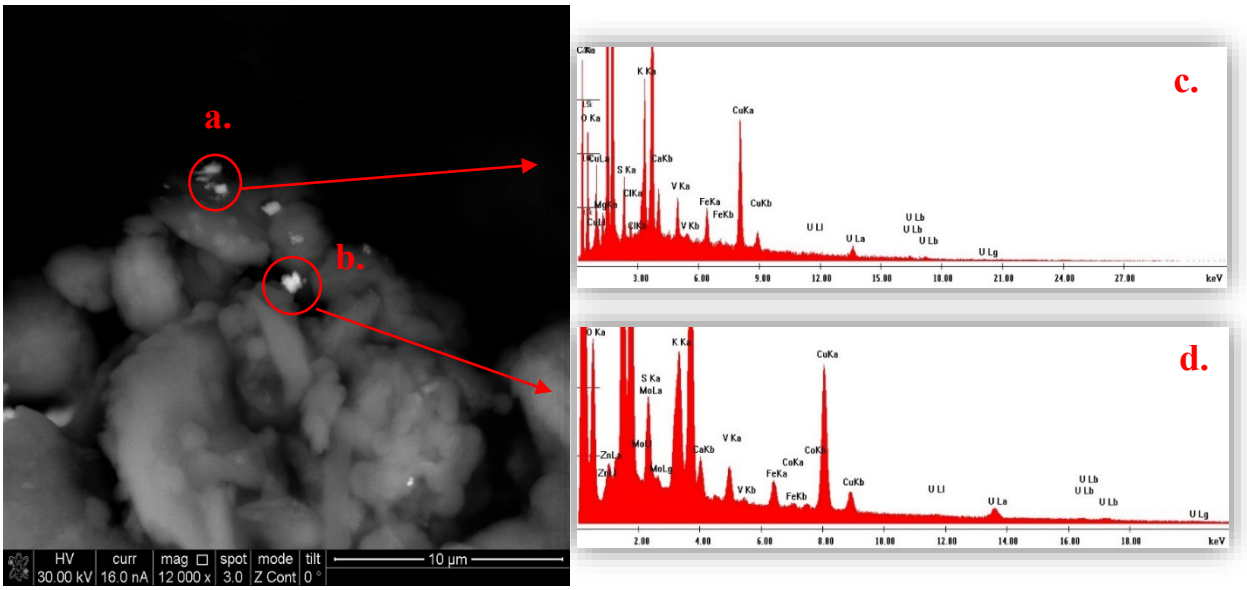

Figure 30: Backscattered electron image and EDS spectra of particulate matter sample 1004 from Mesita Village containing uranyl vanadate grains ranging from 0.391 – 1.13 µm in diameter.

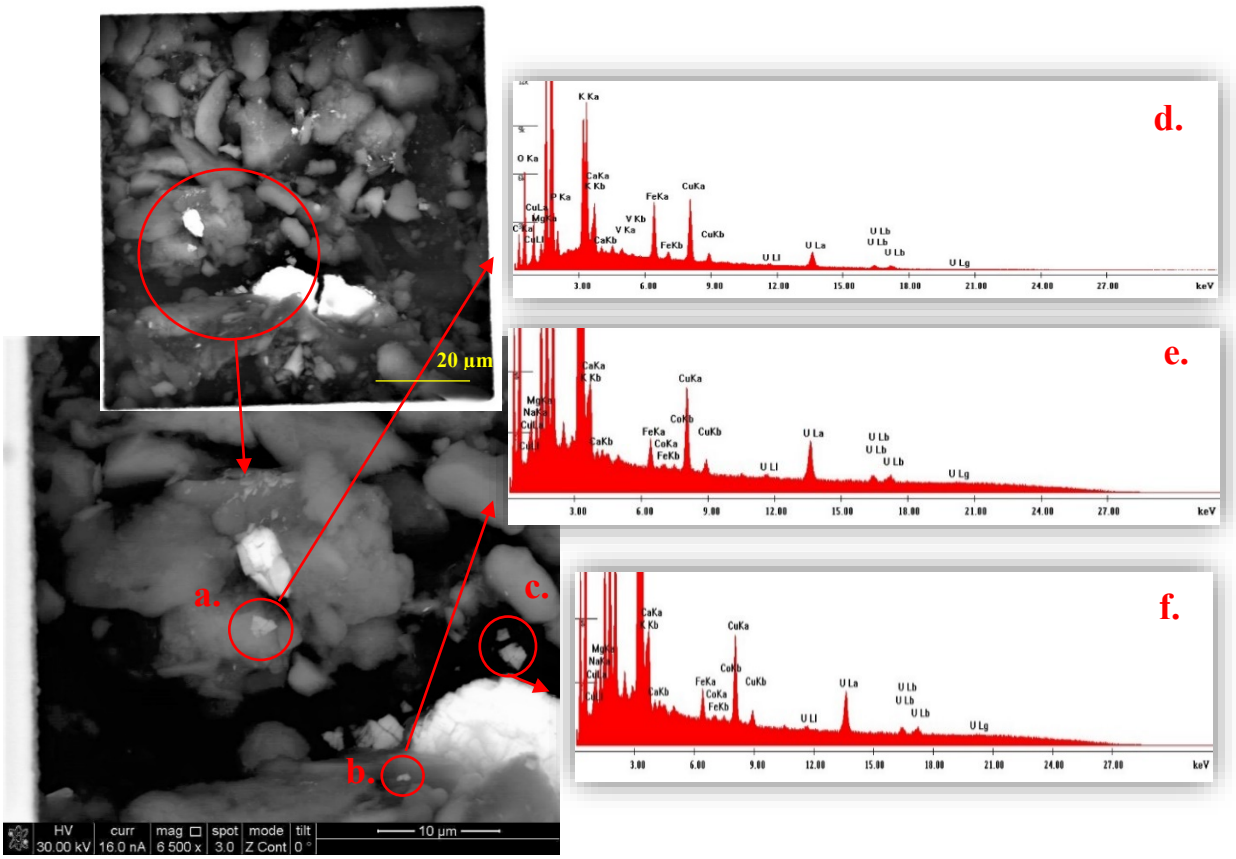

Figure 31: Backscattered electron images and EDS spectra of particulate matter sample 1005 from Old Laguna Village containing several uranyl vanadate particles ranging in size from 1.04 – 5.48 µm.

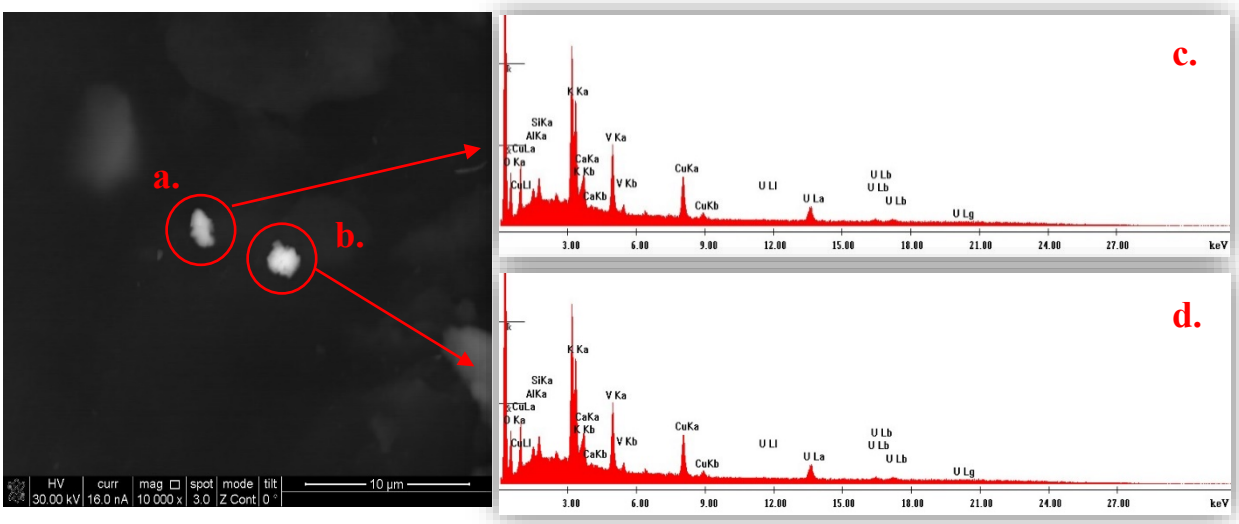

Figure 32: Backscattered electron images and EDS spectra of particulate matter sample 1006 from Mesita Village containing 2 uranyl vanadate particles, 2.10 µm (a) and 2.21µm (b).

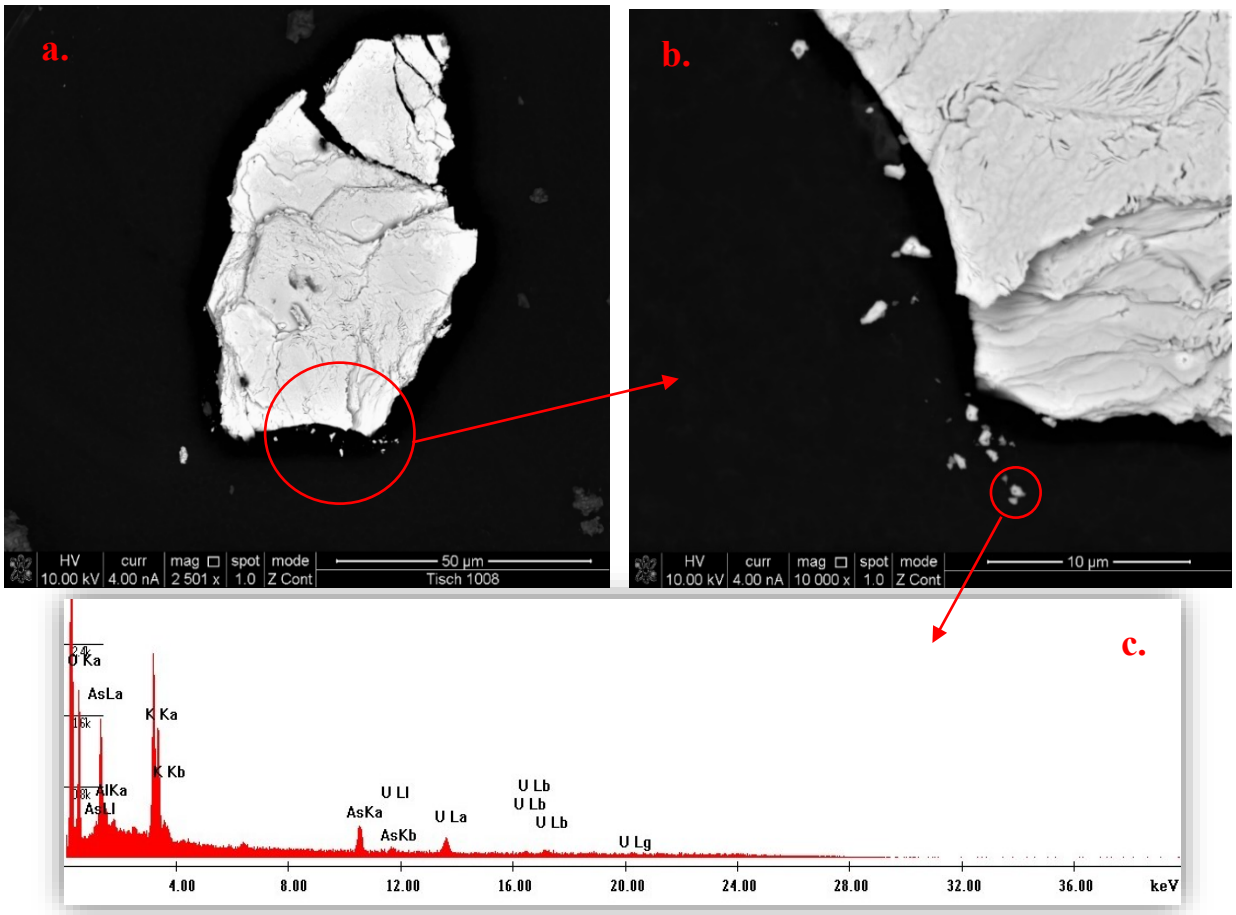

Figure 33: Backscattered electron image and EDS spectrum of particulate matter sample 1008 from Mesita Village containing uranyl arsenate particles ranging in size from 0.274 – 1.43 µm. The largest particle is 87.5 µm in diameter. Each of the particles ~1µm were analyzed with EDS and produced spectra nearly identical to the one presented (c).

The percent of wind detected from the direction of the Jackpile Mine toward each sample station during sample exposure was calculated. Sample 1003 had 0.007% of the wind coming from the direction of the mine during exposure, sample 1004 had 0%, sample 1005 had 11%, sample 1006 had 13%, sample 1007 had 43%, and sample 1008 had 9%. Uranium-bearing particles were identified on all samples except 1007, despite this sample receiving the greatest amount of wind from the direction of the Jackpile Mine. This suggests metal mixtures are widely distributed throughout the region and there is not a strong correlation between wind moving from the direction of the mine and particulate matter containing toxic metal mixtures.

Toxic Metal Concentrations

Several toxic elements were identified in concentrations higher than crustal averages, including U, Pb, As, Zn, and Cu (Fig. 34-38). A few instances of Co were also identified in elevated concentrations compared to crustal averages, as well as several instances of Mo, Cd, and Sn. Metals of concern mentioned by the USEPA that were not identified in concentrations higher than crustal average values include Ba, Mn, and V; other elements analyzed including Ni, La, Li, Ce, and Sr do not show elevated concentrations (Fig. 39-41). The consistency among these elements is as expected, strengthening the efficacy of the overall results, including several toxic metals with values higher than crustal average. Some elemental concentrations, including Mn, Ni, V, Li, Ba, Sr, La, and Ce, are consistent across samples while others show considerable variability, including U, Pb, As, Zn, Cu, Mo, Co, Cd, and Sn. In some cases, results plots show elemental concentrations increasing from left to right, possibly indicating a

seasonal change during the time of data collection, from May to December; however, more data collection is necessary to fully evaluate this trend.

For elements of less concern in terms of potential health risk, the ICP-MS results are also assessed as elements categorized by the Goldschmidt classification. Siderophile elements that have an affinity for iron (Fe) show mixed results; Mn and Ni are consistent with crustal average values, but Co and Mo show several instances of enrichment (Fig. 39). The elements Mo and Co were also notably detected during microscopy analyses. The silicate-forming lithophile elements analyzed, including Mn, V, Li, Ba, and Sr, show consistency with crustal average values; no significant enrichments are observed among these elements compared to crustal average values (Fig. 40). The results for chalcophile elements Cd and Sn both indicate significant enrichments in the particulate matter (Fig. 41); these elements have an affinity for sulfur (S), readily forming sulfates. Sulfur-bearing minerals were also observed several times during microscopy analyses. Several of the elements of concern for health risks observed to be enriched in the particulate matter samples are also chalcophile elements, including As, Pb, Zn, and Cu. The elevated concentrations of Cu compared to crustal average values are likely from anthropogenic activities and could be deposited from brake lining residues.

Absolute concentrations for U, V, Pb, and As were calculated using the ICP-MS results and the Ti crustal average value of 5560 ppm (Table 7). These results are based on samples that collected particulate matter of all sizes, not solely particulate matter of the inhalable size fraction; therefore, comparison to any airborne exposure limits is not direct but provides information about the overall toxic metal mixture concentrations contained in all suspended dust. Particulate matter ≤10 μm generally makes up ~40% of the total volume of dust

components, while PM ≤2.5 μm make up ~20% (Derbyshire, 2007). The USEPA does not currently have standards for toxic substances in air and does not provide limits for this exposure pathway; however, worker standards have been established by the Occupational Safety and Health Administration (OSHA) for exposure to individual toxic metals in air averaged over an 8-hour workday. The limits for soluble and insoluble U are 0.005 ppm and 0.025 ppm, respectively. The limit for V is 0.24 ppm, for Pb the limit is 0.0059 ppm, and for As the limit is 0.0032 ppm. Concentrations of U obtained from the local samples range from 4.17- 223 ppm with an average of 30.9 ppm. Local concentrations of V are consistent between samples and range from 3.91- 5.27 ppm with an average of 4.64 ppm. The local concentrations of Pb range from 15.8- 63.7 ppm with an average of 27.0 ppm. Local concentrations of As range from 24.4- 331 ppm with an average of 76.5 ppm. The sample collection involves a high volume of material collected in a short period of time, at a flow rate of ~1 m^3/min, while humans typically inhale at a rate of 0.015 – 0.06 m^3/min (Rahimi-Gorji et al., 2015). The average volume of air moved through 1 filter exposed for 24 hours at a flow rate of 1.13 m^3/min (the average flow rate of exposure for filters 1001 – 1015) is 1627.2 m^3. The average volume of air inhaled by a human in a 24-hour period at a flow rate of 0.015 – 0.06 m^3/min is 21.6 – 86.4 m^3. Therefore, the volume of air inhaled by a human is much lower than the volume of air moved through the filters; the filters used for ICP-MS analyses were 1/8 sections of a single filter per sample set. An estimate of the volume accumulated on a 1/8 section is 203.4 m^3.

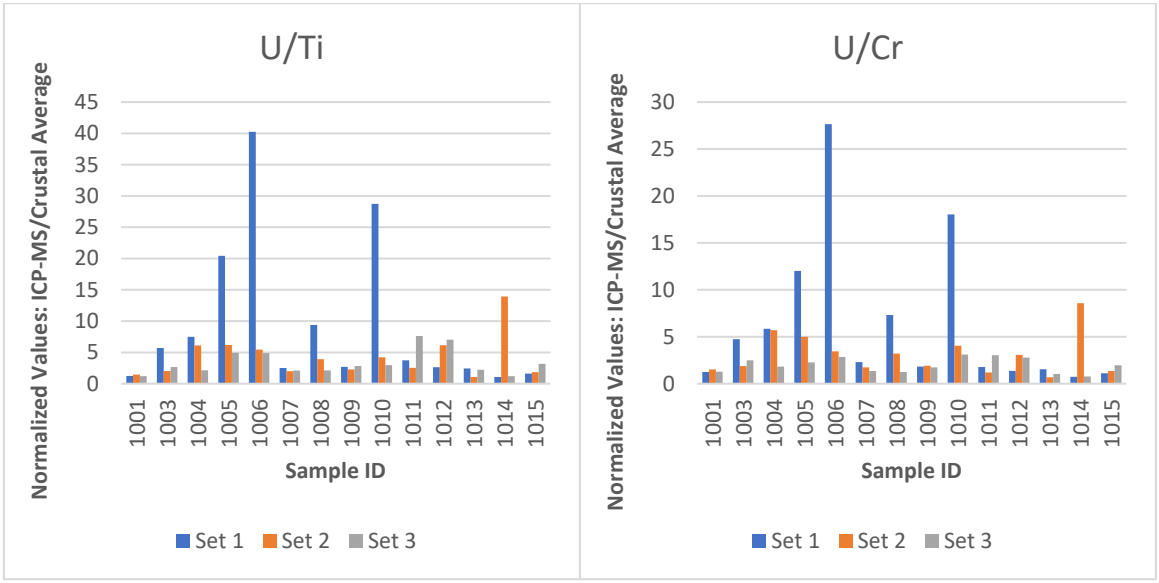

Figure 34: Normalized plots for U/Ti and U/Cr values from ICP-MS results. The normalized values are calculated from a ratio of ICP-MS concentrations of U/Ti to crustal average concentrations of U/Ti, similarly with U/Cr values. The results are for triplicate samples; therefore, set 1, 2, and 3 refer to each of the 3 sample sets for filters 1001 – 1015.

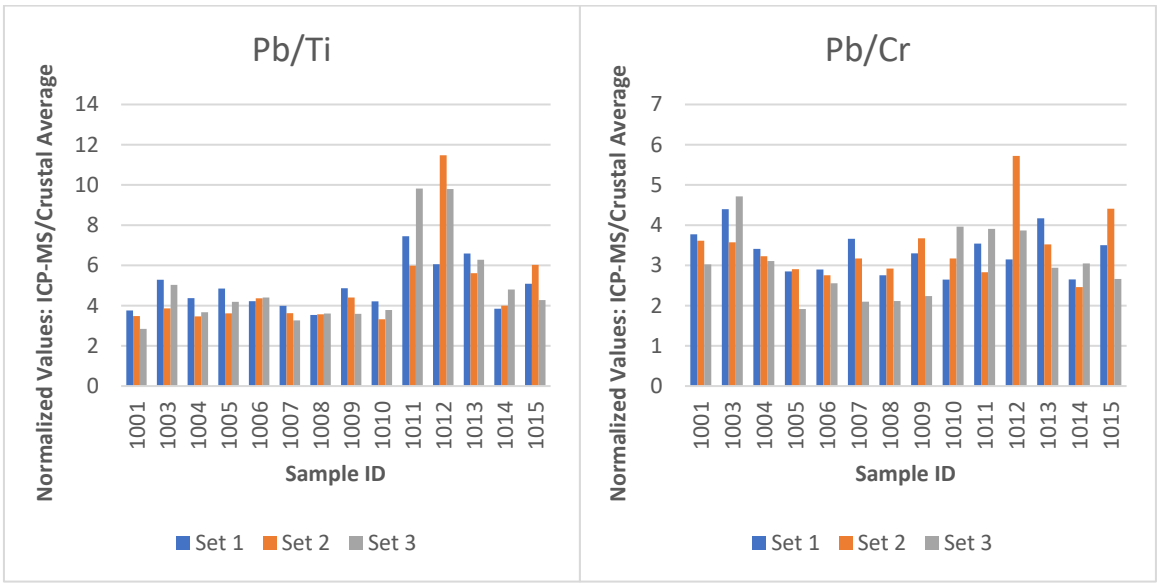

Figure 35: Normalized plots for Pb/Ti and Pb/Cr values from ICP-MS results. The normalized values are calculated from a ratio of ICP-MS concentrations of Pb/Ti to crustal average concentrations of Pb/Ti, similarly with Pb/Cr values. The results are for triplicate samples; therefore, set 1, 2, and 3 refer to each of the 3 sample sets for filters 1001 – 1015.

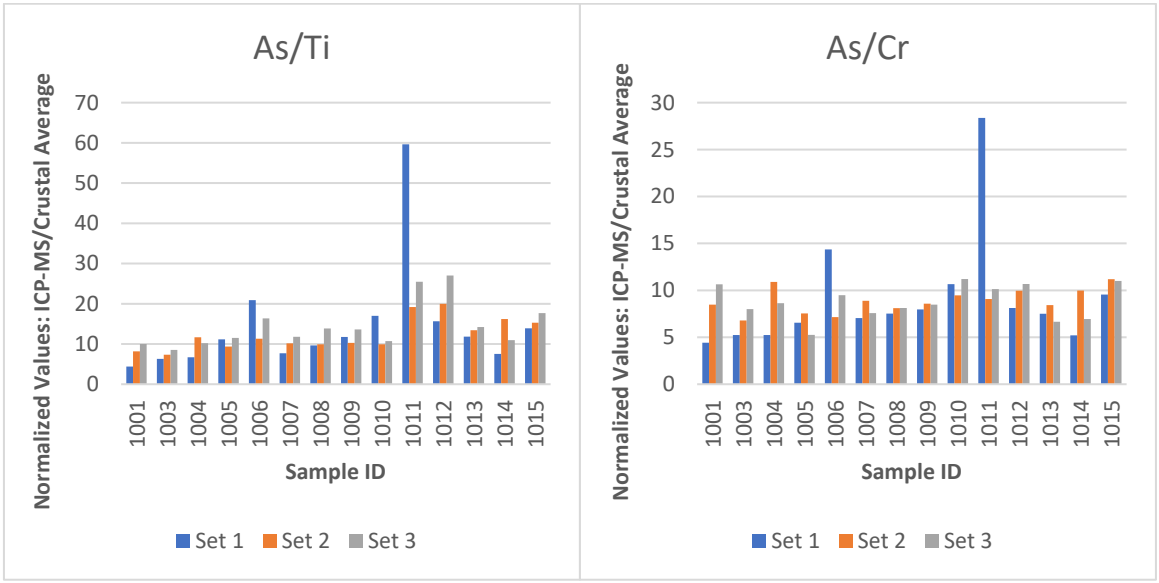

Figure 36: Normalized plot for As/Ti and As/Cr values from ICP-MS results. The normalized values are calculated from a ratio of ICP-MS concentrations of As/Ti to crustal average concentrations of As/Ti, similarly with As/Cr values. The results are for triplicate samples; therefore, set 1, 2, and 3 refer to each of the 3 sample sets for filters 1001 – 1015.

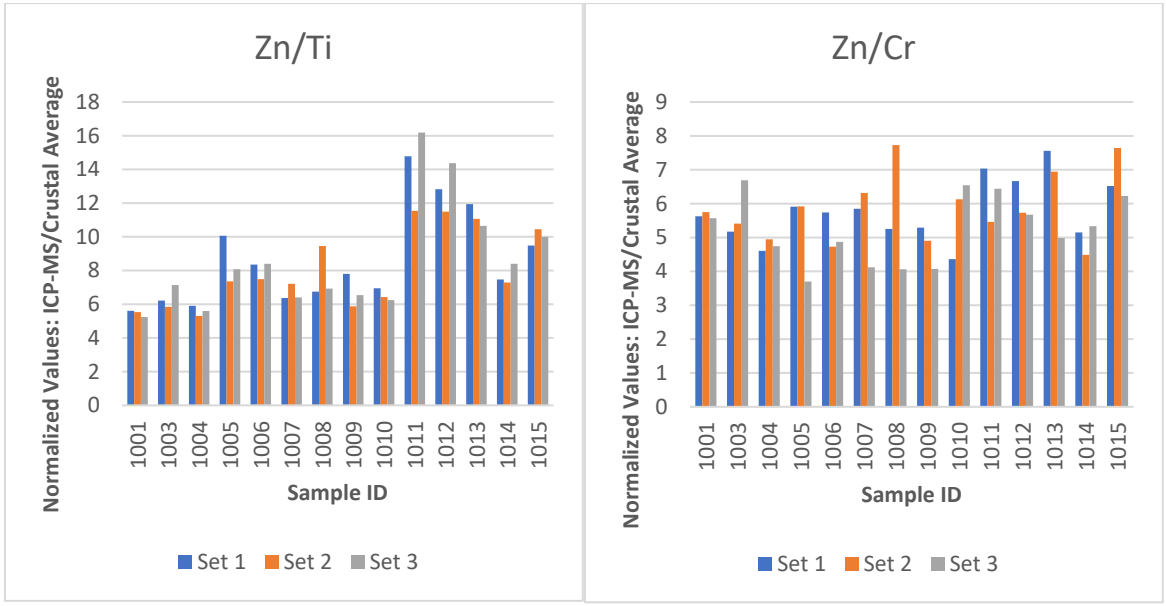

Figure 37: Normalized plot for Zn/Ti and Zn/Cr values from ICP-MS results. The normalized values are calculated from a ratio of ICP-MS concentrations of Zn/Ti to crustal average concentrations of Zn/Ti, similarly with Zn/Cr values. The results are for triplicate samples; therefore, set 1, 2, and 3 refer to each of the 3 sample sets for filters 1001 – 1015.

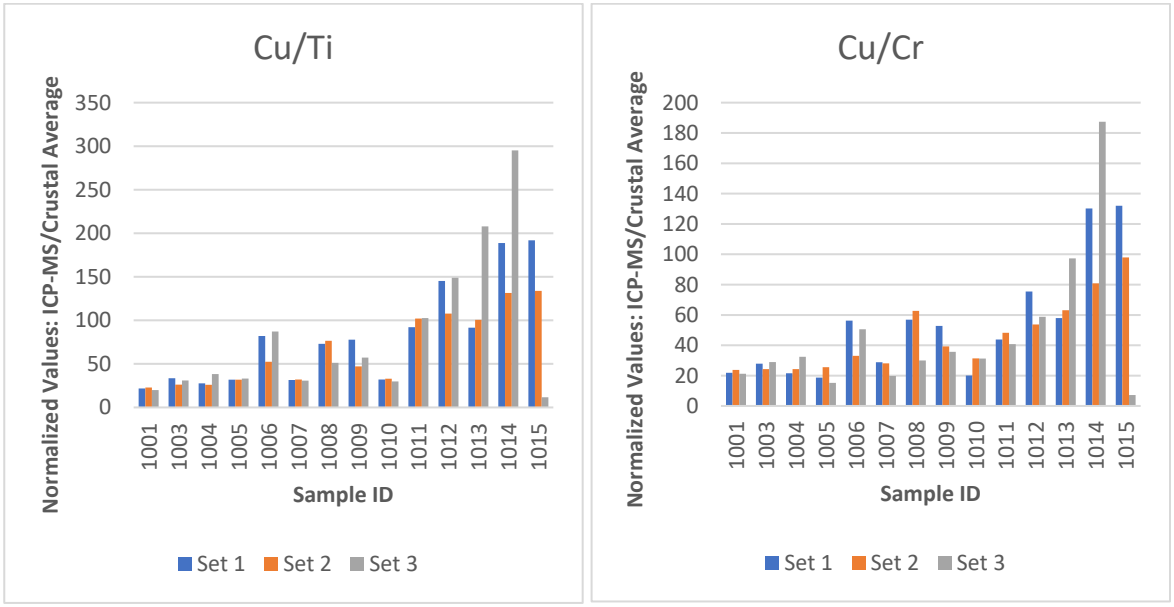

Figure 38: Normalized plot for Cu/Ti and Cu/Cr values from ICP-MS results. The normalized values are calculated from a ratio of ICP-MS concentrations of Cu/Ti to crustal average concentrations of Cu/Ti, similarly with Cu/Cr values. The results are for triplicate samples; therefore, set 1, 2, and 3 refer to each of the 3 sample sets for filters 1001 – 1015.

Siderophile Elements

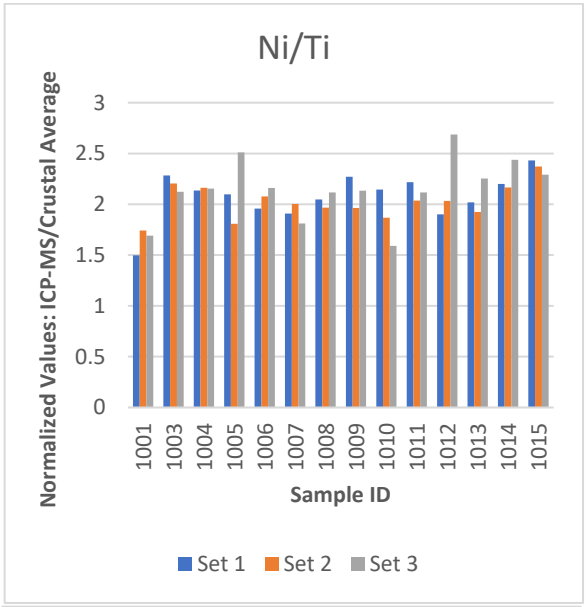

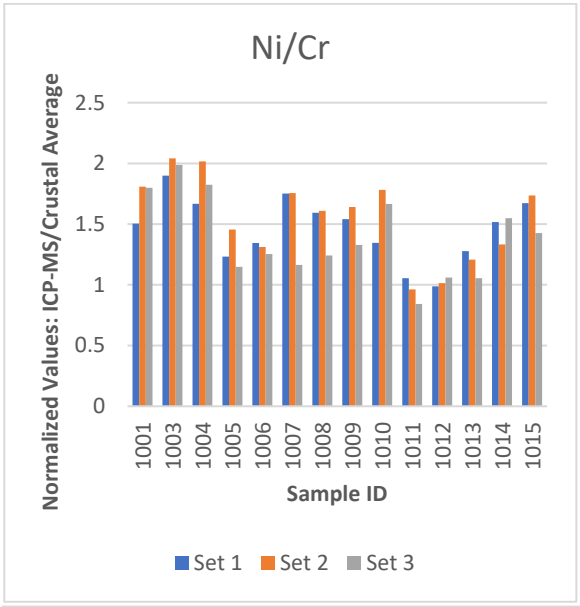

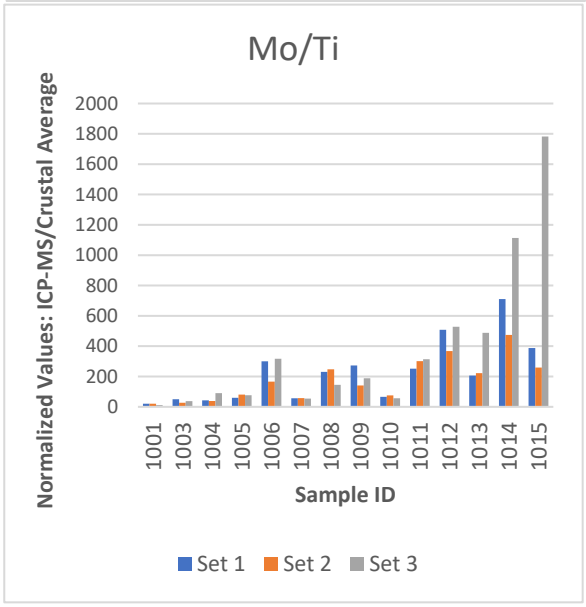

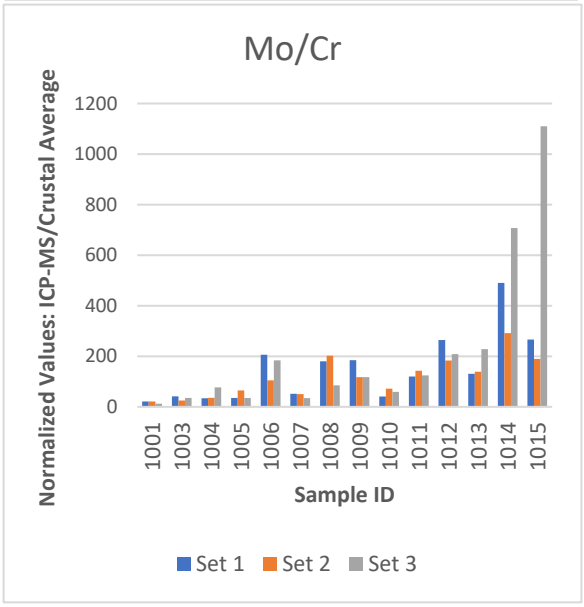

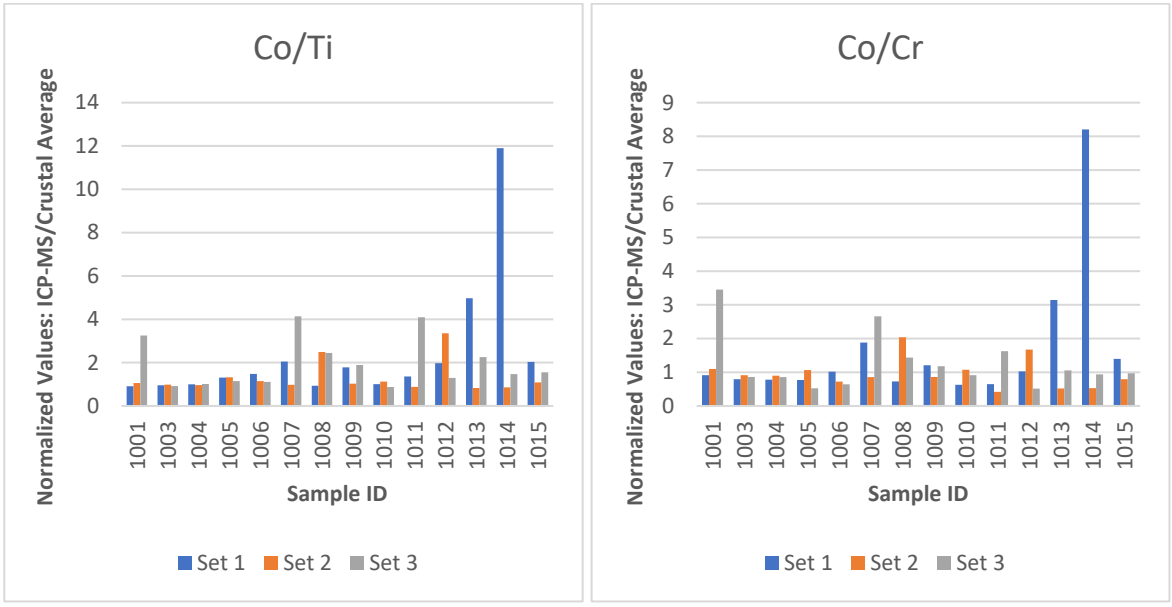

Figure 39: Normalized plots for siderophile elements Ni, Mo, and Co based on ICP-MS results. The normalized values are calculated from a ratio of ICP-MS concentrations of Ni/Ti, Mo/Ti, and Co/Ti to crustal average concentrations of Ni/Ti, Mo/Ti, and Co/Ti, similarly with Ni/Cr, Mo/Cr, and Co/Cr values. The results are for triplicate samples; therefore, set 1, 2, and 3 refer to each of the 3 sample sets for filters 1001 – 1015.

Lithophile Elements

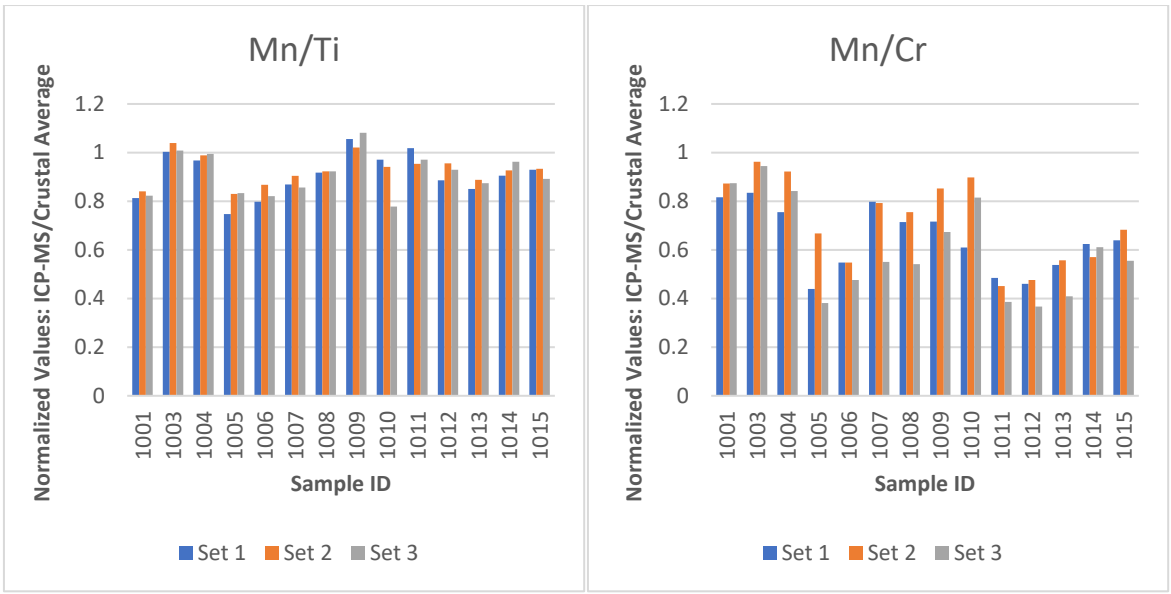

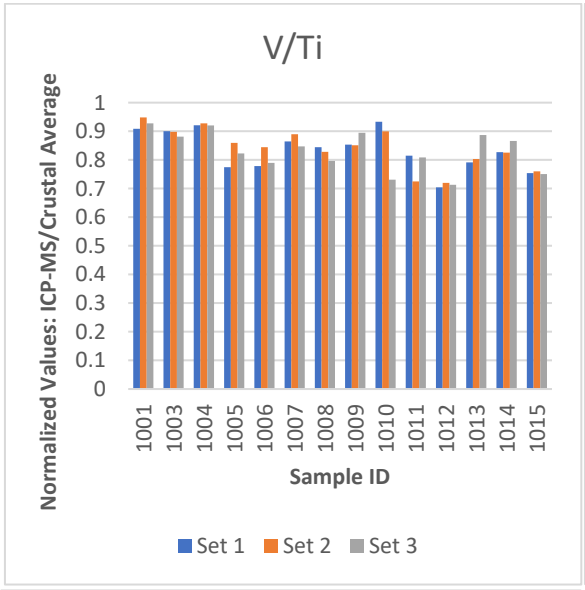
V/Ti
Normalized Values: ICP-MS/Crustal Average
0
0.1
0.2
0.3
0.4
0.5
0.6
0.7
0.8
0.9
1
1001
1003
1004
1005
1006
1007
1008
1009
1010
1011
1012
1013
1014
1015
Sample ID
Set 1
Set 2
Set 3

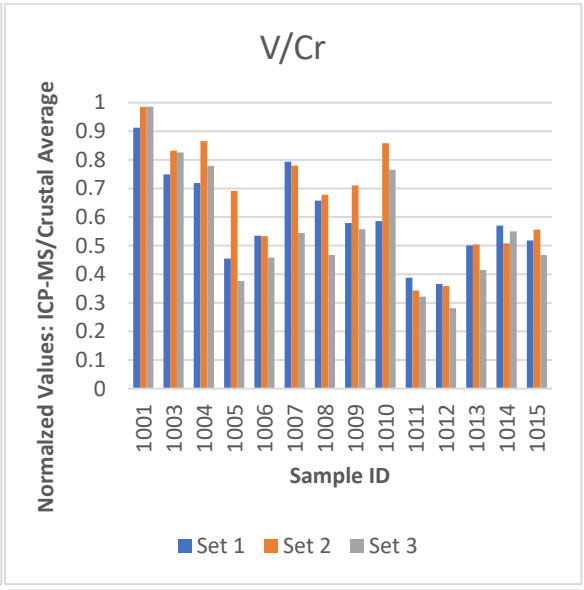
V/Cr
Normalized Values: ICP-MS/Crustal Average
0
0.1
0.2
0.3
0.4
0.5
0.6
0.7
0.8
0.9
1
1001
1003
1004
1005
1006
1007
1008
1009
1010
1011
1012
1013
1014
1015
Sample ID
Set 1
Set 2
Set 3

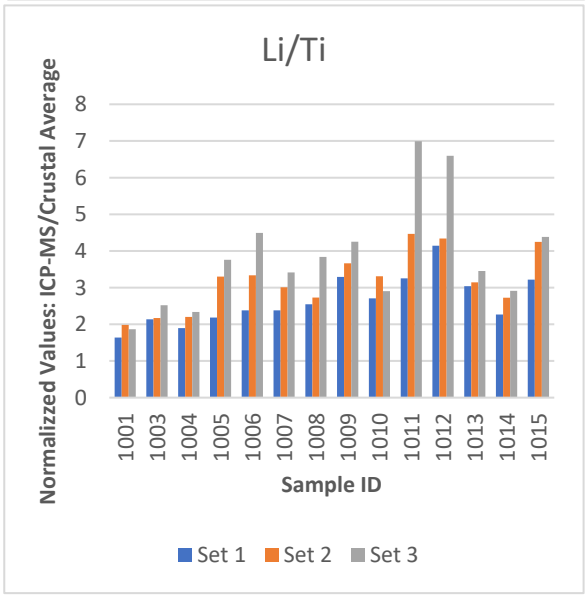
Li/Ti
Normalized Values: ICP-MS/Crustal Average
0
1
2
3
4
5
6
7
8
1001
1003
1004
1005
1006
1007
1008
1009
1010
1011
1012
1013
1014
1015
Sample ID
Set 1
Set 2
Set 3

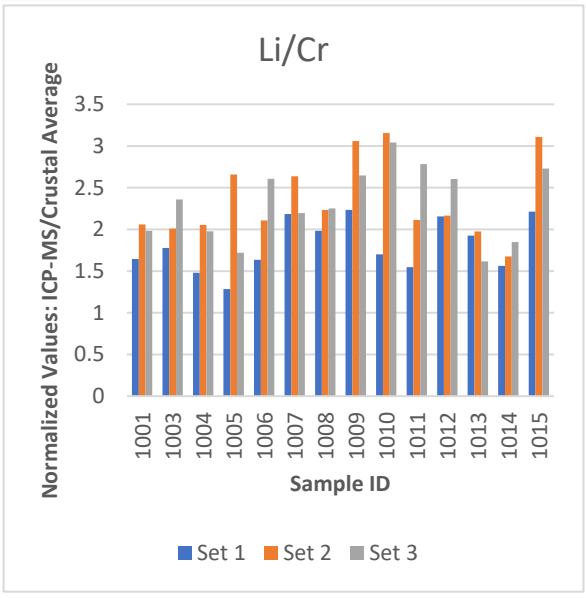
Li/Cr
Normalized Values: ICP-MS/Crustal Average
0
0.5
1
1.5
2
2.5
3
3.5
1001
1003
1004
1005
1006
1007
1008
1009
1010
1011
1012
1013
1014
1015
Sample ID
Set 1
Set 2
Set 3

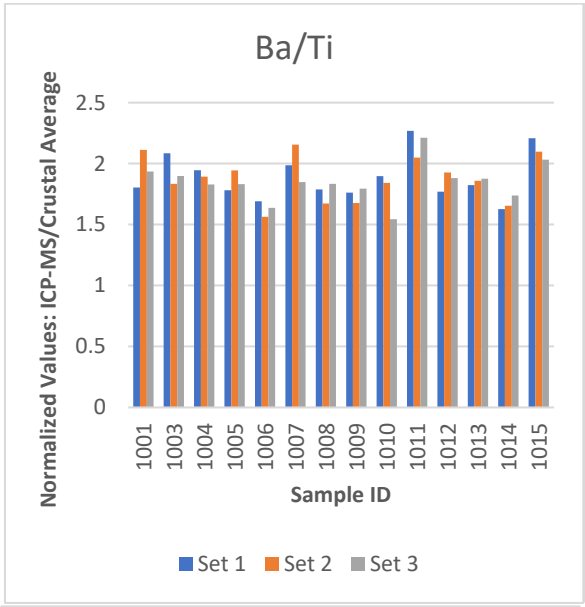
Ba/Ti
Normalized Values: ICP-MS/Crustal Average
2.5
2
1.5
1
0.5
0
1001 1003 1004 1005 1006 1007 1008 1009 1010 1011 1012 1013 1014 1015
Sample ID
Set 1 Set 2 Set 3

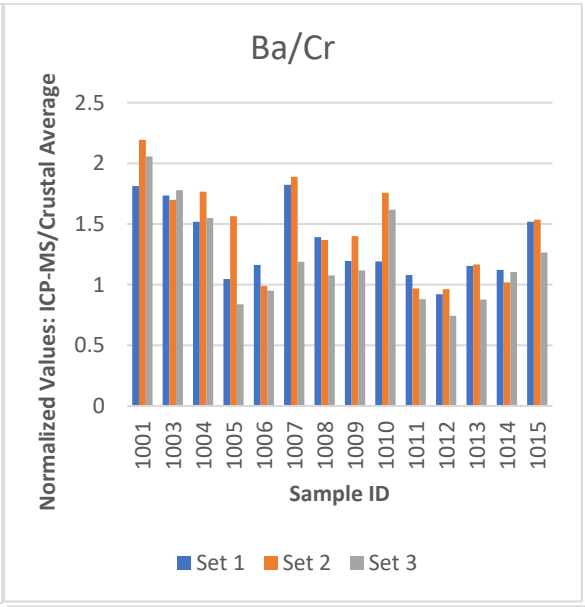
Ba/Cr
Normalized Values: ICP-MS/Crustal Average
2.5
2
1.5
1
0.5
0
1001 1003 1004 1005 1006 1007 1008 1009 1010 1011 1012 1013 1014 1015
Sample ID
Set 1 Set 2 Set 3

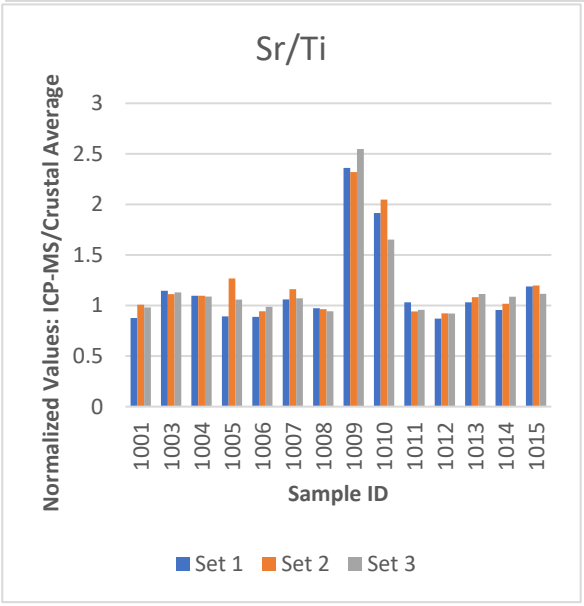
Sr/Ti
Normalized Values: ICP-MS/Crustal Average
3
2.5
2
1.5
1
0.5
0
1001 1003 1004 1005 1006 1007 1008 1009 1010 1011 1012 1013 1014 1015
Sample ID
Set 1 Set 2 Set 3

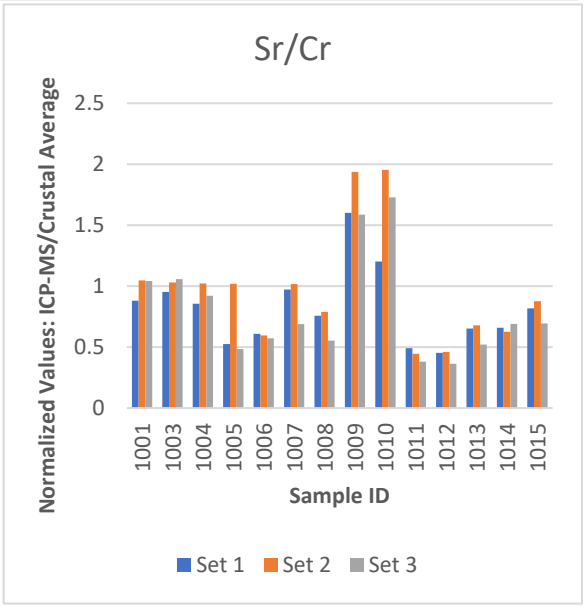
Sr/Cr
Normalized Values: ICP-MS/Crustal Average
2.5
2
1.5
1
0.5
0
1001 1003 1004 1005 1006 1007 1008 1009 1010 1011 1012 1013 1014 1015
Sample ID
Set 1 Set 2 Set 3

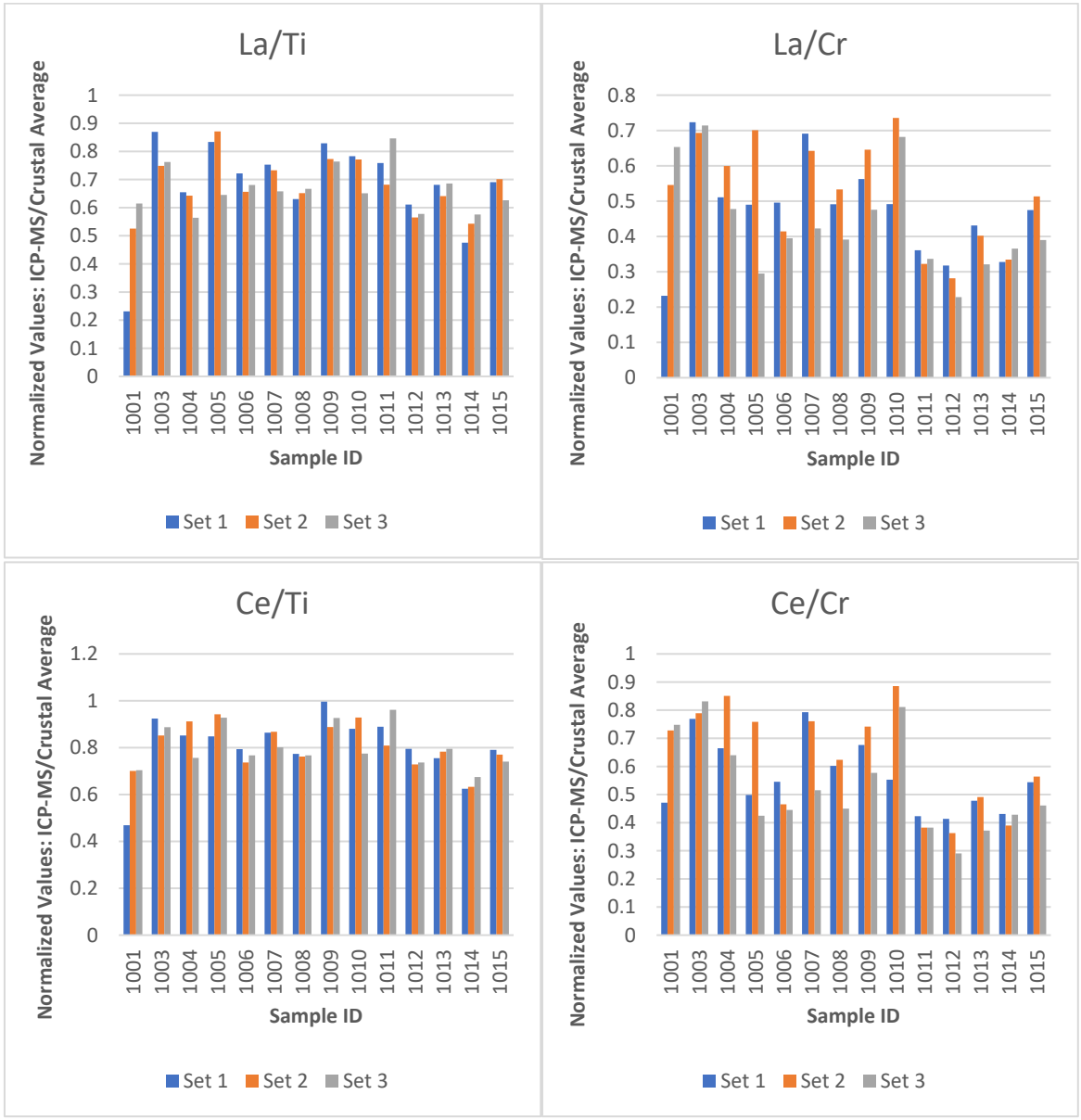

Figure 40: Normalized plots for lithophile elements Mn, V, Li, Ba, Sr, La, and Ce based on ICP-MS results. The normalized values are calculated from a ratio of ICP-MS concentrations of Mn/Ti, V/Ti, Li/Ti, Ba/Ti, Sr/Ti, La/Ti, and Ce/Ti to crustal average concentrations of Mn/Ti, V/Ti, and Li/Ti, Ba/Ti, Sr/Ti, La/Ti, and Ce/Ti, and similarly with Mn/Cr, V/Cr, Li/Cr, Ba/Cr, Sr/Cr, La/Cr, and Ce/Cr values. The results are for triplicate samples; therefore, set 1, 2, and 3 refer to each of the 3 sample sets for filters 1001 – 1015.

Chalcophile Elements

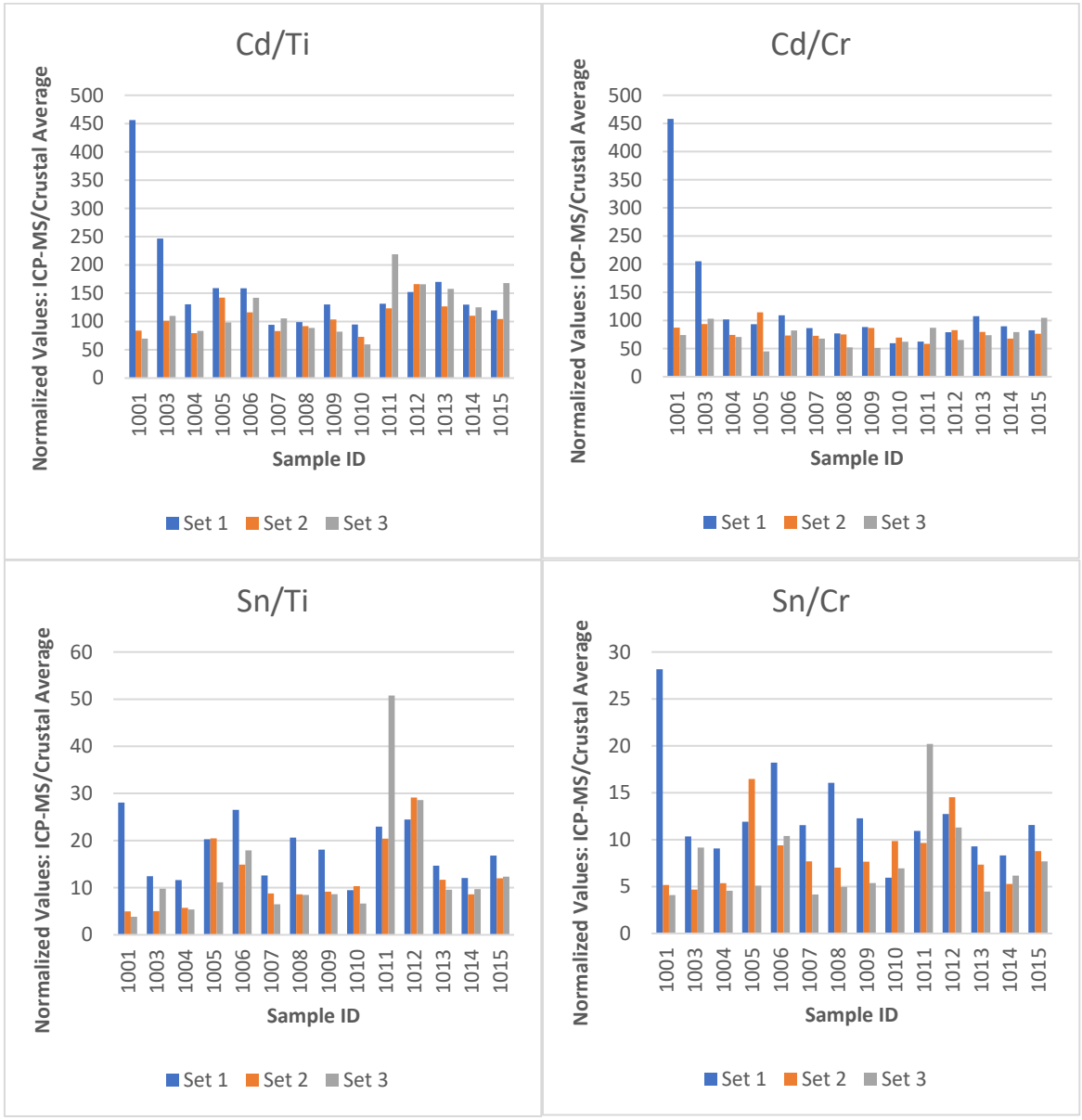

Figure 41: Normalized plots for chalcophile elements Cd and Sn based on ICP-MS results. The normalized values are calculated from a ratio of ICP-MS concentrations of Cd/Ti and Sn/Ti to crustal average concentrations of Cd/Ti and Sn/Ti, similarly with Cd/Cr and Sn/Ti values. The results are for triplicate samples; therefore, set 1, 2, and 3 refer to each of the 3 sample sets for filters 1001 – 1015.

CHAPTER 5- DISCUSSION

Climate analyses from both the NARR model and the local meteorological stations at 4 villages in Laguna Pueblo suggest relative humidity is the most important parameter controlling dust transport in the region, which is notably characterized by semiarid conditions and highly variable topography. A threshold is observed for conditions of relative humidity driving increases in concentrations of respirable particulate matter throughout the year. This threshold is supported by soil matric values that estimate soil moisture content to be extremely low, leaving soils unsaturated and susceptible to windblown transport. This value of relative humidity ≤35% indicates the threshold at which a water layer can develop between particles and allow for soil aggregates to form (Neuman and Sanderson, 2008). A lack of particle cohesion caused by low atmospheric humidity leaves dry particulate matter more susceptible to windblown transport, resulting in higher $PM_{2.5}$ concentrations, which is observed in this study. An increase in soil moisture as a result of increased atmospheric humidity is therefore more effective in reducing dust transport due to a subsequent increase in the threshold friction velocity; additionally, precipitation events remove airborne particulates from the atmosphere, resulting in lower particulate matter concentrations. When conditions at Laguna Pueblo are wetter, there is less dust transport; however, the region is characterized by semiarid conditions that most frequently experience low relative humidity, leaving respirable particulate matter exposed to windblown erosion and transport. The average relative humidity at Laguna Pueblo is 31% based on the available data from the local meteorological stations, which is below the threshold for the development of a water layer between particles. These conditions result in

frequent transport of particulate matter in the area and pose a potential inhalation exposure risk to local tribal communities.

No other meteorological parameter was observed to have a significant relationship to concentrations of PM ≤10 μm for the duration of data collection available. Wind speed likely contributes to dust transport of particulate matter in the inhalable size fraction; however, the data available show very little correlation. Previous studies have found that fine particulate matter of the inhalable size fraction may behave differently in response to wind speed when compared to coarser size fractions (Cichowicz et al., 2020; Zhang et al., 2017). These studies have found that PM ≤10 μm decreases in concentration with increasing wind speeds, while the abundance of larger particles tends to show the opposite effect of increasing with higher wind speeds. This effect was indicated in the data collected by the local stations; however, more data collection is necessary to fully evaluate this effect. Particles with a diameter ≤20 μm can have a residence time of up to 1-2 weeks in the atmosphere after initial suspension; this may explain the presence of high particulate matter concentrations under wind speed conditions of 0 m/s (Kok, et al., 2012). The effect of wind speed and relative humidity together shows very little correlation based on the available data. It is likely that other factors are necessary to consider in future research; similar studies suggest dust transport in low humidity environments is influenced by other factors affecting particle cohesion aside from relative humidity and wind speeds, such as surface roughness and chemical composition of the source materials (Csavina et al., 2014).

The importance of the local meteorological stations for determining relative humidity compared to the regional climate data from the NARR model is less significant than for the

purpose of determining local wind conditions. The NARR model is not refined enough to resolve the small-scale wind processes at the surface, as the best data available are modeled for 10m above the surface. The local meteorological stations are ~1m above the surface and provide more accurate data for the area, which is influenced by highly variable topography. Relative humidity may be more accurate than wind direction and speed from the NARR model because the relative humidity values are represented for 2m above the surface; additionally, this parameter is not influenced by small-scale local variation in the same way that wind conditions are subject to changes due to local topography. For accurate local meteorological data collection as it relates to windblown transport of airborne particulate matter, the local stations at Laguna Pueblo act as a valuable tool. This information can potentially aid in the development of a warning system for the local tribal communities at Laguna Pueblo to prevent against significant exposure to respirable particulate matter.

Relative to crustal average values, the respirable particulate matter collected from Laguna Pueblo is enriched in toxic metal mixtures, as evidenced by mineralogical and geochemical analyses using SEM and ICP-MS techniques. However, constraints have not been made for the abundance of these metals; estimates of some elemental concentrations, such as V, have been detected at concentrations lower than crustal averages despite the presence of uranyl vanadate minerals. During microscopy analyses, uranyl vanadate minerals in the inhalable size fraction were identified in multiple samples and are likely tyuyamunite and carnotite based on knowledge of the local geology and from preliminary research performed in the area. Carnotite [$K_2(UO_2)_2(VO_4)_2 \cdot 3H_2O$] has been identified at the Jackpile Mine in the South Paguate Pit and is typically found in sandstone near carbonaceous fossil matter as an

alteration product of uraninite. Tyuyamunite [$Ca(UO_2)_2V_2O_8 \cdot (5\text{-}8)H_2O$] has been identified at Jackpile Mine in the South Paguate Pit (Anthony et al., 2001).

At least one uranyl arsenate mineral was identified during microscopy analyses and is likely abernathyite; however, there is a possibility a mineral with a similar chemical composition is also present, metazeunerite. The main difference in the composition of these minerals is either the presence of K or Cu concurrent with U and As. Abernathyite [$K(UO_2)(AsO_4) \cdot 4H_2O$] has previously been identified at Temple Mountain, Utah in uriniferous sandstones, as well as in South Dakota, Colorado, and Arizona. This mineral has not been previously identified at the Jackpile Mine (Anthony et al., 2001; U.S. Atomic Energy Commission et al., 1956). Metazeunerite [$Cu(UO_2)_2(AsO_4)_2 \cdot 8H_2O$] has been identified in the Temple Mountain region concurrent with abernathyite. It has also been identified at several other locations including Utah, Nevada, Arizona, and Alaska. (Anthony et al., 2001; U.S. Atomic Energy Commission et al., 1952). The presence of metazeunerite is difficult to detect because the material used for analyses is made of Cu; therefore, further investigation of the mineral composition is necessary for identification.

A common mineralogic property of many of the U-bearing particles observed with SEM is both fracture and cleavage of large particles into several smaller particles of the inhalable size fraction; this indicates particulate matter is susceptible to erosion and fragmentation during windblown transport. These minerals are relatively soft, and many have micaceous cleavage properties, which makes them susceptible to erosion, weathering, and transport throughout the area. While carnotite and tyuyamunite are minerals known to be

present in the area, the presence of uranyl arsenate minerals, possibly abernathyite and metazeunerite, is a new observation that indicates inhalation exposure risks to both U and As.

The results from ICP-MS revealed several toxic metals of concern by the USEPA that are enriched in the particulate matter relative to crustal average values, including U, As, Pb, Zn, and Cu. Other elements observed to be enriched in samples relative to crustal averages which may pose a significant health risk include Cd, Sn, Mo, and Co. Many of the elements identified as enriched in the particulate matter samples relative to crustal averages are chalcophile elements; however, sulfide minerals have not been identified in the soils. Sulfur concentrations were not analyzed using ICP-MS; this element was identified on some of the particulate matter samples during microscopy analyses. Estimations of absolute concentrations of U, As, Pb, and V all indicate values higher than crustal averages. The concentrations are higher than OSHA worker standards, but this is to be expected because the total volume of dust was analyzed, not just the inhalable size fraction, which makes up ~20 – 40% of the total volume of dust (Derbyshire, 2007). There are also no data to support evaluation of exposure to toxic metal mixtures, rather than individual elemental exposure. The samples represent a wide range of particulate matter sizes, and microscopy analyses revealed several instances of respirable uranyl vanadate and uranyl arsenate minerals, but these data do not constrain the abundances of the elements analyzed. The enrichments of toxic metals relative to crustal average values indicate a larger presence of the elements in the region; however, many of the elements are already present in concentrations higher than global crustal averages due to enrichments in the ore material that was sought for mining. Several U-bearing particles observed during microscopy have a tendency to erode and fragment into smaller particles of the inhalable size

fraction, which indicates a possible exposure risk. A study from New Mexico Institute of Mining and Technology by Reid Brown (2017) evaluated toxic metal concentrations in soils at Laguna Pueblo and detected elevated concentrations of U, V, Cr, Mn, Zn, and Pb compared to background concentrations. The background data utilized for this research was gathered from the National Uranium Resource Evaluation (NURE), which was conducted from 1975-1980. This study also determined that toxic metals have an affinity for the smallest size fractions, which have greater mobility in response to windblown transport; however, V was found to have significantly lower concentrations in the dust samples than in the soil. Vegetation type and height was found to be an important variable influencing toxic metal concentrations; variations in the height of the sample equipment resulted in variations of metal concentrations, with greater heights correlating with higher concentrations (Brown, 2017). Toxicologists with UNM METALS have shown that dust profiles with higher U and V concentrations are more toxic to humans; however, it remains unknown if real-life exposures pose significant harm after tests involving exposure of mice to concentrated air from Laguna Pueblo.

CHAPTER 6- CONCLUSIONS AND RECOMMENDATIONS

The most significant atmospheric parameter determining transport of airborne particulate matter in the inhalable size fraction in a semiarid region with variable topography is relative humidity. Low relative humidity conditions are most conducive to windblown transport of PM $\leq$10 μm; these findings are supported by soil moisture estimations derived from soil matric potential calculations based on local meteorological data for relative humidity and

temperature. A threshold for relative humidity ≤35% is observed which prevents the formation of aggregates through a cohesive water layer between particles. Highly unsaturated soils are common in the region, leaving particulate matter sourced from the top layer of soil susceptible to windblown transport; this material is generally only saturated during precipitation events, making particulate matter more difficult to entrain by wind while wet. High evaporation rates in the area result in only short periods of soil saturation before the top layer dries and returns to an unsaturated state.

The influence of slow wind speeds on particulate matter concentrations in the inhalable size fractions is likely significant; however, this variable was unable to be fully evaluated due to lack of data. A seasonal effect should be considered in future research, especially as it relates to changes in relative humidity. A relationship between wind speed and relative humidity may contribute to elevated concentrations of respirable particulate matter; both variables have been found to significantly influence particulate matter concentrations in previous studies. Results indicating high particulate matter concentrations during conditions of wind speed at 0 m/s are most likely the effect of PM ≤20 μm having been found to have long-term suspension and can linger in the atmosphere for 1-2 weeks, especially during periods without precipitation events. Dust particles have greater interparticle cohesive forces than larger particles and are most likely to be lifted by the impacts of saltation from these larger particles ~70-100 μm (Kok et al., 2012). The findings in this study further our scientific understanding of windblown transport in a semiarid region, and more data collection will help to fill the gaps left by this study. Regional climate data with the NARR model is useful for comparison but local data collection is more reliable and can resolve processes on a smaller scale, as the sites represent data closer to the

surface. This effect was more significant with wind data than with relative humidity and temperature data. Maintaining the 4 local stations for meteorological data collection is recommended for research going forward. It is also recommended that the DustTrak Aerosol Monitor be co-located with each of the Kestrel Weather Meters on a regular schedule.

Metal-bearing respirable particulate matter identified with SEM and EDS include uranyl vanadate minerals that are likely tyuyamunite and carnotite, as well as uranyl arsenate minerals that are likely abernathyite and possibly metazeunerite. Only 1of the 6 samples analyzed was found to have no U-bearing particles; this sample was exposed to the largest amount of wind from the direction of the Jackpile Mine. This suggests there is not a significant correlation between U-bearing particulate matter and wind coming directly from the mine; the particulate matter is assumed to be highly distributed throughout the area from the duration of the 30-year mining process and subsequent climatic processes including wind and precipitation events. There are also several other AUMs in the area that cannot be excluded as sources of contamination. At this time, it cannot be determined whether the Jackpile Mine is the source of the minerals collected from Laguna Pueblo; the main ore minerals uraninite and coffinite have not been identified, only uranyl vanadate minerals, which may be present in the local sandstones and could represent background material. The U-bearing particulate matter observed with SEM appears to be susceptible to erosion and fragmentation during windblown transport, increasing the abundance of respirable particulate matter containing toxic metal mixtures. It is recommended that future research analyze particulate matter with other microscopy technologies, such as transmission electron microscopy (TEM) to better identify minerals and their characteristics.

Particulate matter samples from 2 sites on Laguna Pueblo, Mesita Village and Old Laguna Village, are enriched in toxic metal mixtures relative to crustal averages. Several toxic metals were identified in higher than crustal average values, including U, As, Pb, Cu, Cd, and Zn. Additionally, concentrations of Mo and Sn were identified as higher than crustal averages. Individual concentration estimates of U reach concentrations up to 223 ppm; for As the maximum individual sample concentration reaches up to 331 ppm and Pb reaches up to 63.7 ppm. The enrichment relative to crustal average values of these toxic metal mixtures in respirable particulate matter may pose potential health risks for local tribal communities; however, these concentrations are based on samples that also include particulate matter of coarser grain sizes that are too large to be inhaled and at a flow rate higher than the average human inhalation rate.

It is recommended to adjust the Tisch High Volume Air Samplers to filter for collection of only PM $\leq$2.5 μm, allowing for the results from ICP-MS to reflect only that of the respirable particulate matter, which is of most concern for inhalation exposure risk. Continuation of sample analyses for toxic metal concentrations throughout the year is recommended to assess the consistency of toxic metal enrichment in particulate matter samples and analyze seasonal changes that may influence concentrations. It is also recommended that the Tisch High Volume Air Samplers be rotated to each of the 4 local stations, including one to be co-located with the DustTrak Aerosol Monitor at all times. This will allow for direct comparison of respirable particulate matter concentrations with particulate matter enrichment of toxic metal mixtures.

This research identified a potential inhalation exposure risk to toxic metal mixtures that exists for the local tribal communities at Laguna Pueblo based on meteorological,

mineralogical, and geochemical analyses of locally collected data. The direct link to the Jackpile Mine and full potential exposure remains to be established. The combination of these methods for analyses allowed for the evaluation of climatic conditions influencing windblown dust transport of airborne particulate matter, as well as identification of minerals and toxic metal mixture concentrations within the respirable particulate matter collected from Laguna Pueblo.

REFERENCES

Adams, S.S., Curtis, H.S., Hafen, P.L., and Salek-Nejad, H., 1978, Interpretation of postdepositional processes related to the formation and destruction of the Jackpile-Paguate uranium deposit, Northwest New Mexico: Economic Geology, v. 73, p. 1635–1654, doi: 10.2113/gsecongeo.73.8.1635.

Anthony, J.W., Bideaux, R.A., Bladh, K.W., and Nichols, M.C., 2001, Abernathyite; Carnotite; Metazeunerite; Tyuyamunite, in Handbook of Mineralogy, Chantilly, VA, Mineralogical Society of America, v. 4.

ATSDR, 2018, Toxic Substances Portal - Uranium: Centers for Disease Control and Prevention, p.1-11, https://www.atsdr.cdc.gov/PHS/PHS.asp?id=438&tid=77.

Brown, R.D., 2017, Geochemistry and Transport of Uranium-Bearing Dust at Jackpile Mine, Laguna, New Mexico, p. 1-100.

Campbell, G., 2016, Estimating relative humidity in soil: How to stop doing it wrong - enviro...: Environmental Biophysics, https://www.environmentalbiophysics.org/what-is-the-relative-humidity-in-soil/ (accessed August 2021).

CCME, 2007, Canadian Soil Quality Guidelines for Uranium: Environmental and Human Health, Canadian Council of Ministers of the Environment, p. 1-129.

Cichowicz, R., Wielgosiński, G., and Fetter, W., 2020, Effect of wind speed on the level of particulate matter PM10 concentration in atmospheric air during winter season in vicinity of large combustion plant: Journal of Atmospheric Chemistry, v. 77, p. 35–48, doi: 10.1007/s10874-020-09401-w.

Committee on Uranium Mining in Virginia, 2011, Potential Human Health Effects of Uranium Mining, Processing, and Reclamation: Uranium Mining in Virginia: Scientific, Technical, Environmental, Human Health and Safety, and Regulatory Aspects of Uranium Mining and Processing in Virginia., https://www.ncbi.nlm.nih.gov/books/NBK201047/.

Csavina, J., Field, J., Félix, O., Corral-Avitia, A.Y., Sáez, A.E., and Betterton, E.A., 2014, Effect of wind speed and relative humidity on atmospheric dust concentrations in semi-arid climates: Science of The Total Environment, v. 487, p. 82–90, doi: 10.1016/j.scitotenv.2014.03.138.

Derbyshire, E., 2007, Natural minerogenic dust and human health: AMBIO: A Journal of the Human Environment, v. 36, p. 73–77, doi: 10.1579/0044-7447(2007)36[73:nmdahh]2.0.co;2.

Dixon, E., 2015, The Legacy Uranium Mining and Milling Clean Up Plan: Evaluation of the EPA Five-Year Plan, Grants Mining District, New Mexico., p. 1-109.

DuBois, D., 2020, Climate in New Mexico: NM Climate Center | New Mexico State University, https://weather.nmsu.edu/climate/about/.

Gorospe, M. J. (2013). Uranium mobility in vegetation, soils and water below the Jackpile Uranium Mine, New Mexico. New Mexico Institute of Mining and Technology.

HPS, 2018, Health Physics Society Specialists on Radiation Safety: Uranium Fact Sheet, p. 1-5, https://hps.org/documents/uranium_fact_sheet.pdf.

Huggett, R.J., 2017, Fundamentals of geomorphology: Milton Park, Abingdon, Oxon, Routledge.

Kok, J.F., Parteli, E.J.R., Michaels, T.I., and Karam, D.B., 2012, The physics of wind-blown sand and dust: Reports on Progress in Physics, v. 75, p. 1-119, doi: 10.1088/0034-4885/75/10/106901.

Lewis, J., Hoover, J., and Mackenzie, D., 2017, Mining and Environmental Health Disparities in Native American Communities: Current Environmental Health Reports, v. 4, p. 130–141, doi: 10.1007/s40572-017-0140-5.

Liu, J., and Lewis, G., 2014, Environmental Toxicity and Poor Cognitive Outcomes in Children and Adults: J Environ Health, v. 76, p. 130–138.

Martin, R., Dowling, K., Pearce, D.C., Florentine, S., Mcknight, S., Stelcer, E., Cohen, D.D., Stopic, A., and Bennett, J.W., 2016, Trace metal content in inhalable particulate matter (PM2.5–10 and PM2.5) collected from historical mine waste deposits using a laboratory-based approach: Environmental Geochemistry and Health, v. 39, p. 549–563, doi: 10.1007/s10653-016-9833-1.

Moench, R.H., and Schlee, J.S., 1967, Geology and Uranium Deposits of the Laguna District, New Mexico: United States Atomic Energy Commission., p. 1–122.

Naiman, Z., Quade, J., and Patchett, P., 2000, Isotopic evidence for eolian recycling of pedogenic carbonate and variations in carbonate dust sources throughout the southwest United States: Geochimica et Cosmochimica Acta, v. 64, p. 3099–3109, doi: 10.1016/s0016-7037(00)00410-5.

Nash, J.T., 1968, Uranium deposits in the Jackpile Sandstone, New Mexico: Economic Geology, v. 63, p. 737–750, doi: 10.2113/gsecongeo.63.7.737.

Niu, J., Liberda, E.N., Qu, S., Guo, X., Li, X., Zhang, J., Meng, J., Yan, B., Li, N., Zhong, M., Ito, K., Wildman, R., Liu, H., Chen, L.C., et al., 2013, The Role of Metal Components in the Cardiovascular Effects of PM2.5: PLoS ONE, v. 8, doi: 10.1371/journal.pone.0083782.

NOAA., 2000, National Climatic Data Center (NCDC): U.S. Climate Normals., https://www.ncdc.noaa.gov/climatenormals/clim60/states/Clim_NM_01.pdf.

NPS., 2019, Arid and Semi-arid Region Landforms: National Parks Service, https://www.nps.gov/subjects/geology/arid-landforms.htm.

Neuman, C. M. K., & Sanderson, S., 2008, Humidity control of particle emissions in aeolian systems. Journal of Geophysical Research, v. 113. https://doi.org/10.1029/2007jf000780

OSHA., 2019, United States Dept. of Labor: OSHA Annotated PELs | Occupational Safety and Health Administration, https://www.osha.gov/dsg/annotated-pels/tablez-1.html.

Pueblo of Laguna, n.d., Natural Resources Program: Environment and Natural Resources Department, https://www.lagunapueblo-nsn.gov/Natural_Resouces.aspx.

Rahimi-Gorji, M., Pourmehran, O., Gorji-Bandpy, M., and Gorji, T.B., 2015, CFD simulation of airflow behavior and particle transport and deposition in different breathing conditions through the realistic model of Human Airways: Journal of Molecular Liquids, v. 209, p. 121–133, doi: 10.1016/j.molliq.2015.05.031.

Ravi, S., Dodorico, P., Over, T. M., & Zobeck, T. M., 2004, On the effect of air humidity on soil susceptibility to wind erosion: The case of air-dry soils. Geophysical Research Letters, 31(9). doi: 10.1029/2004gl019485

Ravi, S., Zobeck, T. M., Over, T. M., Okin, G. S., & Dodorico, P., 2006, On the effect of moisture bonding forces in air-dry soils on threshold friction velocity of wind erosion. Sedimentology, 53(3), 597–609. doi: 10.1111/j.1365-3091.2006.00775.x

Riley, R., 2019, Testimony: Oversight Field Hearing on “America’s Nuclear Past: Examining the Effects of Radiation in Indian Country”: Senate Committee on Indian Affairs., p. 1-6.

Sittnick, P., 1998, Uranium Mining and Its Impact on Laguna Pueblo: A Study Guide, p. 1-22.

U.S. Atomic Energy Commission., Department of the Interior., Thompson, M.E., Ingram, B., and Gross, E.B., 1952, Reconnaissance for Radioactive Deposits in the Lower Yukon-Kuskokwim Region, Alaska: Grand Junction, Colorado, U.S. Geological Survey, p. 82–90.

U.S. Atomic Energy Commission., Department of the Interior., White, M.G., Killeen, P.L., and West, W.S., 1956, Abernathyite, A New Uranium Mineral of the Metatorbernite Group: Washington, D.C., U.S. Geological Survey, p. 1–10.

U.S. Bureau of Land Management., Bureau of Indian Affairs., Rio Puerco Resource Area., Albuquerque Area Office., 1986, Final environmental impact statement for the

Jackpile-Paguate Uranium Mine Reclamation Project: Laguna Indian Reservation, Cibola County, New Mexico: Albuquerque, NM, U.S. Dept. of the Interior, Bureau of Land Management, Albuquerque District Office, p. 1-252.

U.S. Environmental Protection Agency, and Turner, L., 2012, The Grants Mining District and Jackpile-Paguate Uranium Mine: United States Environmental Protection Agency.

U.S. Environmental Protection Agency., 2015, Jackpile-Paguate Uranium Mine SF Site Status Summary; United States Environmental Protection Agency.

U.S. Environmental Protection Agency., 2017, Jackpile-Paguate Uranium Mine Site Profile: United States Environmental Protection Agency.

Wells, S.G., 1989, A synthesis and review of geomorphic surfaces of the boundary zone Mt. Taylor to Lucero uplift area, West-Central New Mexico: doi: 10.2172/148689.

Wilton, T., 2017, Uranium Deposits at the Cebolleta Project, Laguna Mining District, Cibola Count, New Mexico: New Mexico Geology, v. 39, p. 1–10.

Xing, Y.-F., Xu, Y.-H., Shi, M.-H., and Lian, Y.-X., 2016, The Impact of PM2.5 on the Human Respiratory System: Journal of Thoracic Disease, v. 8, p. 1–6.

Zhang, B., Jiao, L., Xu, G., Zhao, S., Tang, X., Zhou, Y., and Gong, C., 2017, Influences of wind and precipitation on different-sized particulate matter concentrations (PM2.5, PM10, PM2.5–10): Meteorology and Atmospheric Physics, v. 130, p. 383–392, doi: 10.1007/s00703-017-0526-9.

APPENDIX I – *Additional Mineralogical Results & Sample Preparation Procedure*

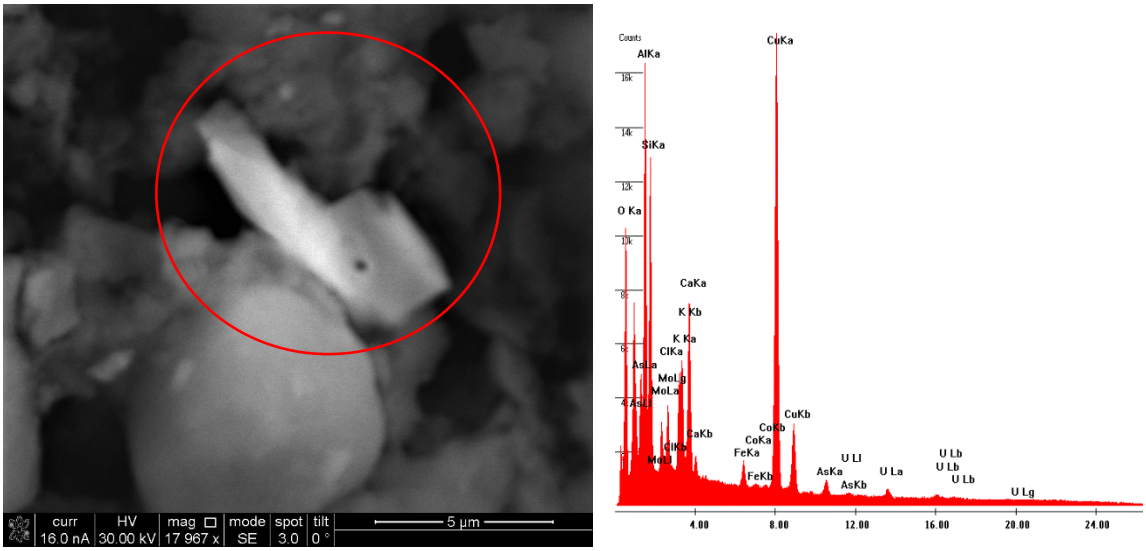

Figure 42: Backscattered electron image and EDS spectrum of 8.32 µm uranyl arsenate particle in sample 1003 from Mesita Village.

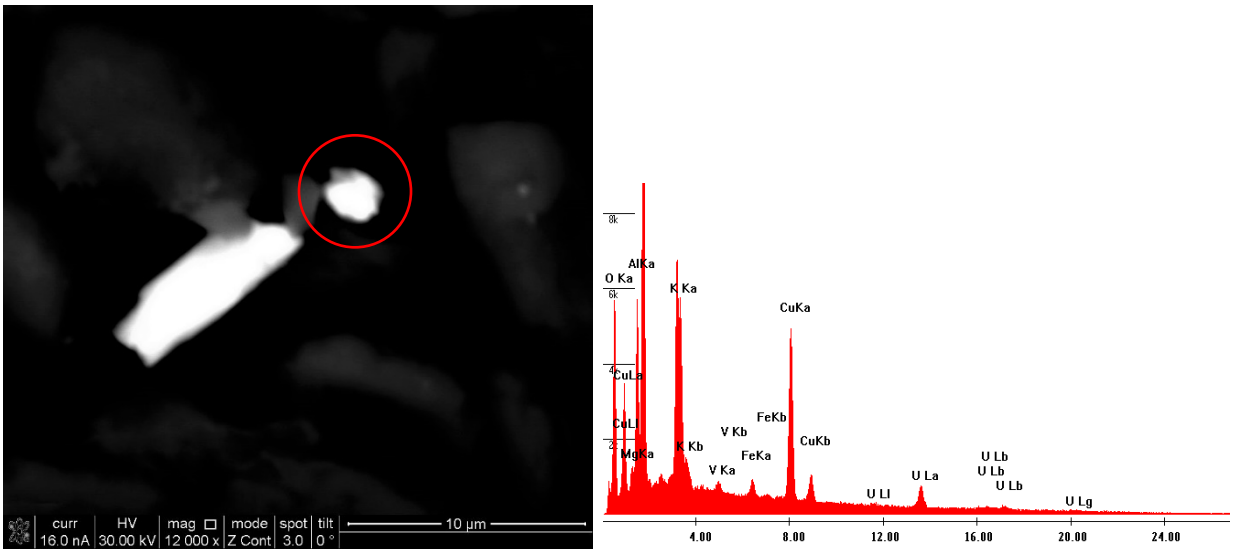

Figure 43: Backscattered electron image and EDS spectrum of 2.55 µm uranyl vanadate particle in sample 1003 from Mesita Village.

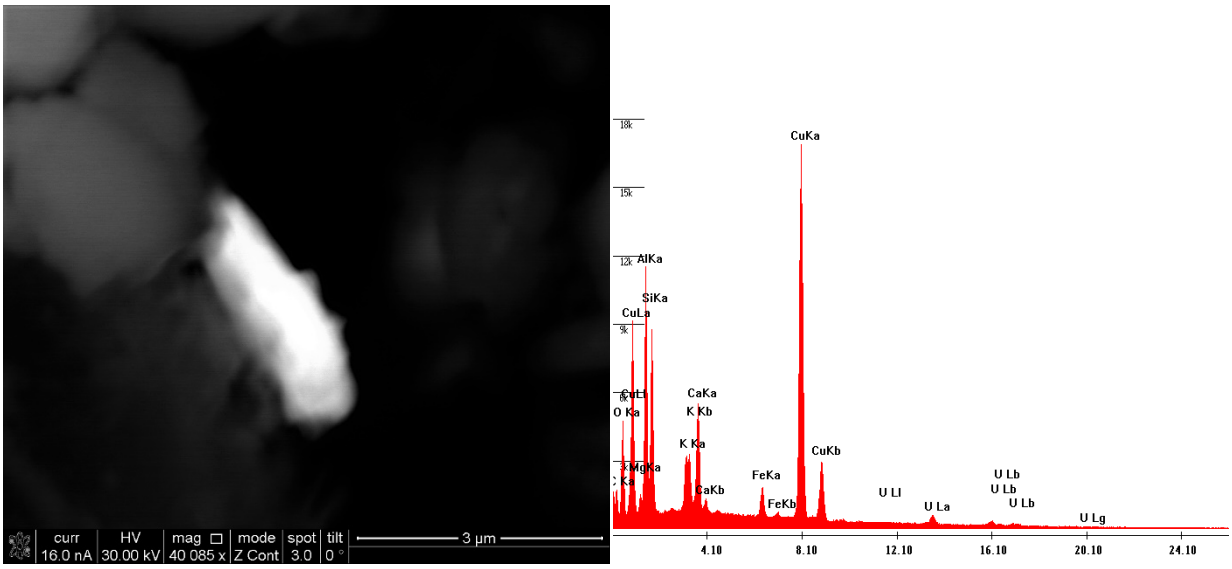

Figure 44: Backscattered electron image and EDS spectrum of 3.06 µm U-bearing particle in sample 1003 from Mesita Village.

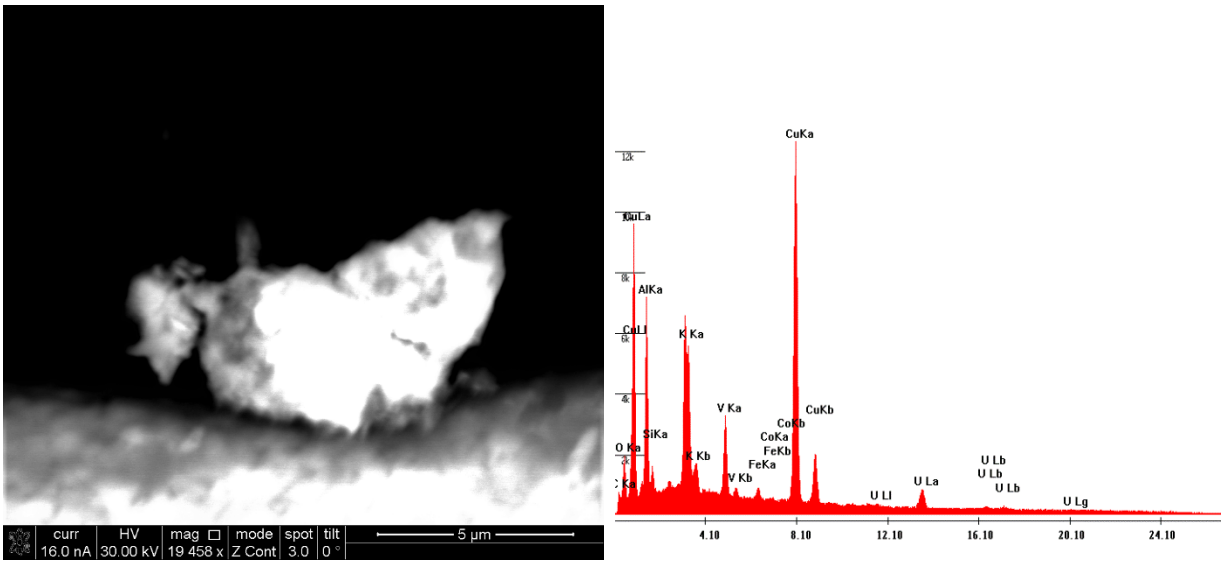

Figure 45: Backscattered electron image and EDS spectrum of 8.48 µm uranyl vanadate particle in sample 1003 from Mesita Village.

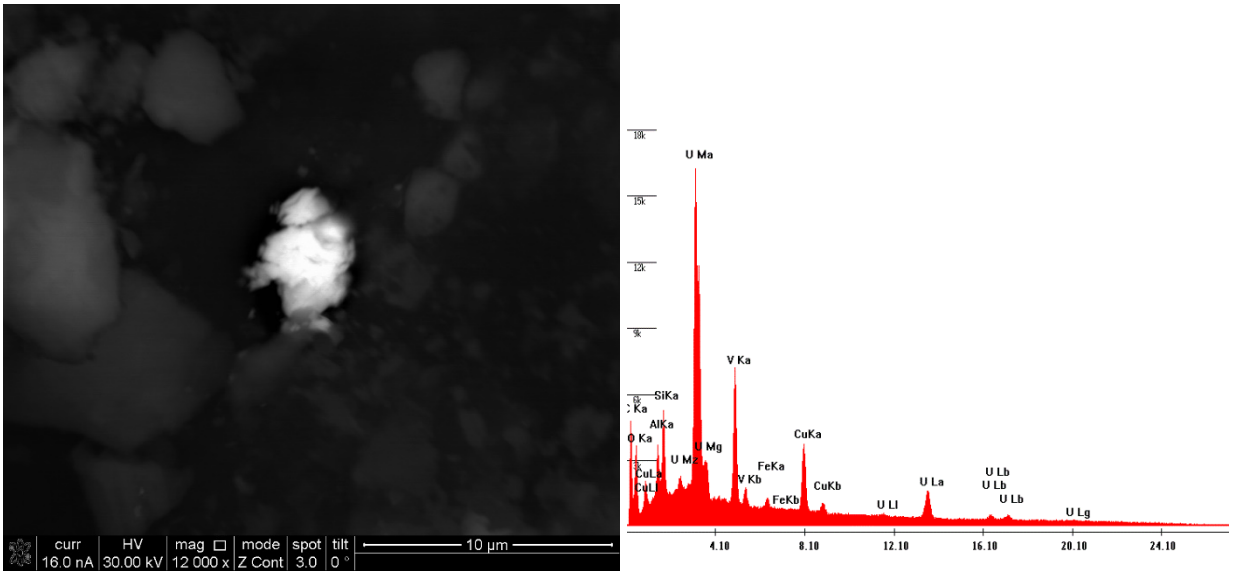

Figure 46: Backscattered electron image and EDS spectrum of 5.53 µm uranyl vanadate particle in sample 1003 from Mesita Village.

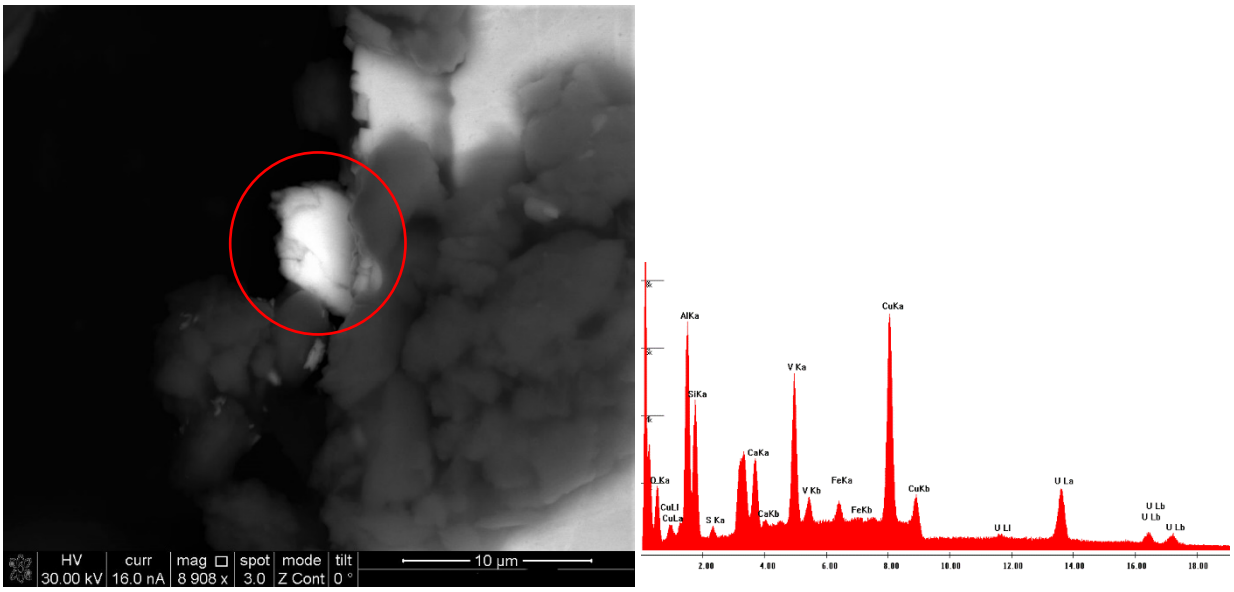

Figure 47: Backscattered electron image and EDS spectrum of 6.98 µm uranyl vanadate particle in sample 1004 from Mesita Village.

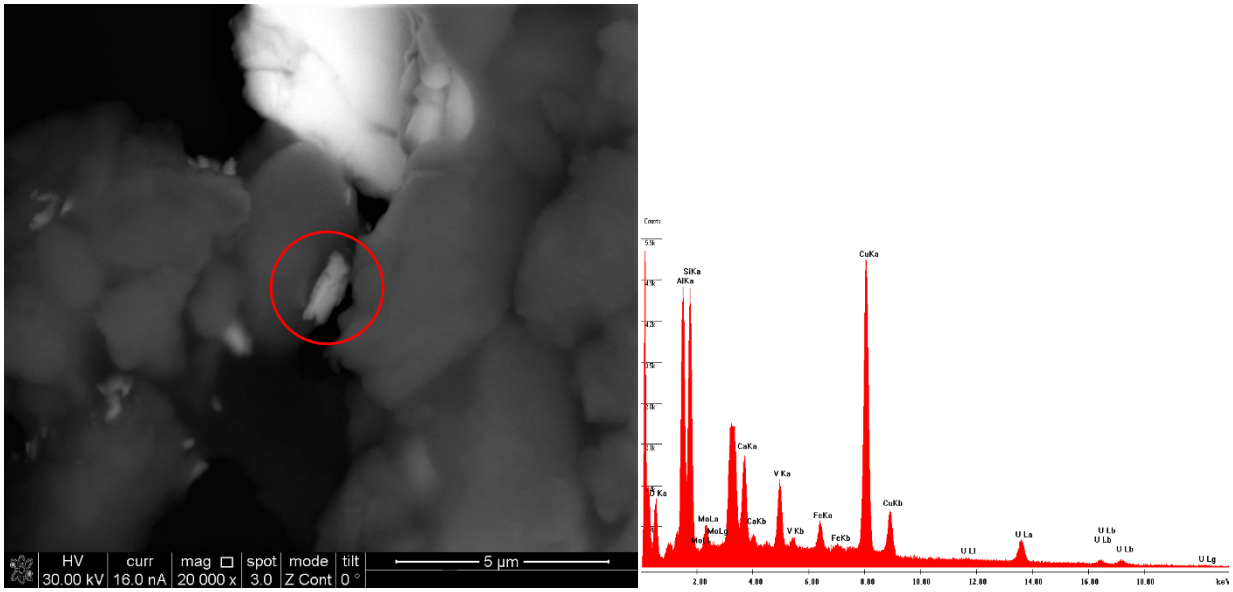

Figure 48: Backscattered electron image and EDS spectrum of 1.64 µm uranyl vanadate particle in sample 1004 from Mesita Village.

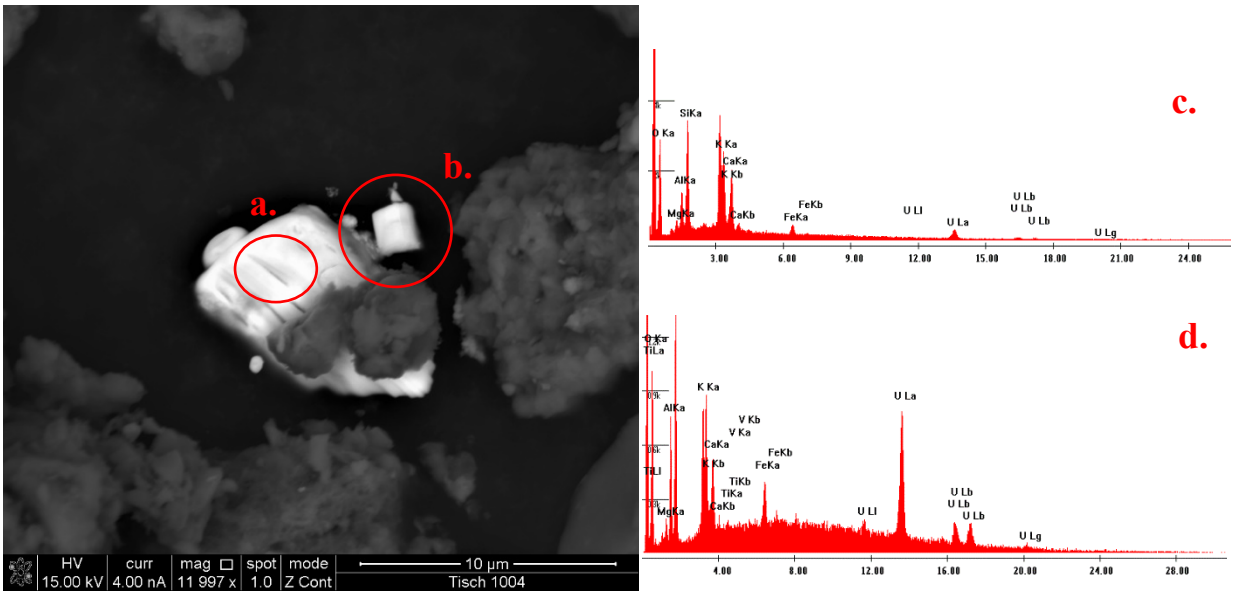

Figure 49: Backscattered electron image and EDS spectra of 9.13 µm (a) and 2.13 µm (b) U-bearing particles in sample 1004 from Mesita Village.

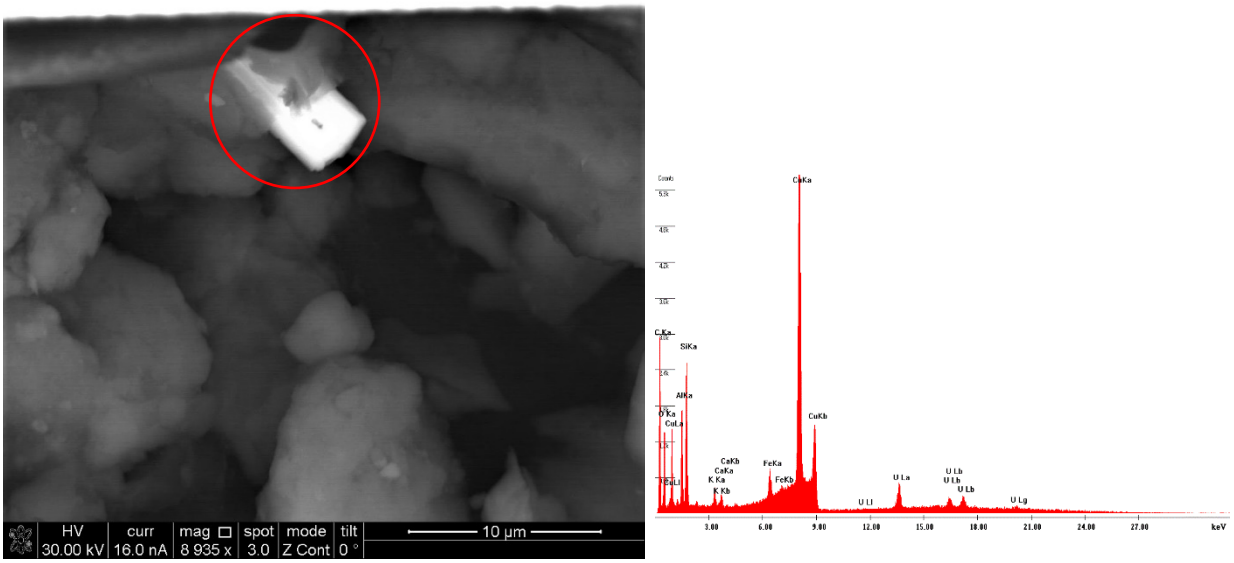

Figure 50: Backscattered electron image and EDS spectrum of 8.07 µm U-bearing particle in sample 1005 from Old Laguna Village.

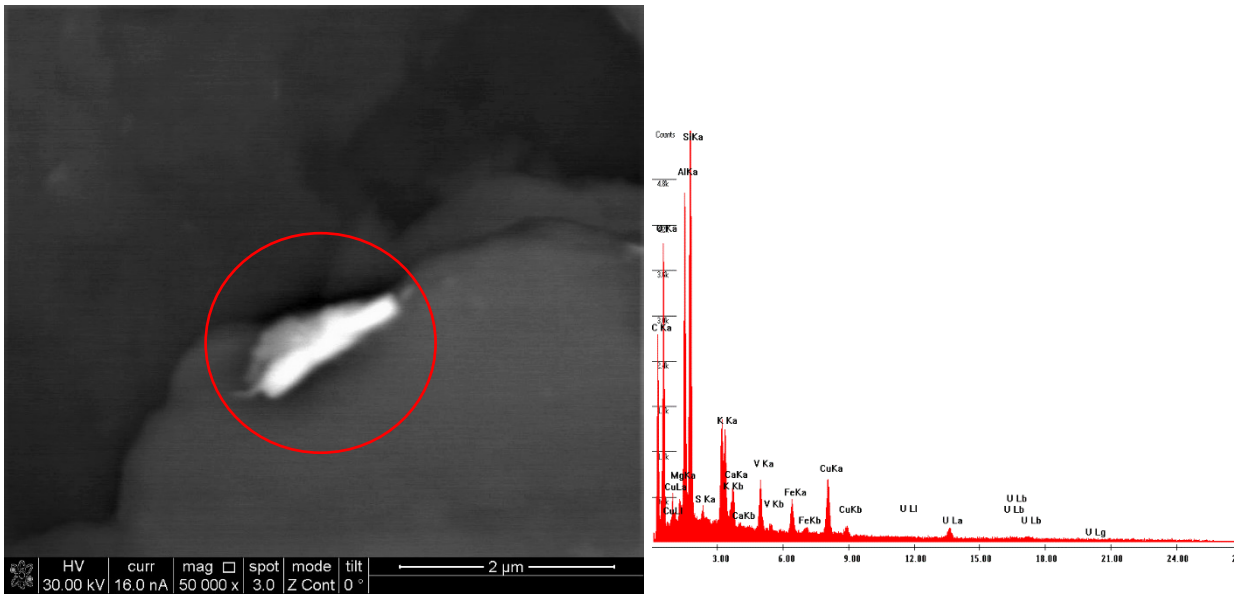

Figure 51: Backscattered electron image and EDS spectrum of 1.56 µm uranyl vanadate particle in sample 1005 from Old Laguna Village.

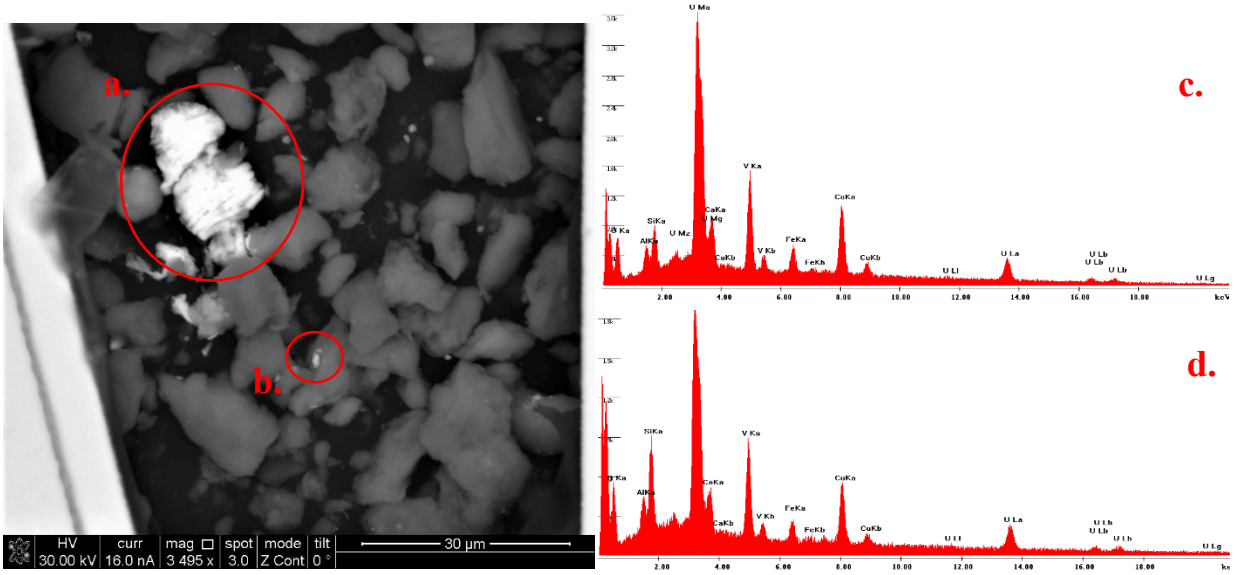

Figure 52: Backscattered electron image and EDS spectra of 19.95 µm (a) and 2.70 µm (b) uranyl vanadate particles in sample 1005 from Old Laguna Village.

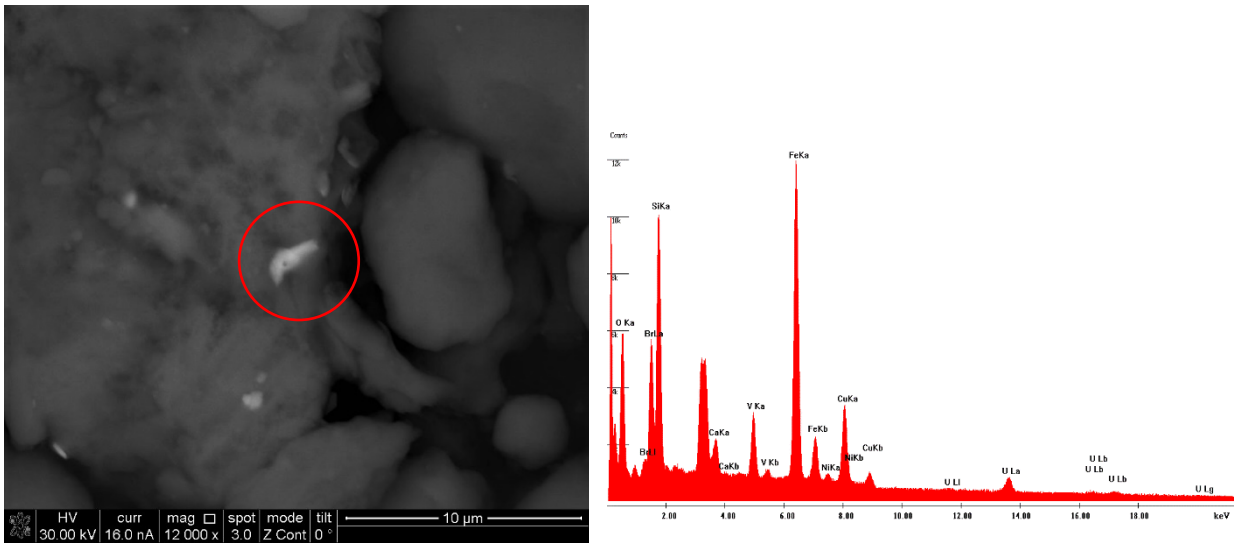

Figure 53: Backscattered electron image and EDS spectrum of 2.16 µm uranyl vanadate particle in sample 1005 from Old Laguna Village.

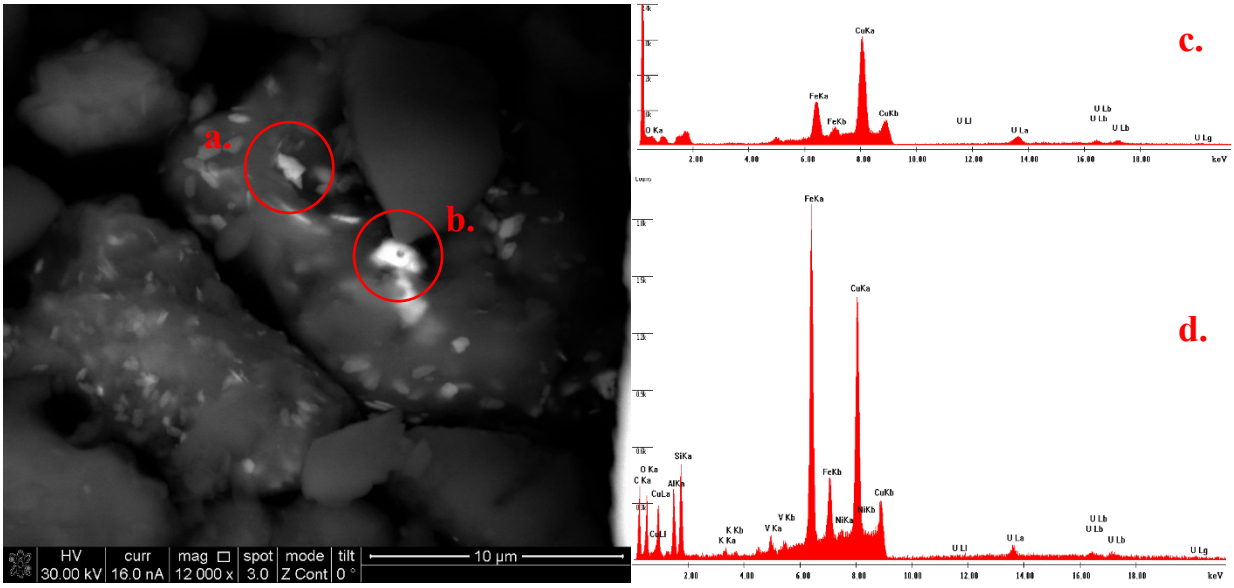

Figure 54: Backscattered electron image and EDS spectra of 1.54 µm (a) and 1.65 µm (b) uranyl vanadate particles in sample 1005 from Old Laguna Village. Each of the particles ~1µm that appear brighter than the background material were analyzed with EDS and produced spectra similar to those presented (c-d).

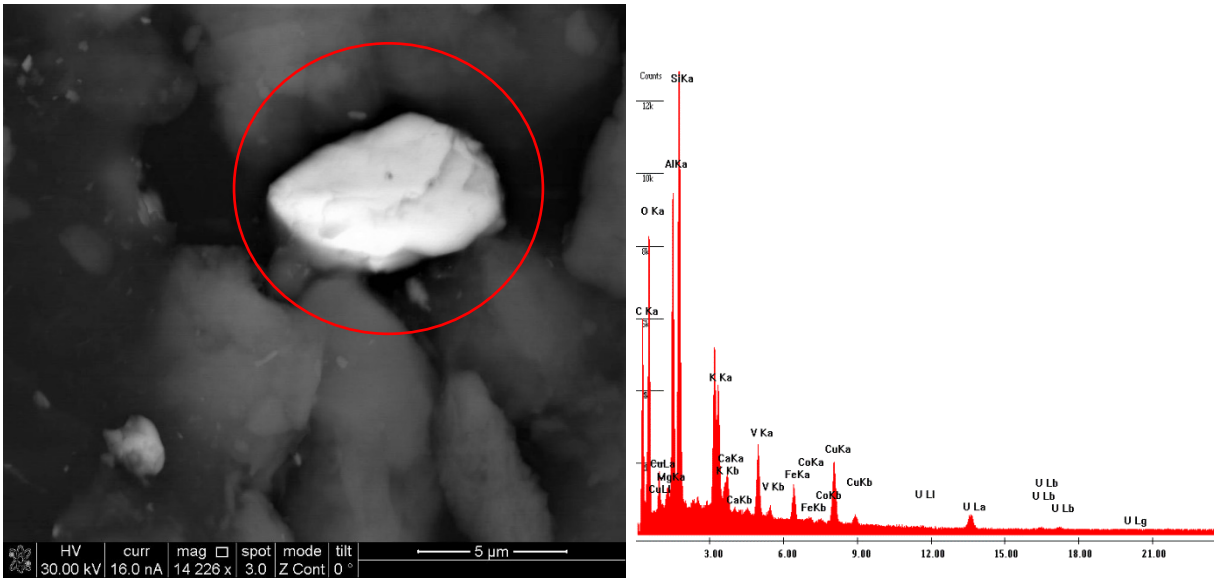

Figure 55: Backscattered electron image and EDS spectrum of 7.73 µm uranyl vanadate particle in sample 1005 from Old Laguna Village.

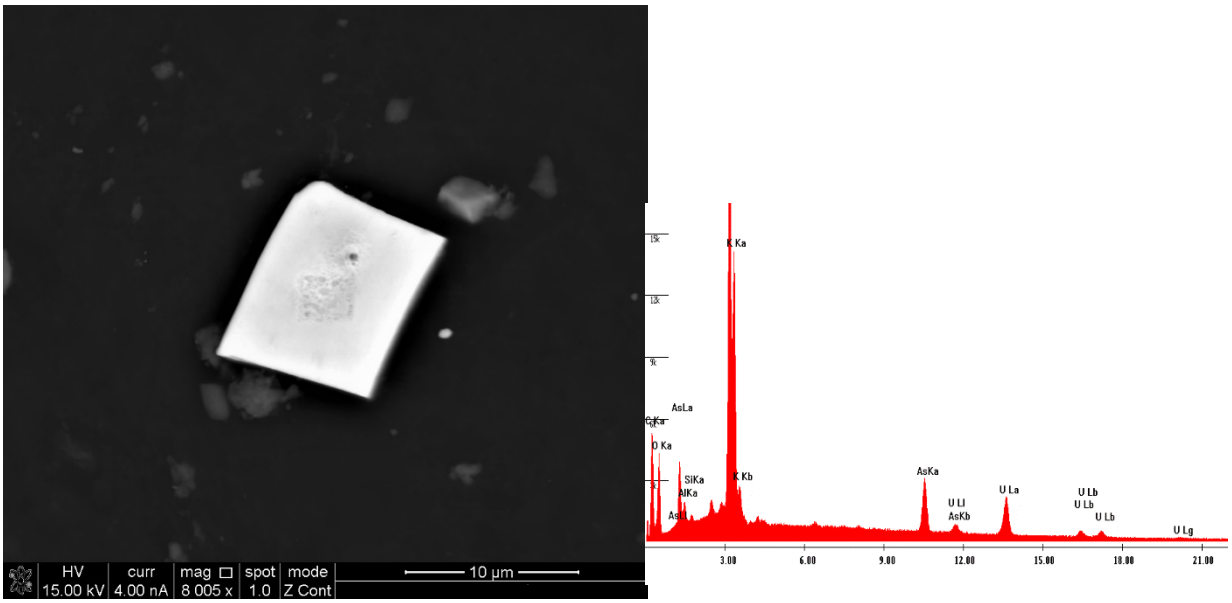

Figure 56: Backscattered electron image and EDS spectrum of 14.5 µm uranyl arsenate particle in sample 1008 from Mesita Village.

UNM METALS Superfund Center
Environmental Project 2
Dept. of Earth & Planetary Sciences
Filter Preparation Procedure for Microscopy: Tisch High Volume Air Samples

Procedure Date: 08/03/2020

Purpose: Preparation of gravimetric samples from a Tisch High Volume Air Sampler for mineralogic analyses with microscopy using both SEM and TEM equipment.

Materials:

- Nitrile gloves
- Tisch Samples: 8" x 10" PTFE Filters
- Small Glassine Envelopes
- Pipettes
- TEM Grids
- KIMTECH Kimwipes
- Ceramic Scissors
- Anti-static Tweezers
- Filter Weight Log (or other recording sheet)
- Pen/Marker (for labeling)
- Acetone
- Glass Vials
- Filter Papers
- Stopwatch

Procedure

Sectioning Filters:

1. Put on a pair of nitrile gloves.
2. Obtain three small glassine envelopes and label with the original sample number followed by C, D and C-I (i.e. 1001C, 1001D, 1001C-I).
3. Use Duster spray to remove dust from the outside of glassine envelopes and table surfaces before removing the filter from its envelope.
    a. After removing, place the filter on top of the envelope with the identification number displayed next to the red dot on the filter and take a picture:

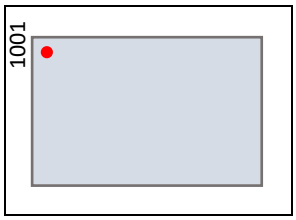

4. Cut filter into roughly equal quadrants with ceramic scissors.
    a. Take a picture:

A	C
B	D

5. Cut a ~2 cm square out of the bottom left corner of filter section C (i.e. 1001C).
    a. Take a picture:

A	C
B	D

6. Place sections A and B back into the original 8" x 10" glassine envelope (i.e. 1001A, 1001B).
    a. Will be used for ICP-MS analyses in the Analytical Chemistry Lab.
7. Gently roll sections C and D (i.e. 1001C, 1001D) inward on themselves, place in their respective small glassine envelopes and then back into the original 8" x 10" glassine envelope.
    a. If necessary, section C may be used to obtain more ~2 cm^2 sections for mineralogical analyses.
    b. To be labeled with sample number, C and progressing roman numerals (i.e. 1001C-I, 1001C-II, 1001C-III, etc.).
8. Place the C-I, ~2 cm^2 filter section into its labeled small glassine envelope.

Weighing Filter Sections Pre-Analysis:

1. Put on a pair of nitrile gloves.
2. Dust off balance and ensure it is stable.
3. Reduce static with mat on desk and anti-static spray (wait two minutes and wipe with a Kimwipe).
4. Place a weigh container on the scale (found in cabinets).
    a. Close microbalance doors and step back ~3ft.
    b. Wait until measurement is no longer fluctuating (or only in the last two decimal places).
    c. Tare the scale, once zero is reached hold zero button for at least 30 seconds.

5. Remove one filter section from glassine envelope using anti-static tweezers and place on the weigh container.
    a. Close microbalance doors and step away for 60 seconds.
    b. After 60 seconds, record pre-analysis measurement from a distance of 2ft from scale.
    c. Replace filter in envelope with tweezers.

Filter Agitation for Microscopy Analysis:

1. Put on a pair of nitrile gloves and dust area before starting sample preparation.
2. Obtain a glass vial for each C-I, ~2 cm^2 filter section to be agitated.
    a. Label each with the date, sample name and intended ultrasonic bath time (see #5 below).
3. Use anti-static scissors to roll filter section into a scroll with the sample side facing outward and place into the corresponding labeled vial.
4. Fill vials with acetone, tighten the lids and place into 50mL beaker with ~10mL DI water.
5. Place the beaker into the ultrasonic bath, close the lid and turn the dial to 10 minutes.
    a. Use a stopwatch/timer to ensure 10 minutes for each vial; do not rely on ultrasonic bath timer.
6. After 10 minutes, remove the beaker and take out the vials.
    a. Allow for particles to settle.
7. Obtain filter paper (FIB lab cabinet) and label one for each of the samples in a vial in preparation for removal.
    a. Also obtain new small glassine envelopes for the filters and label with identification numbers.
8. Carefully and slowly remove filter from vial with anti-static tweezers and place on corresponding filter paper to allow for evaporation.
    a. Attempt to avoid spilling any liquid.
    b. Allow 5-10 minutes for evaporation.
    c. Place cap back on vial and set aside.
9. Once dry, place each filter into the new small glassine envelope and place that back into the original 8” X 10” glassine envelope.

Weighing Filter Sections Post-Analysis:

1. Put on a pair of nitrile gloves.
2. Dust off balance and ensure it is stable.
3. Reduce static with mat on desk and anti-static spray (wait two minutes and wipe with a Kimwipe).
4. Place a weigh container on the scale.
    a. Close microbalance doors and step back ~3ft.

    b. Wait until measurement is no longer fluctuating (or only in the last two decimal places)
    c. Tare the scale, once zero is reached hold zero button for at least 30 seconds.
5. Remove one filter section from glassine envelope using anti-static tweezers and place on the weigh container.
    a. Close microbalance doors and step away for 60 seconds.
    b. After 60 seconds, record post-analysis measurement from a distance of 2ft from scale.
    c. Replace filter in envelope with anti-static tweezers.

Prepare Sample on TEM Grid (for use in SEM):

1. Put on a pair of nitrile gloves.
2. Allow glass vials with sample material to settle before continuing (i.e., glass vials labeled 1001C-I, 1003C-I, etc.).
3. Remove the lid of the glass vial.
    a. Using a pipette, remove ~50-80% of the liquid on top.
    b. Remaining material should be most of the particulate matter of interest.
4. Obtain 3mm copper TEM grid with holy carbon substrate to support particles.
    a. Use carbon tape and anti-static tweezers to adhere TEM grid to SEM pin mount.
5. Shake glass vial and use pipette to collect a small amount of the material in suspension.
    a. Expel the material on TEM grid secured to SEM pin mount.
    b. Only release the amount of material that covers the grid.

APPENDIX II – *Additional Geochemical Results & Sample Preparation Procedure*

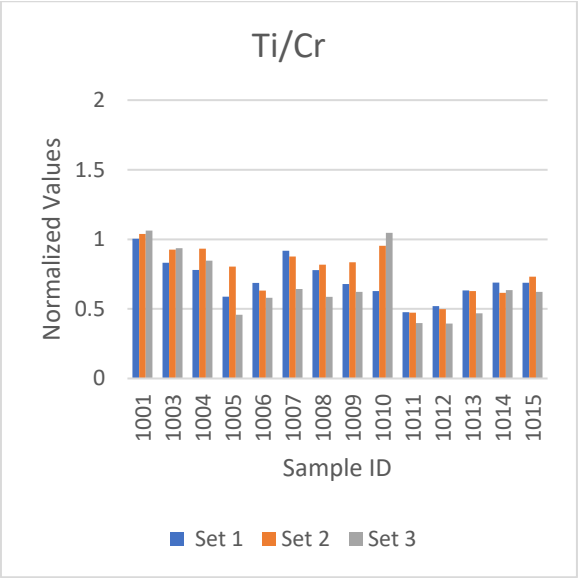

Figure 57: Normalized plot for Ti/Cr using ICP-MS results.

Table 5: ICP-MS Raw Data Results in µg/L as Elemental Ratios.

	U/Ti	V/Ti	Pb/Ti	As/Ti	U/Cr	V/Cr	Pb/Cr	As/Cr
Sample ID								
B1 - 1001	0.000601	0.019610	0.009456	0.001426	0.032878	1.073507	0.517626	0.078048
B1 - 1003	0.002768	0.019426	0.013301	0.002041	0.125531	0.881105	0.603284	0.092573
B1 - 1004	0.003642	0.019876	0.011006	0.002174	0.154921	0.845498	0.468190	0.092465
B1 - 1005	0.009928	0.016713	0.012218	0.003610	0.317979	0.535313	0.391325	0.115620
B1 - 1006	0.019548	0.016801	0.010616	0.006769	0.731927	0.629071	0.397502	0.253434
B1 - 1007	0.001216	0.018663	0.010048	0.002487	0.060807	0.933497	0.502610	0.124400
B1 - 1008	0.004562	0.018224	0.008902	0.003127	0.193648	0.773496	0.377856	0.132703
B1 - 1009	0.001305	0.018414	0.012243	0.003804	0.048250	0.681000	0.452765	0.140689
B1 - 1010	0.013952	0.020139	0.010615	0.005500	0.477480	0.689201	0.363252	0.188227
B1 - 1011	0.001819	0.017590	0.018754	0.019304	0.047171	0.456192	0.486356	0.500625
B1 - 1012	0.001274	0.015193	0.015244	0.005061	0.036115	0.430611	0.432042	0.143434
B1 - 1013	0.001184	0.017079	0.016597	0.003836	0.040836	0.589169	0.572525	0.132342
B1 - 1014	0.000519	0.017848	0.009680	0.002442	0.019497	0.670869	0.363864	0.091777
B1 - 1015	0.000782	0.016266	0.012816	0.004501	0.029311	0.609728	0.480415	0.168713
B2 - 1001	0.000712	0.020468	0.008757	0.002644	0.040322	1.158588	0.495700	0.149675
B2 - 1003	0.000985	0.019387	0.009723	0.002374	0.049728	0.978432	0.490698	0.119797
B2 - 1004	0.002968	0.020027	0.008718	0.003784	0.150878	1.018158	0.443232	0.192401
B2 - 1005	0.003012	0.018550	0.009094	0.003035	0.132075	0.813524	0.398798	0.133110
B2 - 1006	0.002647	0.018223	0.010993	0.003668	0.091088	0.627089	0.378310	0.126211
B2 - 1007	0.000968	0.019203	0.009115	0.003283	0.046251	0.917277	0.435395	0.156843
B2 - 1008	0.001902	0.017870	0.008992	0.003209	0.084806	0.796817	0.400955	0.143076
B2 - 1009	0.001110	0.018366	0.011078	0.003328	0.050530	0.836026	0.504278	0.151496
B2 - 1010	0.002056	0.019418	0.008369	0.003214	0.106865	1.009506	0.435099	0.167101
B2 - 1011	0.001234	0.015646	0.015067	0.006212	0.031803	0.403254	0.388338	0.160105
B2 - 1012	0.002986	0.015541	0.028890	0.006470	0.081149	0.422370	0.785164	0.175836
B2 - 1013	0.000529	0.017329	0.014126	0.004348	0.018080	0.592767	0.483227	0.148743
B2 - 1014	0.006768	0.017810	0.010060	0.005251	0.227059	0.597487	0.337510	0.176173
B2 - 1015	0.000890	0.016400	0.015171	0.004948	0.035485	0.654225	0.605202	0.197368
D1 - 1001	0.000583	0.020022	0.007170	0.003242	0.033769	1.160081	0.415430	0.187857
D1 - 1003	0.001291	0.019026	0.012676	0.002766	0.065902	0.971388	0.647160	0.141238
D1 - 1004	0.001043	0.019860	0.009240	0.003301	0.048122	0.916443	0.426371	0.152319
D1 - 1005	0.002402	0.017753	0.010541	0.003722	0.059914	0.442880	0.262977	0.092851
D1 - 1006	0.002378	0.017038	0.011094	0.005298	0.075192	0.538744	0.350802	0.167518
D1 - 1007	0.001020	0.018283	0.008213	0.003814	0.035740	0.640546	0.287746	0.133609
D1 - 1008	0.001031	0.017189	0.009080	0.004485	0.032980	0.549625	0.290325	0.143403
D1 - 1009	0.001362	0.019311	0.009043	0.004412	0.046215	0.655217	0.306840	0.149693
D1 - 1010	0.001439	0.015774	0.009530	0.003464	0.082118	0.900292	0.543884	0.197680
D1 - 1011	0.003706	0.017455	0.024735	0.008249	0.080356	0.378524	0.536385	0.178891
D1 - 1012	0.003420	0.015390	0.024676	0.008753	0.073608	0.331194	0.531045	0.188375
D1 - 1013	0.001080	0.019144	0.015816	0.004608	0.027539	0.488326	0.403430	0.117546
D1 - 1014	0.000590	0.018693	0.012082	0.003541	0.020427	0.647025	0.418191	0.122578
D1 - 1015	0.001535	0.016195	0.010772	0.005721	0.052082	0.549676	0.365621	0.194183

Table 6: ICP-MS Normalized Data Results

	U/Ti	V/Ti	Pb/Ti	As/Ti	U/Cr	V/Cr	Pb/Cr	As/Cr
Sample ID								
B1 - 1001	1.236761	0.908589	3.755189	4.403828	1.242059	0.912481	3.771275	4.422693
B1 - 1003	5.699274	0.900076	5.28234	6.304417	4.742276	0.748939	4.395352	5.245806
B1 - 1004	7.49945	0.920902	4.370951	6.714048	5.852586	0.718674	3.411099	5.239656
B1 - 1005	20.44348	0.774368	4.852101	11.15017	12.01253	0.455016	2.85108	6.551804
B1 - 1006	40.25487	0.778454	4.216248	20.90776	27.65056	0.53471	2.896087	14.36128
B1 - 1007	2.503359	0.864698	3.990582	7.682121	2.297156	0.793472	3.661876	7.049341
B1 - 1008	9.39518	0.844371	3.535529	9.657527	7.315584	0.657472	2.75295	7.519861
B1 - 1009	2.686731	0.853203	4.862192	11.75099	1.822794	0.57885	3.298719	7.972375
B1 - 1010	28.73181	0.933117	4.215522	16.98953	18.03814	0.585821	2.646549	10.66621
B1 - 1011	3.745593	0.815026	7.447856	59.62736	1.782032	0.387763	3.543448	28.36876
B1 - 1012	2.624063	0.703965	6.054036	15.63239	1.364355	0.36602	3.147735	8.127905
B1 - 1013	2.437716	0.791331	6.591221	11.85018	1.542709	0.500794	4.171253	7.499387
B1 - 1014	1.068126	0.82696	3.844488	7.542029	0.736538	0.570239	2.651009	5.200689
B1 - 1015	1.610248	0.753671	5.089979	13.90279	1.107302	0.518268	3.50017	9.560381
B2 - 1001	1.466904	0.948363	3.477902	8.167789	1.523264	0.9848	3.611526	8.481604
B2 - 1003	2.029055	0.898261	3.861349	7.332047	1.878628	0.831667	3.575082	6.788475
B2 - 1004	6.111219	0.927898	3.462336	11.68964	5.699825	0.865434	3.229259	10.90272
B2 - 1005	6.201726	0.859496	3.611435	9.375496	4.989511	0.691496	2.905529	7.542923
B2 - 1006	5.450725	0.844317	4.365935	11.32872	3.441101	0.533026	2.756261	7.151944
B2 - 1007	1.993857	0.889726	3.619865	10.14212	1.747258	0.779685	3.172162	8.887751
B2 - 1008	3.916495	0.827967	3.571111	9.911265	3.203777	0.677294	2.921245	8.107626
B2 - 1009	2.28586	0.850948	4.399532	10.27997	1.908911	0.710623	3.674028	8.58475
B2 - 1010	4.232882	0.899691	3.323733	9.928252	4.037109	0.85808	3.170009	9.469065
B2 - 1011	2.541059	0.724943	5.983947	19.18838	1.201458	0.342766	2.829318	9.072611
B2 - 1012	6.148787	0.72008	11.47363	19.98498	3.065639	0.359015	5.720478	9.964036
B2 - 1013	1.088406	0.802894	5.610211	13.43131	0.683023	0.503852	3.520656	8.428743
B2 - 1014	13.93713	0.825175	3.995379	16.22057	8.577778	0.507864	2.459005	9.983146
B2 - 1015	1.831774	0.759875	6.025162	15.28273	1.340528	0.556091	4.409332	11.1842
D1 - 1001	1.200177	0.927666	2.847439	10.01473	1.275736	0.986069	3.026704	10.64523
D1 - 1003	2.658117	0.881556	5.034104	8.545097	2.489635	0.82568	4.715023	8.003474
D1 - 1004	2.147407	0.920159	3.669422	10.19574	1.817926	0.778977	3.106415	8.631383
D1 - 1005	4.945563	0.822537	4.186386	11.49641	2.263423	0.376448	1.915973	5.261535
D1 - 1006	4.896822	0.789421	4.405978	16.36424	2.840578	0.457932	2.555846	9.492667
D1 - 1007	2.100657	0.847106	3.261749	11.77961	1.350165	0.544464	2.096438	7.571163
D1 - 1008	2.124015	0.796445	3.606014	13.8534	1.245911	0.467181	2.115226	8.126164
D1 - 1009	2.804833	0.894726	3.591448	13.62747	1.745906	0.556934	2.235545	8.482602
D1 - 1010	2.96288	0.730875	3.784589	10.69869	3.102227	0.765249	3.962581	11.20186
D1 - 1011	7.630665	0.808763	9.823298	25.48148	3.035663	0.321745	3.907945	10.13715
D1 - 1012	7.043344	0.713049	9.799903	27.0377	2.780741	0.281515	3.869042	10.6746
D1 - 1013	2.22323	0.887015	6.281198	14.23438	1.040357	0.415077	2.939276	6.660954
D1 - 1014	1.215266	0.866107	4.798205	10.9389	0.771684	0.549971	3.046823	6.946113
D1 - 1015	3.159966	0.750384	4.278203	17.67244	1.967544	0.467224	2.663812	11.00369

Table 7: Toxic Metal Concentrations Based on Titanium Crustal Average

	U (ppm)	V (ppm)	Pb (ppm)	As (ppm)
Sample ID				
B1 - 1001	6.876390715	5.051753194	20.87885316	24.48528575
B1 - 1003	31.68796446	5.004421524	29.36980781	35.05255615
B1 - 1004	41.69694238	5.120214537	24.30248651	37.33010442
B1 - 1005	113.665724	4.305485349	26.97768231	61.99491865
B1 - 1006	223.8170833	4.328205688	23.44233805	116.2471533
B1 - 1007	13.91867356	4.807718932	22.18763784	42.71259328
B1 - 1008	52.23719917	4.694702501	19.65754024	53.69584939
B1 - 1009	14.93822707	4.743810852	27.03378714	65.33549867
B1 - 1010	159.7488765	5.188132557	23.43830204	94.46180297
B1 - 1011	20.82549868	4.531545202	41.41007927	331.5281491
B1 - 1012	14.58979184	3.914046889	33.66043857	86.91610344
B1 - 1013	13.55370251	4.39980058	36.64718621	65.88701736
B1 - 1014	5.938781872	4.597895246	21.37535056	41.93368034
B1 - 1015	8.952980608	4.190409348	28.30028328	77.29953734
B2 - 1001	8.155987163	5.272897679	19.3371328	45.41290741
B2 - 1003	11.28154548	4.994331441	21.46910233	40.76618194
B2 - 1004	33.97837641	5.159115526	19.25058614	64.99438609
B2 - 1005	34.48159666	4.77880032	20.07957851	52.12775657
B2 - 1006	30.30602933	4.694399842	24.27459808	62.98770023
B2 - 1007	11.08584352	4.946877997	20.12645149	56.39020349
B2 - 1008	21.77571399	4.603493947	19.85537766	55.10663362
B2 - 1009	12.70938411	4.731270247	24.46139901	57.15661027
B2 - 1010	23.53482374	5.002280966	18.47995671	55.20107959
B2 - 1011	14.12829047	4.03068193	33.27074736	106.6874054
B2 - 1012	34.18725502	4.003645737	63.79338411	111.1165017
B2 - 1013	6.05153917	4.464092267	31.19277166	74.67808655
B2 - 1014	77.49045439	4.587970817	22.21430757	90.18635913
B2 - 1015	10.18466414	4.224905638	33.49990298	84.97195804
D1 - 1001	6.672983905	5.157824218	15.83176075	55.68192605
D1 - 1003	14.77912825	4.901453265	27.98961979	47.51073695
D1 - 1004	11.93958168	5.11608158	20.40198362	56.68829102
D1 - 1005	27.49732821	4.573303556	23.27630777	63.92006709
D1 - 1006	27.22632814	4.389182126	24.49723601	90.98517499
D1 - 1007	11.67965393	4.709909464	18.135324	65.49465702
D1 - 1008	11.80952334	4.428234823	20.04943761	77.02487636
D1 - 1009	15.59487113	4.974675597	19.96845276	75.76873259
D1 - 1010	16.47361293	4.063664926	21.04231609	59.48474276
D1 - 1011	42.4264979	4.496720231	54.61753566	141.677011
D1 - 1012	39.16099405	3.964552692	54.48745859	150.3296186
D1 - 1013	12.36115946	4.931804658	34.92346276	79.1431496
D1 - 1014	6.756878172	4.815552711	26.67802115	60.82025704
D1 - 1015	4.172134258	4.172134258	23.78681013	98.25874405

UNM METALS Superfund Center
Environmental Project 2
Dept. of Earth & Planetary Sciences
Filter Preparation Procedure for ICP-MS: Tisch High Volume Air Samples

Procedure Date: 11/11/2020

Purpose: Preparation of gravimetric samples from a Tisch High Volume Air Sampler for geochemical analyses using ICP-MS to determine toxic metal concentrations.

Materials:

- Nitrile gloves
- Tisch Samples: 8" x 10" PTFE Filters
- HF
- HCl
- HNO_3
- KIMTECH Kimwipes
- Small glassine envelopes
- Ceramic Scissors
- Anti-static Tweezers
- Small Ziplock bags
- Glass petri dishes
- Desiccators
- Plastic weigh boats
- Milty Zerostat 3 Anti-static gun
- Plastic test tubes
- Filter caps
- Small plastic test tubes
- Labeling tape & Sharpie
- Parafilm tape
- Filter Weight Log (or other recording sheet)

Procedure

Sectioning Filters:

1. Put on a pair of nitrile gloves.
2. Use ceramic scissors to cut filter sections B and D in half to create B1, B2, D1, D2 filter pieces. Leave sections A and C for other analyses.

a. As follows:

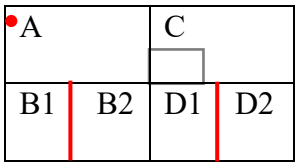

b. The resulting sections for analysis:

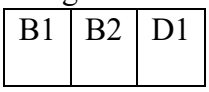

c. Store D2 sections in small glassine envelopes with labels (i.e., 1001-D2, etc.).
d. Use sections B1, B2, and D1 for triplicate sample analysis using ICP-MS; follow steps below for these sections.
    i. If necessary, store sections B1, B2, and D1 in small Ziplock bags until returning to the lab.

3. Use ceramic scissors to cut sections B1, B2, and D1 into several small squares.
    a. Clean scissors between each sample with Kimwipe.

Weighing Filter Sections Pre-Analysis:

4. Wash one glass petri dish for each sample with DI water and sponge.
    a. Dry glass petri dishes with compressed air.
    b. Label one glass petri dish for each filter sample to be analyzed using labeling tape and a Sharpie.
5. Bake samples on glass petri dishes in oven.
    a. Heat to 65°F for 3 hours.
6. Remove samples and cool in desiccators for ~15 minutes.
    a. Periodically vent desiccators by sliding the lid partially open and then closing again.
7. Weigh each sample on microbalance to 5 decimal places.
    a. Use small plastic weigh boats and anti-static tweezers.
    b. Use Milty Zerostat 3 Anti-static gun on each sample before weighing.
        i. Point gun at sample from a distance of 1-3 inches.
        ii. Pull trigger slowly and release slowly- there should be several audible clicks.
        iii. Record sample weight on filter weight log.
        iv. Place sample back in petri dish when finished weighing.

Perform Acid Digestion of Filter Sections:

8. Allow Mehdi or the lab tech to assist when measuring and pouring acid into test tubes.
    a. Obtain and label plastic test tubes and their lids using labeling tape and a Sharpie.

b. Place filter pieces in test tubes and push them down to the bottom of the tube with Teflon tool.
c. Add acid to each sample in the following amounts, making sure to follow the specific safety precautions for each acid type.
    i. 2 mL HF
    ii. 3 mL HNO_3
    iii. 3 mL HCl
d. Allow acid digestion process to take place overnight- Mehdi or lab tech will assist with settings for machine.

After Acid Digestion & Preparation for ICP-MS:

9. Add DI water to each sample to bring to a volume of 25 mL total and shake well.
    a. Place a filter cap on each sample and attach a new, labeled plastic test tube on the other side of the filter cap.
    b. Place a red plug in the bottom hole on the side of the filter cap.
    c. Use the top hole on the filter cap to plug the sample upside-down into the vacuum and turn the blue knob to allow air flow.
    d. Turn on the pump and allow sample to filter into new test tube.
    e. When all the liquid has filtered out, cap the new test tubes.
10. Label new, small test tubes to be used in ICP-MS.
    a. Dilute 10x with 18 molecular weight H_2O.
        i. 1 mL sample
        ii. 1 mL DI water to flush pipet tip
        iii. 8 mL DI water
    b. Provide a list of elements to be analyzed with ICP-MS.
11. The test tubes with the rest of the acid digested samples should be closed tightly.
    a. Wrap parafilm tape tightly around the lid of each sample and store for future analyses.

Weighing Filter Sections Post-Analysis:

12. Repeat steps 4-7 above 3x for oven drying and weighing of samples.
13. Place samples in labeled, small Ziplock bags for storage when complete.